12-6-2016

Electrodermal Activity: What it can Contribute to the Assessment of the Autonomic Nervous System

Hugo F. Posada-Quintero
University of Connecticut - Storrs, hugo.posada-quintero@uconn.edu

Electrodermal Activity: What it can Contribute to the Assessment of the Autonomic Nervous System

Hugo F. Posada-Quintero, PhD

University of Connecticut, 2016

About 70 million people worldwide are affected by dysfunction of the autonomic nervous system (ANS). These dysfunctions can lead to life-threatening conditions, because ANS controls vital functions like heart rate, digestion, respiration, among others. Spectral analysis of heart rate variability (HRV) allows noninvasive assessment of the ANS. However, the low frequencies (0.04-0.15 Hz) of HRV are influenced by the two complementary branches of the ANS, the sympathetic and parasympathetic nervous systems; hence, the spectral analysis cannot separate the dynamics of these autonomic tones. Developing reliable noninvasive techniques for assessment of the ANS dynamics remains a challenge for scientists. Recently, measure of electrodermal activity (EDA) has gained popularity for ANS assessment. EDA signal represents the changes of conductance in the skin, produced by purely sympathetic innervation of sweat glands. Time-domain measures of EDA, such as the skin conductance level (SCL) and skin conductance responses (SCR), are correlated to the sympathetic control, but they lack of consistency. Surprisingly, EDA has been analyzed only in time domain. In this work, using a frequency domain measure via the spectral analysis, we established for the first time that frequency bands of the sympathetic tone in EDA is mostly confined to the 0.045-0.25 Hz range. We termed this power the EDASymp. Furthermore, utilizing a high-resolution time-varying approach we found that the frequency band of 0.08-0.24 Hz is most responsive to sympathetic tone, which we termed, the TVSymp. The EDASymp and TVSymp are more sensitive and consistent discriminators of orthostatic, physical and cognitive stress than time-domain measures of EDA and can quantitatively assess the sympathetic function. Moreover, we found that the sympathetic tone in EDA dynamically changes to higher frequencies when subjects exercise. This result can be useful for adjusting the bounds of HRV when heart rate increases. Currently, the same frequency bounds for the ANS for resting and exercise conditions have been used. Another application of EDA is monitoring of sleep deprivation. Using 24-hour sleep deprivation experiments, we found that high-frequencies (SCR) of EDA relate to vigilance whereas low-frequencies (SCL) relate to

reactiveness. Based on these results, we found that EDA could potentially be used to assist in prevention of fatigue and stress which are the direct and dire consequences of prolonged wakefulness. As a final aim of my dissertation work, evaluations of novel dry carbon/salt/adhesive (CSA) electrodes for obtaining electrocardiogram, surface electromyogram and EDA were investigated. We found non-statistical difference between the carbon/salt/adhesive electrodes for the above mentioned applications when the electrodes were compared to the gold standard silver/silver chloride electrodes. Moreover, it was found that carbon electrodes exhibited better response to noise and motion artifacts when compared to hydrogel Ag/AgCl electrodes. Hence, we concluded that CSA electrodes can be reliably used as a surrogate of the Ag/AgCl electrodes along with the advantage of being more cost effective alternative as they have longer shelf-life.

Electrodermal Activity: What it can Contribute to the Assessment of the Autonomic Nervous System

Hugo F. Posada-Quintero

B. Sc., Universidad Distrital Francisco José de Caldas, Bogotá - Colombia, 2005

M. Sc., Universidad de los Andes, Bogotá - Colombia, 2008

A Dissertation

Submitted in Partial Fulfillment of the

Requirements for the Degree of

Doctor of Philosophy

At the

University of Connecticut

2016

APPROVAL PAGE

Doctor of Philosophy Dissertation

Electrodermal Activity: What it can Contribute to the Assessment of the Autonomic Nervous System

Presented by

Hugo F. Posada-Quintero, B.S., M.S.

Major Advisor _____

Dr. Ki H. Chon

Associate Advisor _____

Dr. Kazunori Hoshino

Associate Advisor _____

Dr. Sabato Santaniello

University of Connecticut

2016

Acknowledgments

To God: He is always with me.

I want to thank the Posada Quintero family, Ana, Albeiro, Diego, Jorge and Andrés. My happy childhood has everything to do with my professional success.

A lot of thanks to Dr. Chon for his stupendous guidance, and for teaching me so many things.

To all the friends I made during these years in the USA, that accompanied and helped me in many aspects, thank you very much.

And many thanks to the ones that make happier a happy person: Caren, Martín and Miguel. There is nothing I wish more than seen you guys to dream and fulfil your dreams.

Table of Contents

Table of Figures

Table of Tables

Chapter 1: Introduction

2.1 Overview

In the autonomic nervous system (ANS), the sympathetic system stimulates the "fight or flight" response, and the parasympathetic system stimulates the "rest and digest" response [1]. The deterioration of autonomic nervous control is a marker for the onset and/or progress of many diseases [2], [3]. Even in healthy subjects, assessing the level of sympathetic arousal or vagal (parasympathetic) control is important for understanding how the ANS maintains body's balance, and detecting when such balance is challenged by internal or external stimuli. We envision simple and reliable technologies for assessment of the branches of the ANS in wearable devices.

Spectral analysis of heart rate variability (HRV) is a noninvasive and quantitative way to assess the dynamics of the ANS [4]. The high-frequency (HF, 0.15 to 0.4 Hz) components of HRV are known to be solely influenced by the parasympathetic system. In contrast, the low-frequency components (LF, 0.045-0.15 Hz), termed HRVLF, are influenced by both the sympathetic and parasympathetic nervous systems. Hence, current HRV analysis techniques cannot separate the dynamics of the sympathetic and parasympathetic nervous systems. Given the current need to fully elucidate and delineate sympathetic dynamics using noninvasive means, new instrumentational devices and signal processing of electrodermal activity (EDA) signals have gained popularity in recent years [5]–[7]. EDA is a measure of the changes in electrical conductance of the skin, also termed galvanic skin response (GSR) for some authors. The attractiveness of EDA is because it is a reflection of the autonomic innervation of sweat glands, reflecting only activity within the sympathetic branch of the ANS because there is no parasympathetic innervation of eccrine sweat glands [8]. It is worth mentioning that EDA can be easily collected using wearable devices.

The overall aim of this thesis work was to determine how EDA signals can be used for assessment of the ANS, specifically elucidating the sympathetic dynamics. For exploring the link between EDA and sympathetic arousal, we considered the spectral analysis of the EDA, studied the variations on EDA signal

under exercise and sleep deprivation, and tested physical media to collect EDA data. The specific aims of this thesis are to assess the dynamics of the sympathetic nervous system, the limitations of the currently available techniques, and the potential of EDA in its contribution to the assessment of the sympathetic nervous system.

2.2 Problem Statement

The need for sensitive measures of sympathetic tone has shown practical relevancy given the important prognostic and diagnostic value of the sympathetic nervous system's impairment to certain cardiovascular diseases and pathophysiological conditions [9], [10]. In many cardiovascular diseases, sympathetic control impairment participates either in the development or in the progression of the pathological process [11], [12]. While there are many and varied approaches to directly measure the sympathetic response, due to high cost, the invasiveness of the technique, the inability to provide continuous monitoring, or the inaccurate assessment of the sympathetic dynamics, the widespread use of these techniques has not been materialized. In cardiovascular autonomic neuropathy, for instance, sympathetic denervation is a marker of the progress of the disease from early to severe stages [2], [3], and the gold standard procedure for sympathetic assessment, the cardiovascular autonomic reflex tests [13], exhibits low sensitivity (50%) for this task [14]. A widely used way to assess the dynamics of the ANS is to compute the power spectral density (PSD) of HRV [4]. Even though HRVLF (low-frequency components of HRV) and HRVLFn (normalized) have shown to be sensitive to postural changes, they are less sensitive to other tests of sympathetic tone [15]. Despite the aforementioned limitation of being also influenced by parasympathetic activity, HRVLF and HRVLFn have been used to assess sympathetic tone [4]. The need for more reliable tools to assess the ANS is evident.

EDA is increasingly used as a surrogate measure of the sympathetic nervous system [6]. Analysis of EDA has been traditionally deployed in time-domain, based on skin conductance level (SCL) and nonspecific skin conductance responses (NS.SCRs) [5]. Because of the high variations of such indices, their use has not yet been popularized. Surprisingly, frequency-domain analysis of EDA, similar to what

is done on HRV, has not been applied as a sympathetic measure. Preliminary exploration showed that a time-frequency analysis of EDA signals can provide a more sensitive and reliable index of sympathetic tone [16]. Frequency-domain and time-frequency spectral analysis are promising techniques to provide more sensitive indices of sympathetic tone. Furthermore, EDA can be a source of information to elucidate the proper adjustment in the low frequency bands of HRV under exercising conditions. When heart rate increases, many studies have found that LF and/or HF bounds vary [17]–[26]. If spectral content of the EDA signal also shifts when heart rate increases (like during exercise), one could utilize that information to correct the HRV's frequency bandwidths. We hypothesize that HRV and EDA can be used together to develop more reliable indices of the sympathetic and parasympathetic tones.

Information on the effect of sleep deprivation on EDA is scarce. However, the effect of sleep deprivation on humans' performance has been widely studied. Prolonged wakefulness has shown to have general detrimental effects on cognitive performance; however, such effect is different depending on the cognitive level of the task. For instance, the effect of sleep deprivation on subjects performing a complex repeated task is much higher than when subjects are asked to perform simple tasks that require little to no vigilant attention (waiting for a stimulus to occur) [27]. For better understanding of the effect of sleep deprivation on humans' physiology, and to evaluate the possibility of predicting the resulting detriment on performance, it is important to evaluate how sleep deprivation affects EDA on subjects performing a cognitive task. We intend to contribute with novel diagnostic markers based on analysis of EDA to prevent detrimental (many times fatal) consequences of sleep deprivation.

Besides the contribution to advance the use of EDA for extraction of the dynamics of the sympathetic nervous system, this work also aimed to explore novel sensing media for acquiring biomedical signals, including EDA. The current gold standard bioelectrical media to obtain EDA and many other signals is the use of Ag/AgCl electrode, mainly because of its property of avoiding polarization. The Ag/AgCl electrodes require application of a paste-like hydrogel over a silver disc. While the hydrogel layer significantly improves the signal quality by effectively lowering the impedance that exists at the electrode-

skin interface, when the hydrogel layer dehydrates impedance increases. This leads to a loss of signal quality and an increased incidence of motion artifacts and noise [28]. Ag/AgCl electrodes are also expensive since silver is an expensive commodity. For measuring EDA signals, Ag/AgCl electrodes need to be taped to the subject's fingers, because they do not have any self-attaching media unlike commercial Ag/AgCl for ECG and surface electromyography (sEMG) that have an adhesive surrounding the hydrogel. We expected CSA electrodes to exhibit low impedance, low cost, long shelf life and the unnecessity of hydrogel layer.

2.3 Summary of Objectives

The hypotheses tested in this thesis are that 1) indices obtained by means of frequency-domain and time-frequency spectral analysis of EDA are sensitive to the sympathetic innervation, 2) EDA can contribute to better understanding of the sympathetic arousal under stressful conditions like exercise or sleep deprivation, and 3) CSA electrodes are a suitable surrogate of Ag/AgCl electrodes for measuring ECG, sEMG and EDA signals. The specific aims of this research are:

Aim 1. Deploy time-frequency domain analysis for better understanding of the interplay between electrodermal activity variability and sympathetic control.

Aim 2. Evaluate heart rate variability and electrodermal activity spectral components under exercises, to get a clearer insight of the sympathetic and parasympathetic tone responses.

Aim 3. Study the effects of sleep deprivation on performance and electrodermal activity signals, to better understand the interplay between these measures and sympathetic arousal.

Aim 4. Test Carbon/Salt/Adhesive electrodes for ECG, sEMG and EDA measurements, in order to examine if these newly developed sensors can potentially be used as an alternative to Ag/AgCl electrodes.

To accomplish **Aim 1**, electrodermal activity (EDA) was explored in time (traditional) and frequency domain separately, to have an initial idea of the nature and characteristics of EDA, for subjects

under several different types of stress. Specifically, we explored the low-frequency range of the power spectrum density (PSD) of EDA, in order to determine whether its dynamics are similar to heart rate variability (HRV), in which the sympathetic tone is reflected in the power of the low-frequency components. Exploring the PSD of EDA gave us a better insight of the interplay between sympathetic control and EDA. Time-frequency spectrum (TFS) analysis was employed to further analyze the EDA and to take advantage of the possibility of tracking the changes of power distribution of EDA components over time. Tests involving orthostatic, cognitive and physical stress were deployed to subjects to test our technique.

For **Aim 2** we proposed to use frequency and time-frequency domain analysis of EDA, to test the autonomic nervous system under strenuous physical activity, specifically the shifting of the frequency bands of the sympathetic and parasympathetic tones. We collected ECG and EDA signals on subjects performing a non-maximal exercise test on a treadmill, to induce a controlled increase on the mean heart rate. By doing this, we were able to see the changes on HRV and EDA frequency components. EDA has never been explored in such conditions, so the observation itself is novel to the field.

In **Aim 3** analyzed the effect of sleep deprivation on subjects performing a cognitive-manual task. Measures of performance were used to assess fatigue and evaluated its correlation with features of EDA. Moreover, the evolution of EDA over time during sleep deprivation was analyzed to procure more comprehension of EDA singularities. Time, frequency and time-frequency domain analysis of EDA signals were deployed to better elucidate the influence of prolonged wakefulness on EDA.

Finally, to achieve **Aim 4**, novel Carbon/Salt/Adhesive (CSA) electrodes were designed and tested for the task of recording biomedical signals, including EDA. The CSA electrodes are intended to overcome the two salient drawbacks of the gold standard Ag/AgCl electrodes for bioelectrical signals collection: short shelf life and the cost. First, the concept of CSA electrodes was explored and its functionality were compared to Ag/AgCl electrodes. Diverse applications of CSA electrodes for collecting biomedical signals

evaluated in terms of quality of the acquired signals. The aim will be finally fulfilled by testing the suitability of CSA electrodes for collecting ECG, sEMG and EDA signals.

2.4 Dissertation Organization

This dissertation is structured in the chapters described below, including the relevant background, methodology and experimental results in accordance to the specific aims. Figure 1.1 shows a diagram of the general methodology and structure of the work. Three main sections conform this thesis dissertation. The first section, which comprises two chapters, is about developing simpler and reliable indices of sympathetic control based on signal processing of EDA, expected to be deployable in wearable devices in the future. The second section, including two chapters, is about using the measures developed in section 1, to explore applications where the sympathetic function assessment can be used. The third section contains three chapters and is a hardware complement to our signal processing work, and is intended to test novel dry electrodes to overcome the limitations of Ag/AgCl electrodes for collecting EDA and other biomedical signals. Chapters 3-9 follow the basic structure of a Journal paper, as they are either already published or in review.

Chapter 2: Background

Presents general information about the physiology of the autonomic nervous system, focusing on the sympathetic branch, and summarizes previous efforts on assessing it. It ends with the definition and meaning of electrodermal activity as well as previously reported measures based on this signal.

Chapter 3: Power Spectral Density Analysis of Electrodermal Activity for Sympathetic Function Assessment

Includes the methodology and experimental results specific to the first part of Aim 1, including the analysis of EDA in frequency domain, and concludes with determination of the frequency bands associated with the

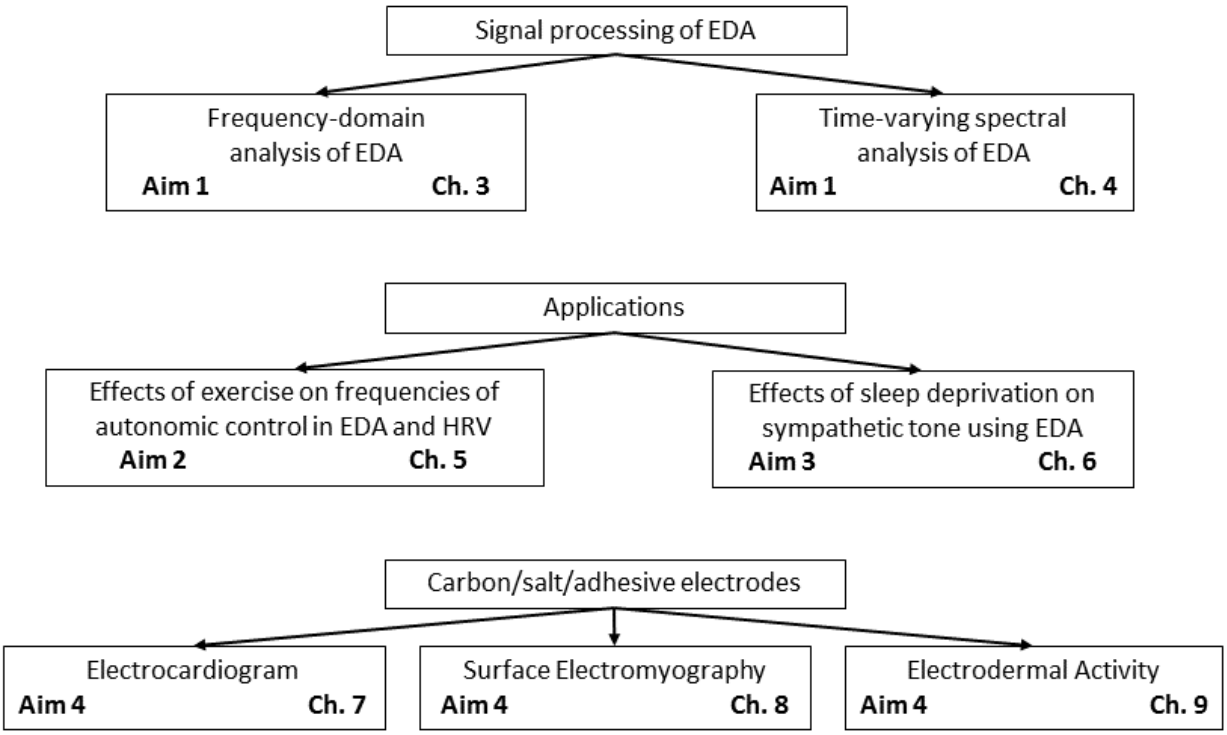

Figure 1.1 – Diagram of the methodology of this research.

sympathetic control. (Posada-Quintero, H. F., Florian, J. P., Orjuela-Cañón, A. D., Aljama-Corrales, T., Charleston-Villalobos, S., & Chon, K. H. (2016). Power Spectral Density Analysis of Electrodermal Activity for Sympathetic Function Assessment. *Annals of Biomedical Engineering*, 1–12)

Chapter 4: Highly Sensitive Index of Sympathetic Activity Based on Time-Frequency Domain Analysis of Electrodermal Activity

Describes the methodology and experimental results regarding the achievement of the remaining portion of Aim 1, expanding the analysis of EDA to the time-frequency domain. The technique used to compute the time-frequency spectra of EDA signals is explained in detail. (Posada-Quintero, H. F., Florian, J. P., Orjuela-Canon, A. D., & Chon, K. H. (2016). Highly Sensitive Index of Sympathetic Activity based on Time-Frequency Spectral Analysis of Electrodermal Activity. *American Journal of Physiology - Regulatory, Integrative and Comparative Physiology*).

Chapter 5: Electrodermal Activity Suggests a Change in Frequencies of Sympathetic Control During Exercise

Defines the methodology and experimental results regarding **Aim 2**, which is focused on understanding how the sympathetic control evolves in the frequency domain when subjects undergo physical activity (Posada-Quintero, H. F., Reljin, N., Mills, C., Mills, I., Florian, J. P., VanHeest, J. & Chon, K. H. Chapter 5: Electrodermal Activity Suggests a Change in Frequencies of Sympathetic Control During Exercise. *American Journal of Physiology - Exercise*. Submitted).

Chapter 6: Electrodermal Activity Can Track the Effects of Sleep Deprivation on Reactiveness and Vigilance

Reports the methodology and experimental results of studying EDA signals as subjects are sleep deprived for 24 hours. This chapter fulfills the purposes of **Aim 3**. (Posada-Quintero, H. F., Bolkhovsky, J. B., Reljin, N. & Chon, K. H.. Electrodermal Activity Can Track the Effects of Sleep Deprivation on Reactiveness and Vigilance. To be published).

Chapter 7: Low Impedance Carbon Adhesive Electrodes with Long Shelf Life

Aim 4 involves the testing of carbon/salt/adhesive (CSA) electrodes for collecting EDA signals. To fulfill this, three studies have been deployed: first, assessment of CSA electrodes to collect ECG; second, evaluation of CSA electrodes to collect surface electromyography (sEMG) signals; finally, testing of CSA electrodes to collect EDA. The first part of this aim is covered in this chapter. (Posada-Quintero, H. F., Reyes, B. A., Burnham, K., Pennace, J., & Chon, K. H. (2015). Low Impedance Carbon Adhesive Electrodes with Long Shelf Life. Annals of Biomedical Engineering, 43(10), 2374–2382)

Chapter 8: Assessment of Carbon/Salt/Adhesive Electrodes for Surface Electromyography Measurements

Describes the methods and results to fulfill the second part of **Aim 4**, evaluating CSA electrodes to collect sEMG signals. A succinct yet effective methodology is described to assess sEMG CSA electrodes (Posada-Quintero, H., Rood, R., Burnham, K., Pennace, J., & Chon, K. (2016). Assessment of Carbon/Salt/Adhesive Electrodes for Surface Electromyography Measurements. *IEEE Journal of Translational Engineering in Health and Medicine*, PP(99), 1–1).

Chapter 9: Dry Carbon/Salt Adhesive Electrodes for Recording Electrodermal Activity

The methods and results of the final part of **Aim 4**, evaluating CSA electrodes to sense EDA signals using different types of technologies and tests that are available to EDA (Posada-Quintero, H. F., Rood, R., Noh, Y., Burnham, K., Pennace, J. and Chon, K. H.. Dry Carbon/Salt Adhesive electrodes for recording Electrodermal Activity. Sensors & Actuators: A. Physical. In process of revision for publication).

Chapter 10: Conclusions and Future work

Summarizes the main findings of this dissertation as well as the limitations and areas of future development and application of the methods proposed in this research.

2.5 References

[1] V. Higgins, “Human physiology: the basis of medicine,” *Br. J. Sports Med.*, vol. 40, no. 10, p. 880, Oct. 2006.

[2] D. J. Ewing and B. F. Clarke, “Diagnosis and management of diabetic autonomic neuropathy.,” *Br. Med. J. Clin. Res. Ed*, vol. 285, no. 6346, pp. 916–918, Oct. 1982.

[3] C. J. Mathias and R. Bannister, “Investigation of autonomic disorders,” in *Autonomic failure: a textbook of clinical disorders of the autonomic nervous system*, C. J. Mathias and R. Bannister, Eds. Oxford: Oxford University Press, 1999, pp. 169–195.

[4] Task Force of the European Society of Cardiology and the North American Society of Pacing and Electrophysiology, “Heart rate variability. Standards of measurement, physiological interpretation, and clinical use,” *Eur. Heart J.*, vol. 17, no. 3, pp. 354–381, Mar. 1996.

[5] W. Boucsein *et al.*, “Publication recommendations for electrodermal measurements,” *Psychophysiology*, vol. 49, no. 8, pp. 1017–1034, Aug. 2012.

[6] R. Freeman and M. W. Chapleau, “Testing the autonomic nervous system,” *Handb. Clin. Neurol.*, vol. 115, pp. 115–136, 2013.

[7] A. P. Colbert, K. Spaulding, A. Larsen, A. C. Ahn, and J. A. Cutro, “Electrodermal activity at acupoints: literature review and recommendations for reporting clinical trials,” *J. Acupunct. Meridian Stud.*, vol. 4, no. 1, pp. 5–13, Mar. 2011.

[8] H. D. Critchley, “Electrodermal responses: what happens in the brain,” *Neurosci. Rev. J. Bringing Neurobiol. Neurol. Psychiatry*, vol. 8, no. 2, pp. 132–142, Apr. 2002.

[9] K. H. Chon *et al.*, “A novel quantitative method for diabetic cardiac autonomic neuropathy assessment in type 1 diabetic mice,” *J. Diabetes Sci. Technol.*, vol. 8, no. 6, pp. 1157–1167, Nov. 2014.

[10] G. Grassi and M. Esler, “How to assess sympathetic activity in humans,” *J. Hypertens.*, vol. 17, no. 6, pp. 719–734, Jun. 1999.

[11] M. Esler *et al.*, “Assessment of human sympathetic nervous system activity from measurements of norepinephrine turnover,” *Hypertension*, vol. 11, no. 1, pp. 3–20, Jan. 1988.

[12] J. L. Rouleau *et al.*, “Activation of neurohumoral systems following acute myocardial infarction,” *Am. J. Cardiol.*, vol. 68, no. 14, p. 80D–86D, Nov. 1991.

[13] P. Schwartz, M. La Rovere, and E. Vanoli, “Assessment: Clinical autonomic testing report of the Therapeutics and Technology Assessment Subcommittee of the American Academy of Neurology,” *Neurology*, vol. 46, no. 3, pp. 873–880, Mar. 1996.

[14] V. Spallone, R. Morganti, T. Fedele, C. D’Amato, and M. R. Maiello, “Reappraisal of the diagnostic role of orthostatic hypotension in diabetes,” *Clin. Auton. Res. Off. J. Clin. Auton. Res. Soc.*, vol. 19, no. 1, pp. 58–64, Feb. 2009.

[15] H. F. Posada-Quintero, J. P. Florian, A. D. Orjuela-Cañón, T. Aljama-Corrales, S. Charleston-Villalobos, and K. H. Chon, “Power Spectral Density Analysis of Electrodermal Activity for Sympathetic Function Assessment,” *Ann. Biomed. Eng.*, vol. 44, no. 10, pp. 3124–3135, Apr. 2016.

[16] H. F. Posada-Quintero and K. H. Chon, “Frequency-domain electrodermal activity index of sympathetic function,” in *2016 IEEE-EMBS International Conference on Biomedical and Health Informatics (BHI)*, 2016, pp. 497–500.

[17] R. Bailón, G. Laouini, C. Grao, M. Orini, P. Laguna, and O. Meste, “The integral pulse frequency modulation model with time-varying threshold: application to heart rate variability analysis during exercise stress testing,” *IEEE Trans. Biomed. Eng.*, vol. 58, no. 3, pp. 642–652, Mar. 2011.

[18] R. Bailón, N. Garatachea, I. de la Iglesia, J. A. Casajús, and P. Laguna, “Influence of running stride frequency in heart rate variability analysis during treadmill exercise testing,” *IEEE Trans. Biomed. Eng.*, vol. 60, no. 7, pp. 1796–1805, Jul. 2013.

[19] A. Benítez *et al.*, “Ventilatory threshold prediction by spectral analysis of heart rate variability in incremental maximal tests,” in *Computing in Cardiology, 2010*, 2010, pp. 939–942.

[20] G. Blain, O. Meste, T. Bouchard, and S. Bermon, “Assessment of ventilatory thresholds during graded and maximal exercise test using time varying analysis of respiratory sinus arrhythmia,” *Br. J. Sports Med.*, vol. 39, no. 7, pp. 448-452-452, Jul. 2005.

[21] F. Cottin, C. Médigue, P. Lopes, P.-M. Leprêtre, R. Heubert, and V. Billat, “Ventilatory thresholds assessment from heart rate variability during an incremental exhaustive running test,” *Int. J. Sports Med.*, vol. 28, no. 4, pp. 287–294, Apr. 2007.

[22] M. J. Gaitan-Gonzalez, S. Carrasco-Sosa, R. Gonzalez-Camarena, and O. Yanez-Suarez, “Non-linear relationship between heart period and root mean square of successive differences during ramp exercise and early recovery,” in *Computers in Cardiology, 2005*, 2005, pp. 727–730.

[23] K. Martinmäki, K. Häkkinen, J. Mikkola, and H. Rusko, “Effect of low-dose endurance training on heart rate variability at rest and during an incremental maximal exercise test,” *Eur. J. Appl. Physiol.*, vol. 104, no. 3, pp. 541–548, Oct. 2008.

[24] O. Meste, G. Blain, and S. Bermon, “Analysis of the respiratory and cardiac systems coupling in pyramidal exercise using a time-varying model,” in *Computers in Cardiology, 2002*, 2002, pp. 429–432.

[25] E. F. Sierra-Alonso, L. M. Sepulveda-Cano, R. Bailon-Luesma, P. Laguna, and G. Castellanos-Dominguez, “Estimating respiratory frequency from HRV during treadmill exercise testing,” in *Computing in Cardiology Conference (CinC), 2013*, 2013, pp. 121–124.

[26] M. P. Tulppo, T. H. Mäkikallio, T. Seppänen, R. T. Laukkanen, and H. V. Huikuri, “Vagal modulation of heart rate during exercise: effects of age and physical fitness,” *Am. J. Physiol.*, vol. 274, no. 2 Pt 2, pp. H424-429, Feb. 1998.

[27] J. Lim and D. F. Dinges, “A meta-analysis of the impact of short-term sleep deprivation on cognitive variables.,” *Psychol. Bull.*, vol. 136, no. 3, p. 375, 2010.

[28] A. Searle and L. Kirkup, “A direct comparison of wet, dry and insulating bioelectric recording electrodes,” *Physiol. Meas.*, vol. 21, no. 2, pp. 271–283, May 2000.

Chapter 2: Background

2.1 The autonomic nervous system

The autonomic nervous system (ANS) provides a rapidly responding neural control to regulate a wide range of unconscious body actions. The sympathetic and the parasympathetic systems are the two main divisions of the ANS [1]. The primary function of the sympathetic branch is to stimulate the body's fight or flight response, and the parasympathetic activity has an antagonist or complementary function. Renal, endocrine, respiratory, cardiovascular and other systems are controlled by the sympathetic or the parasympathetic branch, or both [2].

2.1.1 The sympathetic function

In terms of physiological importance, sympathetic influences on the heart and peripheral circulation have been shown to control heart rate and blood pressure both at rest and during physiological stimuli, such as orthostatic stress [6]. In response to stressors of any kind, the stress system is activated to coordinate the adaptive responses of the organism [7]. This leads to peripheral and behavioral changes that improve the ability of the organism to adjust homeostasis and have better chances for survival. The sympathetic innervation of peripheral organs is derived from the efferent preganglionic fibers, which synapse in the bilateral chains of sympathetic ganglia with postganglionic sympathetic neurons that innervate eccrine sweat glands, among many other organs. Sympathetic preganglionic neurons are cholinergic, whereas the postganglionic neurons are mostly noradrenergic [8].

2.2 Sympathetic function assessment

Assessment of sympathetic function is one of the major research fields in cardiovascular research, because alterations in sympathetic tone have been conclusively demonstrated to have important pathophysiological, physiological and clinical relevance [9]. The sympathetic nervous system has pathophysiological relevance in several diseases directly or indirectly affecting the cardiovascular system. This is especially important for the neuropathies [10] because sympathetic function is affected in early

stages [11], and in general for cardiovascular diseases in which the sympathetic activation occurring has been shown to participate either in the development or in the progression of the pathological process [12], [13].

Techniques to assess the sympathetic activity include hemodynamic measurements [14], [15], adrenergic and ganglionic pharmacological blockade [16]–[19], noradrenaline measurement in urine or plasma [12], [20], [21], neurophysiological approach [22], [23], plasma noradrenaline kinetics [24], [25], heart rate variability (HRV) analysis [26]–[28] or imaging techniques [29]. Haemodynamic measurements and pharmacological blockade are invasive and present limited reproducibility. Noradrenaline measurement provides only a 'static' picture of sympathetic function. Neurophysiological approach is the only method for directly recording efferent postganglionic muscle sympathetic nerve activity, and allows a continuous measurement; however, it is an invasive technique. Imaging techniques, including positron emission tomography and single photon emission computed tomography scanning, have been applied to visualize the sympathetic enervation of human organs with a good success in studying, for example, the various syndromes causing postural hypotension. Nevertheless, neuroimaging techniques require an elevated level of financial and technical support.

2.2.1 Heart Rate Variability

Given the widespread of the technique, HRV will be a common reference to compare the results of this work to. HRV is a noninvasive indicator that reflects the homeostatic interplay between perturbations in cardiovascular functions and the dynamic responses of the cardiovascular regulatory systems [28]. HRV is extracted from the R-R peak series of the electrocardiogram (ECG), and spectral analysis of the R–R series has been widely used in HRV studies to discriminate between subjects with different cardiac conditions as well as to predict mortality in some groups of patients [30], [31]. HRV analysis has been widely deployed because it can overcome the high cost, invasiveness and inability to provide continuous monitoring with other techniques.

The power spectra of HRV is usually calculated using Welch's periodogram method. From spectral analysis, two frequency bands are considered: low frequency (LF) band (0.045 to 0.15 Hz) and high frequency (HF) band (0.15 to 0.4 Hz) (see Figure 2.1) [28]. Very low frequency (VLF) band is not taken into account because their physiological correlates are still unknown [28]. The spectral frequency band is computed as the sum of the products of power spectral densities of the band harmonics by the sharpness of the spectrum (Nyquist cointerval). The LF and HF oscillatory components are reported in absolute (square milliseconds, ms^2) and normalized (to the total power of HRV) units. These spectral parameters are known to reflect autonomic activity. Indeed, the parasympathetic nervous system activity is the major contributor to the HF component [32], [33]. The interpretation of the LF component is very difficult, but previous research has demonstrated that it reflects both sympathetic and parasympathetic influences [32], [34]. Many studies have highlighted the need for an adjustment in the frequency bands of HRV during exercise [31], [35]–[43]. Even though there is evidence of the frequency shifts during exercises, there is not enough evidence to elucidate the proper frequency bounds of HF and LF bands. It remains unclear what is the evolution of the frequencies of the sympathetic and parasympathetic tones on the HRV, when subjects exercise.

Although traditional spectral analysis of HRV is not reliable for separate assessment of sympathetic and parasympathetic functions, we used this technique as a comparison reference for assessing the ANS in this dissertation. We did not directly compare the indices by merely computing the correlation of the sympathetic indices we developed in this work to HRVLF (normally used to assess sympathetic control); instead, we always showed how indices of HRV were not reliable indices for the assessment of autonomic control, for the tests we deployed to elicit sympathetic response on subjects.

2.2.2 Electrodermal Activity

Sudomotor activity is linked to the sympathetic function, and has the potential to be used to evaluate the autonomic functions and assess stress levels [44]–[46]. However, measuring the amount of sweat produced is impractical. Nevertheless, sweat glands activity modulates conductance of an applied current

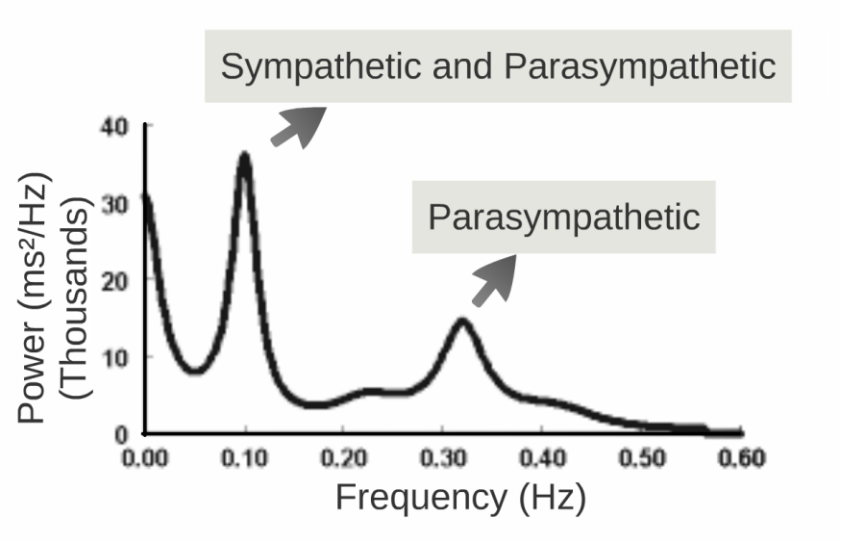

Figure 2.1 – Spectral analysis of HRV.

[47]–[50]. Changes in electrical conductance of the skin are termed electrodermal activity (EDA). Sweating influences the electrical conductance of the skin, because although sweat contains minerals, lactic acid and urea, it is mostly water. EDA has shown strong correlation to sweat production, and is thought to provide a quantitative functional measure of sudomotor activity [51], [52]. In other words, we can get signals from control centers in the brain by taking advantage of the fact that their arrival at the skin is indicated by EDA [50].

2.2.2.1 Relevant physiology

Although primary function of most sweat glands is thermoregulation, those located on the palmar and plantar surfaces are thought to be more concerned with grasping performance than with temperature control. Thus, they are more responsive to psychologically significant stimuli than to thermal stimuli [50]. This is most evident in these areas because of the high gland density concentration, but all eccrine sweat glands are believed to be involved in emotion-evoked sweating [53]. The most widely accepted model for EDA is the single effector model of the sweat glands, with the level and phasic changes in EDA as outputs. We can think of the sweat ducts as a set of variable resistors wired in parallel. Sweat comes through the ducts in in varying numbers of sweat glands in variable amounts, depending on the degree of sympathetic

activation. The higher the sweat rises, the lower the resistance in that variable resistor. Changes in the level of sweat in the ducts produce observable variations in EDA [54].

Neurotransmitter involved in the mediation of eccrine sweat glands activity is acetylcholine, which is generally a parasympathetic neurotransmitter, rather than noradrenaline, typically associated with peripheral sympathetic activation [55]. For that reason both the sympathetic and parasympathetic branches of the ANS were thought to control EDA. It is currently accepted that human sweat glands have predominantly cholinergic innervation from sudomotor fibers originating in the sympathetic chain [53]. Evidence for the sympathetic control of EDA has been provided by studies which simultaneously recorded sympathetic action potentials in peripheral nerves and EDA. A high correlation between bursts of sympathetic nerve activity and SCRs was shown [56].

At least three pathways lead to production of SCRs: hypothalamic control, contralateral and basal ganglion influences (involves one pathway of excitatory control by the premotor cortex and another pathway of exhibitory and excitatory influences in the frontal corterx) and the reticular formation in the brainstem [57], [58]. These pathways imply different functional roles associated with the central mechanisms: activation of the reticular formation is associated with gross movements and increased muscle tone; hypothalamic activity controls the thermoregulatory sweating; amygdala activation is reflecting affective processes; premotor cortex occur in situations requiring fine motor control; and prefrontal cortical activity is associated with orienting and attention [54], [59], [60]. All these processes, at certain level, influence the EDA signal.

Electrodermal activity (EDA) has a long history on psychophysiological research, since Vigouroux studies in France, 1879. Historically, most of the studies evaluated EDA as a response to mental (e.g. emotional, cognitive) stress. However, skin resistance varies with the state of sweat glands in the skin, controlled by the sympathetic nervous activity, making skin conductance an indication of not only psychological but also general sympathetic arousal. Despite the wide acceptation of this concept, using EDA for pathophysiological assessment is rather novel.

2.2.2.2 Recording devices

Although it is possible to collect EDA signals without an external source (endosomatic recording), most EDA devices involve the application of an external constant current or voltage source (exosomatic recordings) via electrodes on the skin [49]. Endosomatic devices are simpler as they require only a high input impedance amplifier (>10 MΩ), However, they are not. Requirement on amplifier's gain and the need for a floating reference to measure the potential difference between the two electrodes, make this approach difficult.

Exosomatic devices measure the modulated current or voltage, depending on whether the constant source is voltage or current, to compute the skin conductance. The constant source can be either direct current (DC) or alternating current (AC). Electrodermal measurements with DC source is accomplished by means of operational amplifiers [61]. Although constant current and constant voltage can be used, the latter is widely preferred [62]. Given that the floating reference is common to output and input, the voltage difference is independent of a reference electrode position, preventing endosomatic contamination of exosomatic measurements.

Measuring EDA using AD devices requires more elaborate instrumentation than the DC approach, because of the capacitive properties of the stratum corneum. Given that conductance and capacitance are physically in parallel, constant amplitude excitation is preferred (measuring changes in current). A phase-sensitive rectifier can be used to separate components of conductive and capacitive contributions. The main advantage of AC source devices is avoiding electrode polarization [49]. In spite of this advantage of AC-source devices over DC-source devices, both types are still widely used [49].

2.2.2.3 Electrodes for collecting EDA

Special electrodes, electrode gels, and recording devices may be required for recording EDA. Those can be different from the ones utilized for other psychophysiological measures, given the nature of EDA and the location where the signal is acquired. Electrodes are an important factor for the quality of the measures because they are the biomedical sensors. Electrodes for EDA recording are normally of metal,

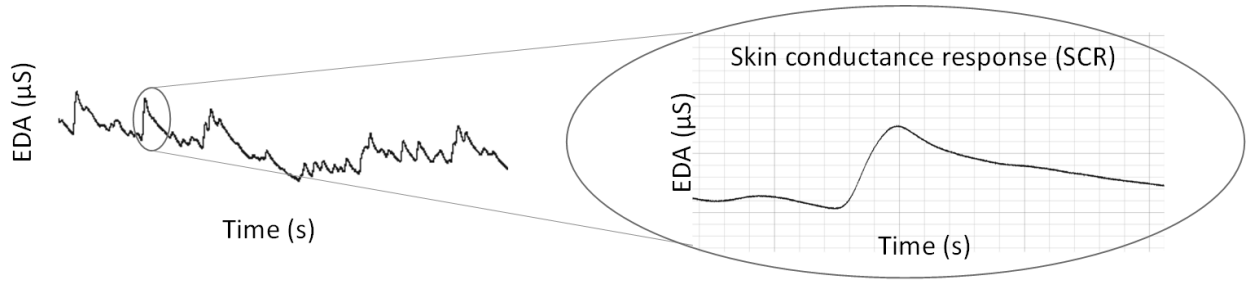

Figure 2.2 – Electrodermal activity signal and skin conductance response.

but can be potentially made with carbon [49]. Using the same metal for the two electrodes is important, mainly in DC-source devices, because the difference in metals will introduce a potential difference.

In exosomatic DC-source devices the electrodes carry a DC current and become anode and cathode in an electric system. The electrodes are polarized by electrolysis. The use of silver-silver chloride (Ag/AgCl) electrodes is standard in order to minimize both polarization of the electrode and the bias potential between the electrodes. Reusable EDA electrodes, often commercially available are much more expensive than disposable AgCl electrodes with very thin layers of silver chloride. With low DC current in prolonged use, the charge may be high enough to remove part of the AgCl layer at the cathode and increase the layer at the anode. After some time, large bias voltage levels may result [62].

For its part, stainless steel electrodes have the advantages of not corroding and also being mechanically strong. However, they are more prone to polarizing effects than Ag/AgCl electrodes. Carbon is a promising alternative to metal for both the wires and the electrodes. Besides reducing polarization effects , using carbon can make the electrodes radiotranslucent, and compatible with MRI [49].

2.2.2.4 Measures of EDA

The most salient characteristic of EDA signal is the occurrence of skin conductance responses (SCR), as a result of instantaneous or tonic stimuli. The SCRs are those noticeable rapid transient events. SCRs have the smooth waveform as shown in Figure 2.2. Elicited SCRs are used to evaluate subjects' response on event-related experiments ("startle-like" stimuli) or tonic stimuli tests (like a change in condition, workload, cognitive stress, etc.). In event-related experiments, the occurrence of a SCR is

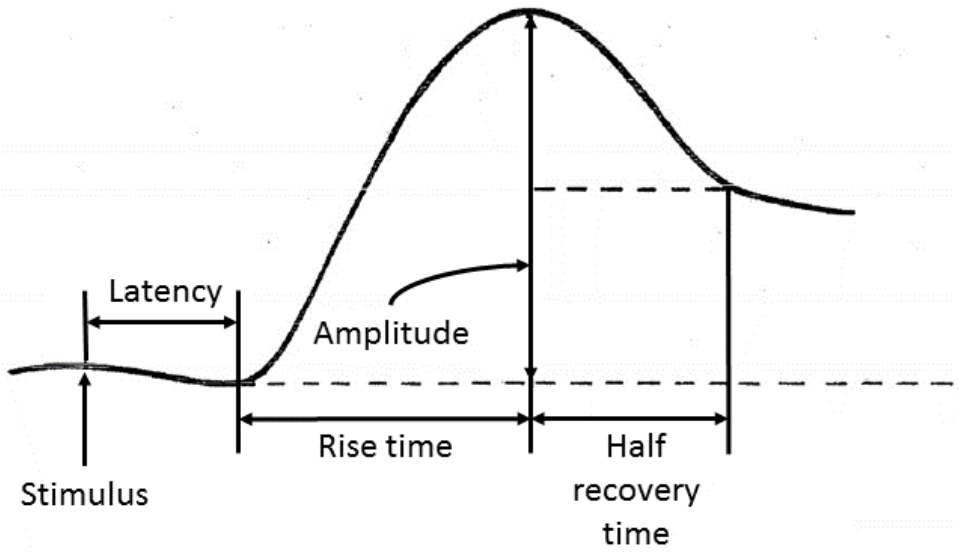

Figure 2.3 – Time-domain measures of EDA based on the specific SCR caused by an instantaneous stimulus

expected after the stimulus is applied. In such experiments the SCRs are usually called event related SCRs (ER.SCRs). ER.SCRs' stimulus-onset latency, amplitude (peak-to-onset value difference), rise time (also called onset-to-peak time), among others, are measures used to assess the level of stress induced by the stimulus (Figure 2.3).

In tonic stimulus tests, skin conductance level (SCL) and nonspecific skin conductance responses (NS.SCRs) [49], are the used measures (Figure 2.4). SCL (usually expressed in microsiemens, μS) is a measure related to the slow shifts of EDA, and specifically refers to the level of skin conductance. SCL is typically computed as a mean of several measurements taken during a specific non-stimulation rest period, e.g. the mean of the "tonic EDA" component shown in Figure 2.4. The non-specific SCRs (NS.SCRs) are the number of SCRs in a period of time, and are considered a tonic measure because they occur post-stimuli, over a period of time, e.g. the SCRs that overpass the defined threshold in Figure 2.4. A key concern for the SCL and NS.SCRs is that these indices are highly variable between subjects [63]. This is due to the frequent occurrence of a second response before the completion of a given SCR, which can be detected by visual inspection, but its detection is not easy to automate [49]. In addition, periodic shifts in the background SCL (like a DC shift) could be important if they appear to occur in conjunction with specific components

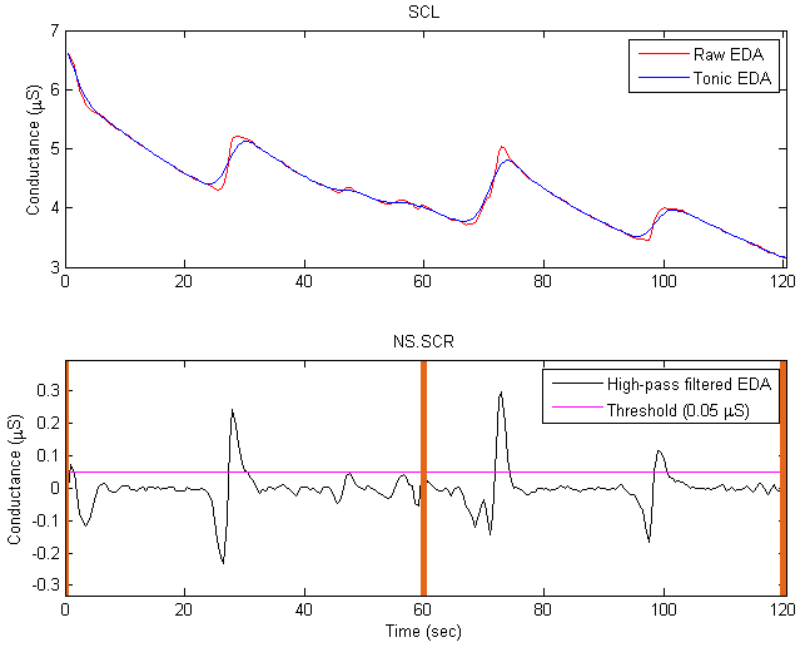

Figure 2.4 – Time-domain measures of EDA signal resulting from a tonic stimulus.

of the experiment, and only a visual analysis would reveal the difference between a SCR and unimportant drift factors (artifacts) [64]. Furthermore, obtaining NS.SCRs requires an observer to count SCRs, which could be problematic if there are motion artifacts during EDA measurements.

2.3 References

[1] C. Tsigos and G. P. Chrousos, "Physiology of the hypothalamic-pituitary-adrenal axis in health and dysregulation in psychiatric and autoimmune disorders," *Endocrinol. Metab. Clin. North Am.*, vol. 23, no. 3, pp. 451–466, Sep. 1994.

[2] M. P. Gilbey and K. M. Spyer, "Essential organization of the sympathetic nervous system," *Baillières Clin. Endocrinol. Metab.*, vol. 7, no. 2, pp. 259–278, Apr. 1993.

[3] J. T. Shepherd and G. Mancia, "Reflex control of the human cardiovascular system," *Rev. Physiol. Biochem. Pharmacol.*, vol. 105, pp. 1–99, 1986.

[4] G. P. Chrousos and P. W. Gold, "The concepts of stress and stress system disorders. Overview of physical and behavioral homeostasis," *JAMA*, vol. 267, no. 9, pp. 1244–1252, Mar. 1992.

[5] C. Tsigos and G. P. Chrousos, "Hypothalamic-pituitary-adrenal axis, neuroendocrine factors and stress," *J. Psychosom. Res.*, vol. 53, no. 4, pp. 865–871, Oct. 2002.

[6] G. Grassi and M. Esler, “How to assess sympathetic activity in humans,” *J. Hypertens.*, vol. 17, no. 6, pp. 719–734, Jun. 1999.

[7] C. J. Mathias and R. Bannister, “Investigation of autonomic disorders,” in *Autonomic failure: a textbook of clinical disorders of the autonomic nervous system*, C. J. Mathias and R. Bannister, Eds. Oxford: Oxford University Press, 1999, pp. 169–195.

[8] D. J. Ewing and B. F. Clarke, “Diagnosis and management of diabetic autonomic neuropathy.,” *Br. Med. J. Clin. Res. Ed*, vol. 285, no. 6346, pp. 916–918, Oct. 1982.

[9] M. Esler *et al.*, “Assessment of human sympathetic nervous system activity from measurements of norepinephrine turnover,” *Hypertension*, vol. 11, no. 1, pp. 3–20, Jan. 1988.

[10] J. L. Rouleau *et al.*, “Activation of neurohumoral systems following acute myocardial infarction,” *Am. J. Cardiol.*, vol. 68, no. 14, p. 80D–86D, Nov. 1991.

[11] J. Brod, V. Fencl, Z. Hejl, and J. Jirka, “Circulatory changes underlying blood pressure elevation during acute emotional stress (mental arithmetic) in normotensive and hypertensive subjects,” *Clin. Sci.*, vol. 18, pp. 269–279, May 1959.

[12] C. B. Thomas, J. A. Stanley, and M. A. Kendrick, “Observations on some possible precursors of essential hypertension and coronary artery disease. VII. The subjective reaction to the cold pressor test as expressed in the verbal response,” *J. Chronic Dis.*, vol. 14, pp. 355–365, Sep. 1961.

[13] G. Grassi *et al.*, “Heart rate as marker of sympathetic activity,” *J. Hypertens.*, vol. 16, no. 11, pp. 1635–1639, Nov. 1998.

[14] S. Julius, A. V. Pascual, and R. London, “Role of parasympathetic inhibition in the hyperkinetic type of borderline hypertension,” *Circulation*, vol. 44, no. 3, pp. 413–418, Sep. 1971.

[15] N. K. Hollenberg *et al.*, “Renal vascular tone in essential and secondary hypertension: hemodynamic and angiographic responses to vasodilators,” *Medicine (Baltimore)*, vol. 54, no. 1, pp. 29–44, Jan. 1975.

[16] B. Egan, R. Panis, A. Hinderliter, N. Schork, and S. Julius, “Mechanism of increased alpha adrenergic vasoconstriction in human essential hypertension.,” *J. Clin. Invest.*, vol. 80, no. 3, pp. 812–817, Sep. 1987.

[17] R. D. Hoeldtke, K. M. Cilmi, G. A. Reichard, G. Boden, and O. E. Owen, “Assessment of norepinephrine secretion and production,” *J. Lab. Clin. Med.*, vol. 101, no. 5, pp. 772–782, May 1983.

[18] I. J. Kopin, “Catecholamine metabolism: basic aspects and clinical significance,” *Pharmacol. Rev.*, vol. 37, no. 4, pp. 333–364, Dec. 1985.

[19] A. B. Vallbo, K. E. Hagbarth, H. E. Torebjörk, and B. G. Wallin, “Somatosensory, proprioceptive, and sympathetic activity in human peripheral nerves,” *Physiol. Rev.*, vol. 59, no. 4, pp. 919–957, Oct. 1979.

[20] W. Delius, K. E. Hagbarth, A. Hongell, and B. G. Wallin, “General characteristics of sympathetic activity in human muscle nerves,” *Acta Physiol. Scand.*, vol. 84, no. 1, pp. 65–81, Jan. 1972.

[21] G. L. Brown and J. S. Gillespie, “The output of sympathetic transmitter from the spleen of the cat,” *J. Physiol.*, vol. 138, no. 1, pp. 81–102, Aug. 1957.

[22] T. Bradley and P. Hjemdahl, “Renal extraction of endogenous and radiolabelled catecholamines in the dog,” *Acta Physiol. Scand.*, vol. 126, no. 4, pp. 505–510, Apr. 1986.

[23] S. Akselrod, D. Gordon, J. B. Madwed, N. C. Snidman, D. C. Shannon, and R. J. Cohen, “Hemodynamic regulation: investigation by spectral analysis,” *Am. J. Physiol.*, vol. 249, no. 4 Pt 2, pp. H867-875, Oct. 1985.

[24] A. Malliani, M. Pagani, F. Lombardi, and S. Cerutti, “Cardiovascular neural regulation explored in the frequency domain,” *Circulation*, vol. 84, no. 2, pp. 482–492, Aug. 1991.

[25] Task Force of the European Society of Cardiology and the North American Society of Pacing and Electrophysiology, “Heart rate variability. Standards of measurement, physiological interpretation, and clinical use,” *Eur. Heart J.*, vol. 17, no. 3, pp. 354–381, Mar. 1996.

[26] D. S. Goldstein, “Clinical assessment of catecholaminergic function,” *Stress Catecholamines Cardiovasc. Dis. N. Y. Oxf. Univ. Press*, pp. 234–286, 1995.

[27] R. E. Kleiger, J. P. Miller, J. T. Bigger Jr, and A. J. Moss, “Decreased heart rate variability and its association with increased mortality after acute myocardial infarction,” *Am. J. Cardiol.*, vol. 59, no. 4, pp. 256–262, 1987.

[28] M. P. Tulppo, T. H. Mäkikallio, T. Seppänen, R. T. Laukkanen, and H. V. Huikuri, “Vagal modulation of heart rate during exercise: effects of age and physical fitness,” *Am. J. Physiol.*, vol. 274, no. 2 Pt 2, pp. H424-429, Feb. 1998.

[29] S. Akselrod, D. Gordon, F. A. Ubel, D. C. Shannon, A. C. Berger, and R. J. Cohen, “Power spectrum analysis of heart rate fluctuation: a quantitative probe of beat-to-beat cardiovascular control,” *Science*, vol. 213, no. 4504, pp. 220–222, Jul. 1981.

[30] B. Pomeranz *et al.*, “Assessment of autonomic function in humans by heart rate spectral analysis,” *Am. J. Physiol.*, vol. 248, no. 1 Pt 2, pp. H151-153, Jan. 1985.

[31] M. L. Appel, R. D. Berger, J. P. Saul, J. M. Smith, and R. J. Cohen, “Beat to beat variability in cardiovascular variables: noise or music?,” *J. Am. Coll. Cardiol.*, vol. 14, no. 5, pp. 1139–1148, Nov. 1989.

[32] R. Bailón, G. Laouini, C. Grao, M. Orini, P. Laguna, and O. Meste, “The integral pulse frequency modulation model with time-varying threshold: application to heart rate variability analysis during exercise stress testing,” *IEEE Trans. Biomed. Eng.*, vol. 58, no. 3, pp. 642–652, Mar. 2011.

[33] R. Bailón, N. Garatachea, I. de la Iglesia, J. A. Casajús, and P. Laguna, “Influence of running stride frequency in heart rate variability analysis during treadmill exercise testing,” *IEEE Trans. Biomed. Eng.*, vol. 60, no. 7, pp. 1796–1805, Jul. 2013.

[34] A. Benítez *et al.*, “Ventilatory threshold prediction by spectral analysis of heart rate variability in incremental maximal tests,” in *Computing in Cardiology, 2010*, 2010, pp. 939–942.

[35] G. Blain, O. Meste, T. Bouchard, and S. Bermon, “Assessment of ventilatory thresholds during graded and maximal exercise test using time varying analysis of respiratory sinus arrhythmia,” *Br. J. Sports Med.*, vol. 39, no. 7, pp. 448-452-452, Jul. 2005.

[36] F. Cottin, C. Médigue, P. Lopes, P.-M. Leprêtre, R. Heubert, and V. Billat, “Ventilatory thresholds assessment from heart rate variability during an incremental exhaustive running test,” *Int. J. Sports Med.*, vol. 28, no. 4, pp. 287–294, Apr. 2007.

[37] M. J. Gaitan-Gonzalez, S. Carrasco-Sosa, R. Gonzalez-Camarena, and O. Yanez-Suarez, “Non-linear relationship between heart period and root mean square of successive differences during ramp exercise and early recovery,” in *Computers in Cardiology, 2005*, 2005, pp. 727–730.

[38] K. Martinmäki, K. Häkkinen, J. Mikkola, and H. Rusko, “Effect of low-dose endurance training on heart rate variability at rest and during an incremental maximal exercise test,” *Eur. J. Appl. Physiol.*, vol. 104, no. 3, pp. 541–548, Oct. 2008.

[39] O. Meste, G. Blain, and S. Bermon, “Analysis of the respiratory and cardiac systems coupling in pyramidal exercise using a time-varying model,” in *Computers in Cardiology, 2002*, 2002, pp. 429–432.

[40] E. F. Sierra-Alonso, L. M. Sepulveda-Cano, R. Bailon-Luesma, P. Laguna, and G. Castellanos-Dominguez, “Estimating respiratory frequency from HRV during treadmill exercise testing,” in *Computing in Cardiology Conference (CinC), 2013*, 2013, pp. 121–124.

[41] B. M. W. Illigens and C. H. Gibbons, “Sweat testing to evaluate autonomic function,” *Clin. Auton. Res.*, vol. 19, no. 2, pp. 79–87, Apr. 2009.

[42] C. Setz, B. Arnrich, J. Schumm, R. La Marca, G. Tröster, and U. Ehlert, “Discriminating stress from cognitive load using a wearable EDA device,” *IEEE Trans. Inf. Technol. Biomed. Publ. IEEE Eng. Med. Biol. Soc.*, vol. 14, no. 2, pp. 410–417, Mar. 2010.

[43] J. . Healey and R. W. Picard, “Detecting stress during real-world driving tasks using physiological sensors,” *IEEE Trans. Intell. Transp. Syst.*, vol. 6, no. 2, pp. 156–166, Jun. 2005.

[44] J. T. Cacioppo, L. G. Tassinary, G. Berntson, and & 0 more, *Handbook of Psychophysiology*, 3 edition. Cambridge England ; New York: Cambridge University Press, 2007.

[45] “Techniques in Psychophysiology. By I. Martin and P. H. Venables. (Pp. 669; illustrated; £19.50.) John Wiley & Sons: Chichester. 1980.,” *Psychol. Med.*, vol. 10, no. 4, pp. 806–806, 1980.

[46] W. Boucsein *et al.*, “Publication recommendations for electrodermal measurements,” *Psychophysiology*, vol. 49, no. 8, pp. 1017–1034, Aug. 2012.

[47] N. S. Greenfield and R. A. Sternbach, *Handbook of psychophysiology*, vol. xii. Oxford, England: Holt, Rinehart & Winston, 1972.

[48] P. H. Ellaway, A. Kuppuswamy, A. Nicotra, and C. J. Mathias, “Sweat production and the sympathetic skin response: Improving the clinical assessment of autonomic function,” *Auton. Neurosci.*, vol. 155, no. 1–2, pp. 109–114, Jun. 2010.

[49] M. Benedek and C. Kaernbach, “A continuous measure of phasic electrodermal activity,” *J. Neurosci. Methods*, vol. 190, no. 1–5, pp. 80–91, Jun. 2010.

[50] S. A. Shields, K. A. MacDowell, S. B. Fairchild, and M. L. Campbell, “Is mediation of sweating cholinergic, adrenergic, or both? A comment on the literature,” *Psychophysiology*, vol. 24, no. 3, pp. 312–319, May 1987.

[51] R. Edelberg, “Electrodermal Mechanisms: A Critique of the Two-Effector Hypothesis and a Proposed Replacement,” in *Progress in Electrodermal Research*, J.-C. Roy, W. Boucsein, D. C. Fowles, and J. H. Gruzelier, Eds. Springer US, 1993, pp. 7–29.

[52] M. J. Christie, “Electrodermal activity in the 1980s: a review.,” *J. R. Soc. Med.*, vol. 74, no. 8, pp. 616–622, Aug. 1981.

[53] B. G. Wallin, “Sympathetic nerve activity underlying electrodermal and cardiovascular reactions in man,” *Psychophysiology*, vol. 18, no. 4, pp. 470–476, Jul. 1981.

[54] H. Sequeira and J.-C. Roy, “Cortical and Hypothalamo-Limbic Control of Electrodermal Responses,” in *Progress in Electrodermal Research*, J.-C. Roy, W. Boucsein, D. C. Fowles, and J. H. Gruzelier, Eds. Springer US, 1993, pp. 93–114.

[55] J.-C. Roy, H. Sequeira, and B. Delerm, “Neural Control of Electrodermal Activity: Spinal and Reticular Mechanisms,” in *Progress in Electrodermal Research*, J.-C. Roy, W. Boucsein, D. C. Fowles, and J. H. Gruzelier, Eds. Springer US, 1993, pp. 73–92.

[56] W. Boucsein, *Electrodermal Activity*. Boston, MA: Springer US, 2012.

[57] R. J. Davidson, “Psychophysiology: The Mind–Body Perspective. By Kenneth Hugdahl. Cambridge: Harvard University Press, 1995, 429 pp.,” *Psychophysiology*, vol. 35, no. 3, pp. 352–353, May 1998.

[58] R. Lowry, “Active circuits for direct lenear measurement of skin resistance and conductance,” *Psychophysiology*, vol. 14, no. 3, pp. 329–331, May 1977.

[59] D. C. Fowles, M. J. Christie, R. Edelberg, W. W. Grings, D. T. Lykken, and P. H. Venables, “Committee report. Publication recommendations for electrodermal measurements,” *Psychophysiology*, vol. 18, no. 3, pp. 232–239, May 1981.

[60] A. Crider and R. Lunn, “Electrodermal lability as a personality dimension,” *J. Exp. Res. Personal.*, vol. 5, no. 2, pp. 145–150, 1971.

[61] J. J. Braithwaite, D. G. Watson, R. Jones, and M. Rowe, “A guide for analysing electrodermal activity (EDA) & skin conductance responses (SCRs) for psychological experiments,” University of Birmingham, UK, Technical, 2013.

Chapter 3: Power Spectral Density Analysis of Electrodermal Activity for Sympathetic Function Assessment

(Posada-Quintero, H. F., Florian, J. P., Orjuela-Cañón, A. D., Aljama-Corrales, T., Charleston-Villalobos, S., & Chon, K. H. (2016). Power Spectral Density Analysis of Electrodermal Activity for Sympathetic Function Assessment. Annals of Biomedical Engineering, 44(10))

3.1 Introduction

In this study we are more interested in the post-transient SCRs (the NS.SCRs) due to posture, cold pressor or Stroop test, which occur after the ER-SCR (Event-related SCR). A key concern for the SCL and NS.SCRs is that these indices are highly variable between subjects [15]. This is due to the frequent occurrence of a second response before the completion of a given SCR, which can be detected by visual inspection, but its detection is not easy to automate [10]. In addition, periodic shifts in the background SCL (like a DC shift) could be important if they appear to occur in conjunction with specific components of the experiment, and only a visual analysis would reveal the difference between a SCR and unimportant drift factors (artifacts) [16]. Furthermore, obtaining NS.SCRs requires an observer to count SCRs but this could be problematic if there are motion artifacts during EDA measurements. These circumstances necessitate a trained observer to compute NS.SCRs, thereby limiting the full potential of the usefulness of EDA. Moreover, it has not yet been established whether or not dynamics of the sympathetic tone measured from EDA can be used as a surrogate for HRV's derived LF response. This would require EDA analysis similar to HRV analysis using the PSD. The response to stress of the spectral components of EDA signals has rarely been examined. To the best of our knowledge, only one study has explored the matter. This study found elevation of power within the 0.03 to 0.5 Hz band in response to increased mental workload [17].

Thus, the aim of this work is to examine if a similar association of LF components of HRV to sympathetic function also exists with the sudomotor function as measured by EDA. Specifically, we are

interested in examining if EDA analysis yields similar frequency dynamics at the HRV's prescribed LF range of 0.045-0.15 Hz. If such relation occurs, we can overcome the main disadvantage of LF domain analysis of HRV because EDA is not influenced by the parasympathetic branch of the autonomic nervous system, and we could provide a better quantitative evaluation of sympathetic tone. To test our aim, we determined the EDA differences between baseline conditions and three maneuvers to elicit sympathetic activation: postural stimulation, cold pressor test, and Stroop test. These tests were selected because they are among the stimuli that most efficiently release sympathetic neurotransmitters [18], and they cover three relevant types of stressors (i.e. orthostatic, physical and cognitive).

3.1 Materials and Methods

3.1.1 Protocol

Twelve healthy volunteers (10 males, 2 female) of ages ranging from 19 to 36 years old (26.2 ± 6.14; mean ± SD), weight 64.63 ± 7.01 kg, and height 171.45 ± 9.64 cm, were enrolled in this study. No gender-related differences have been reported for EDA or sympathetic function. To induce a wide variety of sympathetic arousal types, subjects underwent three tests: postural stimulation (orthostatic stress), cold pressor (physical stress) and Stroop task (cognitive stress).

Before any test, subjects were asked to stay in the supine position for at least 5 minutes to ensure hemodynamic stabilization, before the start of data recording. Postural stimulation tests consisted of 5 minutes in the supine position (baseline) followed by 5 minutes standing. Similarly, the cold-pressor test included 5 minutes of baseline with the subjects supine; then the subjects were asked to immerse their left hand to the wrist level into a 0-1 °C water bath for a period of 3 minutes. For Stroop tests, 5 minutes of baseline were also recorded with subjects relaxing in the supine position. Then, subjects were asked to speak a word which named a color. They were shown a congruent visualization (the word was written in the color it expressed) and an incongruent visualization (the word and the color it was printed in were different) to induce cognitive stress [19]. The words and colors were "blue," "yellow," "green," "red," "purple," and "black." The background also changed to be randomly congruently or incongruently colored

with the word. A computerized version of the original Stroop task was developed in our lab using customized software. The Stroop task was 5 minutes total, and the first minute was used for training.

Participants were asked to avoid caffeine and alcohol for 24 hours preceding the test, and instructed to fast for at least 3 hours before testing. The experiments were carried out in a quiet, dimly lit room (ambient temperature 26-27 °C), in order to avoid other stimuli. The study protocol was approved by the Institutional Review Board of The University of Connecticut and all volunteers consented to be subjects for the experiment. ECG and EDA signals were simultaneously recorded throughout all tests. An HP 78354A (Hewlett-Packard, FDA approved) and a GSR amplifier FE116 (fully isolated AC excitation and automatic zeroing low voltage amplifier, 22 mVrms @75 Hz, ADINSTRUMENTS) were used to collect ECG and EDA, respectively. No on-line filtering was applied during the signal recording. ECG electrodes were placed following the recommendation to acquire Lead I, and EDA electrodes were placed on the index and middle fingers for all subjects. Skin was prepared with alcohol before placing the electrodes. Signals were digitized using a PowerLab system at 400 Hz, 12 bits resolution.

3.1.2 Signal processing

Figure 3.1 shows heart rate and EDA signals for two minutes of baseline and the corresponding three tests (postural, cold pressor and Stroop) for a given subject. Negative values in EDA signals refer to a reduction of the skin conductance with respect to the level at the beginning of the test, when the calibration was performed (zeroing of the signal). Note that HR and EDA differences between the baseline and each of the test cases are pronounced. Figure 3.2 delineates the signal processing procedures used to compute the set of HRV and EDA indices used in this study. The HRVLF power (and normalized power, HRVLFn), SCL, NS.SCRs, and the PSD of high-pass filtered data of EDA were computed in order to quantify the elicited changes of the sympathetic nervous system due to postural stimulation and the cold pressor and Stroop tests.

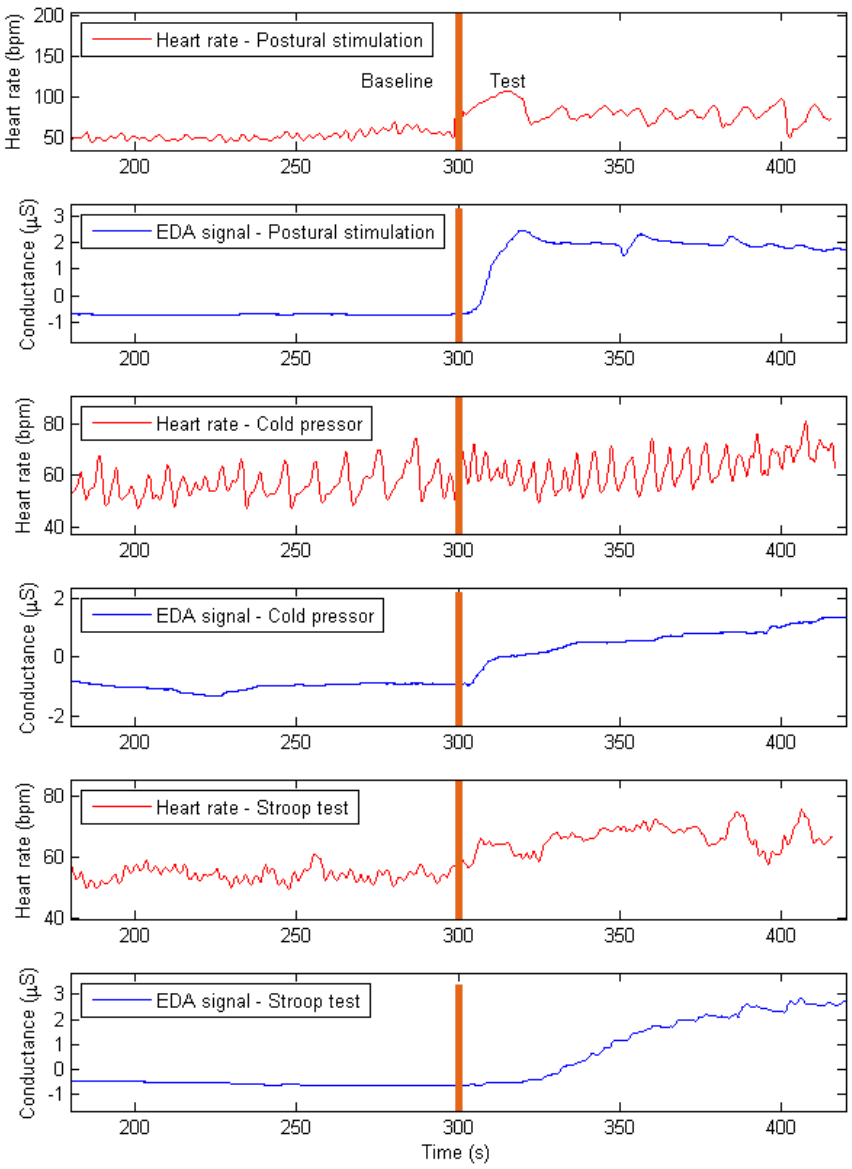

Figure 3.1 – ECG and EDA signals for a given subject, undergoing postural stimulation (top), cold pressor test (middle) and Stroop test (bottom).

3.1.2.1 Heart rate variability indices

For HRV analysis, ECG signals were band-pass filtered (0.05-40 Hz) to reduce noise and motion artifacts. The R-waveform peaks were detected using the detection algorithm that defines a delineation function based on the envelope of the ECG signal [20], [21]. All the segments were visually inspected to

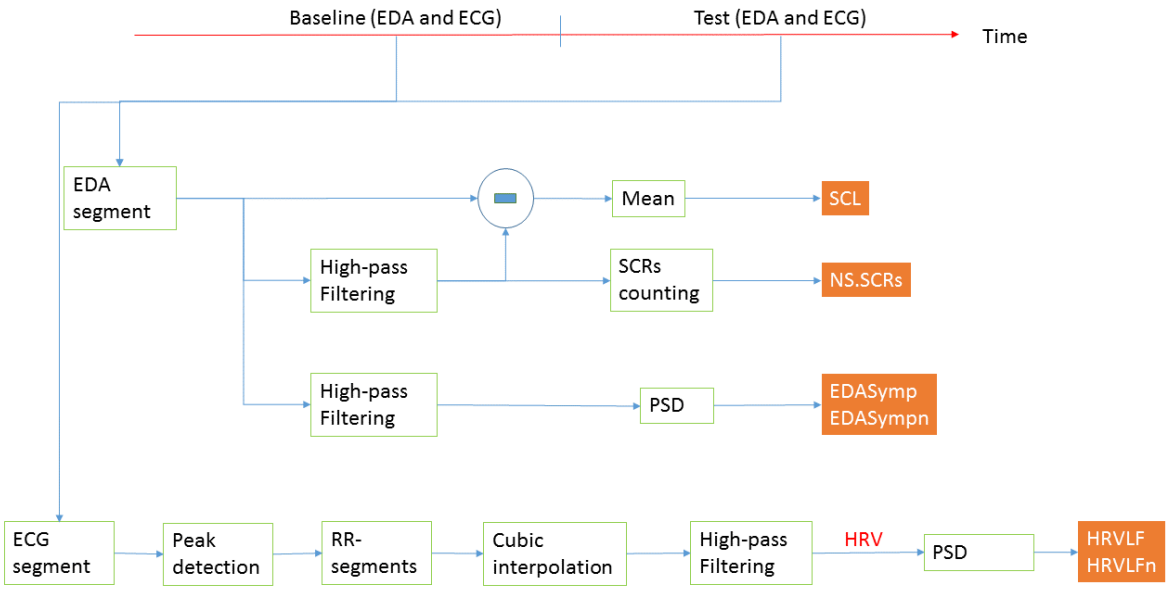

Figure 3.2 – Signal processing procedures to compute HRV and EDA indices.

ensure that no beat was missed. After accounting for the missed R-wave beats, the HR time series were computed. The power spectra of HRV were then calculated using Welch's periodogram method with 50% data overlap. The RR interval series were converted to an evenly time-sampled signal (4 Hz) by cubic spline interpolation. A Blackman window (length of 256 points) was applied to each segment and the Fast Fourier Transform was calculated for each windowed segment. Finally, the power spectra of the segments were averaged. The low-frequency index (HRVLF [ms2], 0.045 to 0.15 Hz) [9] and normalized LF (HRVLFn = (HRVLF)/Total power, normalized units [n.u.]) were computed. Four minutes of clean ECG signals were used to compute HRV for postural stimulation and the Stroop test, and three minutes for the cold pressor test as most subjects could not withstand the cold temperature for four minutes. For each test, the same data length was used consistently for baseline and test segments.

3.1.2.2 Time-domain indices of Electrodermal Activity

Two minutes of baseline EDA and two minutes of test EDA were selected for each test. Figure 3.3 illustrates the process of computing SCL and NS.SCRs. Baseline signals were always the two minutes

prior to the subject performing a test. For the postural stimulation test, the two-minute EDA test signal was extracted starting from 30 seconds after the subject stood up, to avoid the motion artifacts during the movement process. For the cold pressor test, the first minute was avoided because the maximal discomfort occurs during this time. The subsequent two minutes were used as the test EDA signals. For the Stroop test, the two-minute segments were extracted after discarding the first minute of data after the training period.

To extract the tonic component of the EDA signals (SCL), a 10th-order low-pass finite impulse response filter with a cut-off frequency of 0.0004 Hz was applied. The remaining signal (raw signal minus tonic component) was used to compute the NS.SCRs. The SCL index was computed using the mean of the tonic EDA over the two-minute period. NS.SCRs were obtained manually for each minute and then averaged over the two-minute period. It is important to note that for defining a non-negligible occurrence of NS.SCRs, a minimum change in conductance needs to be considered. A recommended threshold value of 0.05 μS was used [10]. In addition, when a second response occurred before completion of the prior response, the two responses were counted as two positive NS.SCRs even though they overlapped.

3.1.2.3 Power spectral density analysis of Electrodermal Activity

For frequency-domain analysis, EDA signals were down–sampled to 2 Hz. Before down-sampling, the data was filtered with an 8th-order Chebyshev Type I low-pass filter (0.8 Hz). Down-sampling from 400 Hz to 2 Hz was performed in two steps (using consecutive down-sampling factors of 1/20 and 1/10, respectively). Finally, signals were high-pass filtered (0.01 Hz, Butterworth, 8th order) to remove any trend. The power spectra of EDA signals were calculated using Welch's periodogram method with 50% data overlap. A Blackman window (length of 128 points) was applied to each segment, the Fast Fourier Transform was calculated for each windowed segment, and the power spectra of the segments were averaged. Note that the down-sampling frequency for EDA was half of the sampling frequency for HRV. This down-sampling frequency (2 Hz) is sufficient given that the dynamics of the EDA spectrum are largely confined to frequencies less than 0.4 Hz as observed in this work and as reported [17]. Total power [μS2]

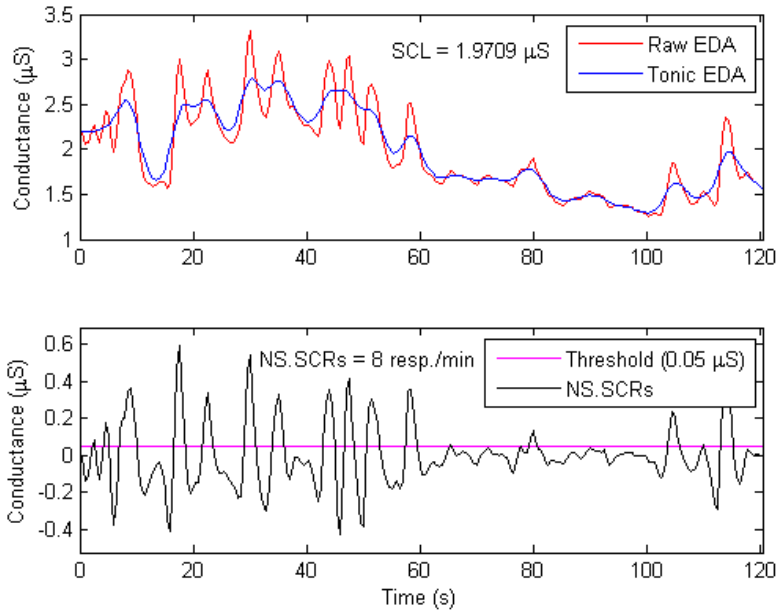

Figure 3.3 – Exemplification of acquired measures of tonic EDA (SCL and NS.SCRs).

and the power within the frequency bands of interest (VLF = 0 to 0.045 Hz, LF = 0.045 to 0.15 Hz, HF1 = 0.15 to 0.25 Hz, HF2 = 0.25 to 0.4 Hz and VHF = 0.4 to 0.5 Hz) were computed. After determining the frequency range for sympathetic assessment, EDASymp and EDASympn [n.u.] = EDASymp/(Total power) were computed.

3.1.3 Statistics

The full set of indices is HRVLF, HRVLFn, SCL, NS.SCRs, EDA-Total power, EDASymp and EDASympn. First, the paired t-test was applied to test the null hypothesis that elicited responses as measured by each of the above-defined indices are equal to the baseline values. These results are useful to evaluate the suitability of the indices to quantitatively assess the sympathetic function on healthy subjects, for the types of stress induced in the present study.

Time- and frequency-domain indices of EDA (SCL, NS.SCRs and EDASympn) were further compared using a detection theory for which summary statistics are provided, including the maximum Youden's index (J = Sensitivity + Specificity – 1, a measure of the performance of the detector), the area

Table 3.1 Percentage of energy within the frequency bands for EDA and HRV

		Postural Stimulation		Cold Pressor		Stroop Test	
		Baseline	**Test**	**Baseline**	**Test**	**Baseline**	**Test**
EDA	**VLF (0 to 0.045 Hz)**	86.2 %	65 %	79.2 %	51.2 %	87.3 %	51.6 %
	LF (0.045 to 0.15 Hz)	11.6 %	28.5 %	14.6 %	31.7 %	8.07 %	32.9 %
	HF1 (0.15 to 0.25 Hz)	1.24 %	4.67 %	3.7 %	10.9 %	2.07 %	10.7 %
	HF2 (0.25 to 0.4 Hz)	0.36 %	1.3 %	1.35 %	4.44 %	1.44 %	3.77 %
	VHF (0.4 to 0.5 Hz)	0.19 %	0.25 %	0.86 %	1.72 %	0.7 %	0.96 %
HRV	**VLF (0 to 0.045 Hz)**	36.8 %	36 %	29.2 %	34.8 %	27.8 %	29.6 %
	LF (0.045 to 0.15 Hz)	23.5 %	51.4 %	32.1 %	27 %	36.6 %	39.2 %
	HF (0.15 to 0.4 Hz)	36.5 %	10.9 %	35.6 %	34.4 %	32.8 %	25.9 %
	VHF (0.4 to 1 Hz)	2.17 %	0.93 %	2.53 %	2.91 %	2.33 %	4.63 %

Values represent percentage of power considering all the subjects together.

under the ROC curve (AUC, the probability that the index will assign to a positive instance a higher value than to a negative one), and the maximum accuracy of the given index used as detector. This analysis allows us to test the ability of these indices to correctly identify the presence of the stressors.

In order to assess inter-subject variability and degree of consistency of each index, the coefficient of variation (CV) (i.e. the standard deviation between all the measurements divided by the mean) and the intra-class correlation (ICC) were computed for the SCL, NS.SCRs and EDASympn indices, respectively. ICC has been computed as defined in the literature [22], for the N=12 independent subjects, using the 6 available measures (3 tests, baseline and test measure).

3.2 Results

Figure 3.4 shows the NS.SCRs throughout the experiment (during postural stimulation, cold pressor and Stroop tests), for a given subject. Note that during baseline periods, there were no positive NS.SCRs for this subject, for any test. Some subjects exhibited a few NS.SCRs in the supine position but this was a rare occurrence. All subjects consistently produced more NS.SCRs when performing the tests than during the baseline for all three tests.

The power spectra of the HRV series and the EDA signal for a given subject are included in Figure 3.5 and Figure 3.6. Note that for both, this subject exhibits marked differences between baselines and

each of the three induced tests. As expected, HRV power spectra show frequency components above 0.15 Hz. These components are known to be related to parasympathetic function. For EDA spectra, spectral power beyond 0.25 Hz is minimal at best for all three induced stimuli.

HRV is heart rate variability, EDA is electrodermal activity, VLF is power of very low-frequency components, LF is power of low-frequency components, HF is power of high-frequency components, and VHF is power of very high-frequency components.

To quantitatively assess the dynamic frequency ranges of the EDA, we computed the percentage of energy within the five frequency bands as shown in Table 1. For HRV, the HF was computed from the standard frequency band of 0.15 to 0.4 Hz. As shown in Table 1, the VLF power is consistently high for EDA for all three baseline and test stimuli conditions. The largest increase in EDA spectral power was found in the LF, post-stimuli, for all three test conditions. With stimuli, the EDA's HF1 (0.15-0.25 Hz) and HF2 (0.25-0.4 Hz) contain 5-10% and 1-4%, respectively, of the total spectral power, and the VHF of

Table 3.2 Sympathetic function indices.

	Postural Stimulation		**Cold Pressor**		**Stroop task**	
	Baseline	**Test**	**Baseline**	**Test**	**Baseline**	**Test**
HRV indices						
HRVLF (ms^2)	4.8 ± 5.98	27.67 ± 31.45*	7.14 ± 6.396	4.77 ± 3.27	4.18 ± 3.36	6.11 ± 4.44*
HRVLFn (n.u.)	0.24 ± 0.06	0.54 ± 0.17*	0.33 ± 0.13	0.27 ± 0.14	0.35 ± 0.13	0.39 ± 0.08
Time-domain indices of EDA						
SCL (μS)	4.14 ± 8.11	10.79 ± 7.47*	0.77 ± 4.68	4.47 ± 7.50*	-1.28 ± 3.92	6.31 ± 4.01*
NS.SCRs (#/min)	1.83 ± 2.03	6.00 ± 2.86*	2.67 ± 2.9	4.958 ± 4.53*	0.96 ± 1.5	9.75 ± 3.89*
Frequency-domain indices of EDA						
Total EDA (μS^2)	1.71 ± 4.49	0.50 ± 0.46	0.11 ± 0.19	0.24 ± 0.42	0.019 ± 0.036	0.46 ± 0.45*
EDASymp (μS^2)	0.82 ± 2.48	0.28 ± 0.31	0.028 ± 0.056	0.15 ± 0.28	0.008 ± 0.016	0.198 ± 0.25*
$EDASymp_n$ (n.u.)	0.29 ± 0.17	0.47 ± 0.22*	0.23 ± 0.158	0.42 ± 0.20*	0.28 ± 0.20	0.48 ± 0.18*

Values are expressed as mean ± standard deviation.
*Statistically significantly higher with respect to baseline ($p<0.05$)
HRV is heart rate variability, LF is power of low-frequency components, LFn is normalized power of low-frequency components, SCL is skin conductance level, NS.SCRs ares non-specific skin conductance responses, EDASymp and EDASympn indicate non-normalized and normalized power spectra, respectively, in the frequency band between 0.045 and 0.25 Hz.

EDA contains less than at most 2% of the total spectral power. Given that HF1 comprises 5-10% of the power associated with the sympathetic dynamics, and as 95% of the total spectral power of EDA is accounted for by including VLF, LF and HF1, the frequency range relevant to the sympathetic component of the EDA (EDASymp) can be defined to be in the range of 0.045-0.25 Hz. This excludes VLF because, as shown in Table 1, its power decreases with stress induction. Henceforth, "EDASymp" refers to spectral dynamics in the frequency range of 0.045 to 0.25 Hz.

HRV is heart rate variability, LF is power of low-frequency components, LFn is normalized power of low-frequency components, SCL is skin conductance level, NS.SCRs ares non-specific skin conductance responses, EDASymp and EDASympn indicate non-normalized and normalized power spectra, respectively, in the frequency band between 0.045 and 0.25 Hz.

Table 2 incorporates the mean time- and frequency-domain results for all subjects. The postural stimulation test (orthostatic stress) produced significant increases in HRVLF, HRVLFn, SCL, NS.SCRs and EDASympn indices. Total EDA and EDASymp were not found to be statistically different under this test. The cold pressor test (physical stress) elicited differences in the SCL, NS.SCRs and EDASympn.

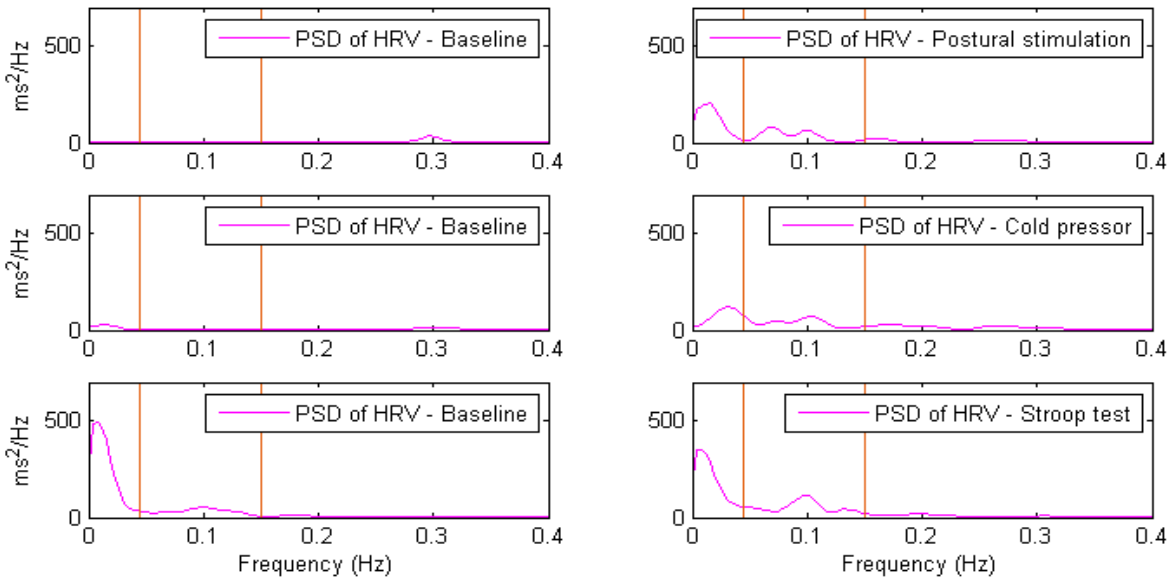

Figure 3.5 – Power spectra of HRV for a given subject during baseline (left) and test (right), for postural stimulation, cold pressor and Stroop test. Lines denote 0.045 and 0.15 Hz.

Table 3.3 Statistics of EDA indices

	Postural Stimulation			Cold Pressor			Stroop task				
	J	**AUC**	**Acc**	**J**	**AUC**	**Acc**	**J**	**AUC**	**Acc**	**Average CV**	**ICC (LB UB)**
SCL	0.58	0.69	0.79	0.50	0.66	0.75	0.83	0.85	0.92	1.32	0.88 (0.68 0.98)
NS.SCRs	0.83	0.87	0.92	0.33	0.61	0.67	0.92	0.92	0.96	0.93	0.93 (0.79 0.99)
EDASymp$_n$	0.5	0.6	0.75	0.7	0.78	0.85	0.5	0.71	0.75	0.55	0.82 (0.48 0.97)

EDA is electrodermal activity, SCL is skin conductance level, NS.SCRs are the non-specific skin conductance responses, EDASympn indicates the normalized spectral power in the frequency band between 0.045 to 0.25 Hz, J is Youden's index, AUC is Area under the ROC curve, Acc is accuracy; CV is coefficient of variation, ICC is Intra-class correlation, and LB and UB are upper and lower bounds of the ICC with a level of significance of 0.05.

Note that these three indices were found to be statistically different than under postural stimulation. However, HRV indices were not significantly different during this test. Total EDA and EDASymp were not found to be statistically different either. The stroop task test (cognitive stress) induced differences in HRVLF, SCL, NS.SCRs, total EDA, EDASymp and EDASympn. In other words, while low-frequency components of HRV (HRVLF) were sensitive to orthostatic and cognitive stress, normalized HRVLF (HRVLFn) was different only under orthostatic stress. The SCL and NS.SCRs always exhibited statistically-significant differences under any kind of stress tested in this study. EDASymp and total power of EDA were significantly increased by only cognitive stress, and normalized low-frequency components of EDA were sensitive to all three types of stress. This suggests that the normalized low-frequency components of EDA and the time domain SCL and NS.SCRs are the most sensitive markers for differentiating changes induced by stressors.

We used a detection theory and receiver operating characteristic (ROC) curves to test the ability of the different indices to correctly identify the presence of the stressors (orthostatic, physical or cognitive) when compared to their baseline conditions. Table 3 shows the maximum Youden's index, the area under the ROC curve, and the highest possible accuracy for each index used as a detector. EDASympn had better results than SCL and NS.SCRs for these three measures for the cold pressor test. However, for both orthostatic and Stroop stimuli, the NS.SCRs provided the best results for the Youden's index, AUC, and the accuracy values.

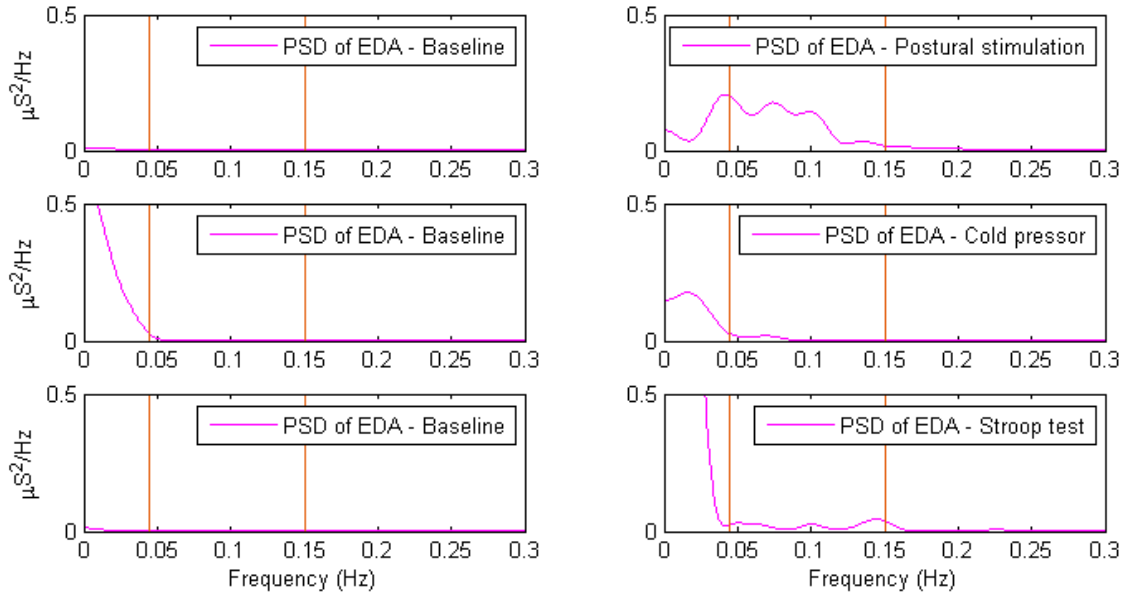

Figure 3.6 – Power spectra of EDA for a given subject during baseline (left) and test (right), for postural stimulation, cold pressor and Stroop test. Lines denote 0.045 and 0.15 Hz.

The high variability of EDA measurements has been a concern among researchers, impeding the widespread use of these indices for assessing the general state of activation of the sympathetic system. Table 3 shows the coefficient of variation (CV) and intra-class correlation (ICC) for SCL, NS.SCRs and EDASympn. The total average of CV for the given index is also shown. Although the NS.SCRs showed lower variability than did SCL, both SCL and NS.SCRs exhibited higher variability compared to EDASympn for all stimuli. Finally, ICC was higher for the SCL and NS.SCRs, which suggests that these indices are more consistent than EDASympn.

3.3 Discussion

The main goal of this work was to determine the dynamic frequency response characteristics of EDA through the use of power spectral density. Specifically, the intent was to systematically determine the frequency band limits of the sympathetic nervous activities derived from the EDA signal. Moreover, we were interested in examining the hypothesis that if EDA does represent the dynamics of the cardiac and peripheral sympathetic nervous systems, the spectral power should be largely present in the low frequency band (0.04-0.15 Hz). Indeed, this was the case, as we found that most of the significant increase in the

spectral power is confined in the low frequency band for all three test stimuli and this observation is in agreement with the LF band derived from HRV which contains the dynamics of the cardiac sympathetic nervous system. To account for the additional 5-10% of spectral power largely seen in the HF band with induction of stimuli, we determined that the frequency response of the sympathetic activities represented in the EDA signal can be defined to be within 0.045-0.25 Hz (EDASymp).

EDA data analysis in either the time or frequency domain consistently provided significantly elevated responses for all test stimuli in this study. However, for HRV, the cold pressor stimulus did not provide significant changes whereas the other two stimuli (posture and Stroop tests) did. The increase of the sympathetic tone with postural stimulation is a consistent finding when compared to previous studies [7], [23], [24]. However, the reliability of low-frequency components of HRV for sympathetic assessment is a sustained scientific concern. For example, in the supine position, it has been shown that HRVLF and HRVLFn exhibit poor relative reliability (i.e. high inter-subject variability), and all HRV indices have poor absolute reliability (i.e. high intra-subject variability) [25], [26]. Another study reported poor reproducibility of HRV measured after an orthostatic challenge in healthy subjects, also suggesting an even poorer reproducibility in a clinical population [27]. EDA has been used to provide a quantitative functional measure of sudomotor activity [28], [29], which is controlled by the sympathetic nervous system [30]–[32]. More recently, EDA has been used as a surrogate measure of the sympathetic activities [11]. However, due to the high variability of the time-domain measures of EDA, which largely consist of the SCL and NS.SCRs, its use has not yet been popularized. Surprisingly, the PSD of EDA, similar to the PSD of HRV, is not yet a widely-adopted measure. With EDASympn, we found evidence that postural stimulation invokes the central and cardiac sympathetic nervous dynamics [11]. The added benefit of analyzing EDA in the frequency domain is that it can lead to less variability in the features estimated due to the inherent filtering properties of the frequency domain. More importantly, the EDA represents only the sympathetic nervous activities whereas the LF of the HRV exhibits both the parasympathetic in addition to the sympathetic tone. The other main objective of this work was to determine if non-cardiac related sympathetic-inducing

stressors such as the cold pressor test could also be assessed via EDA analysis, and if their frequency responses are also in the prescribed LF range.

Scant results have been reported about the influence of postural changes on EDA, because EDA measurement has been mainly used in psychophysiological research [10]. However, the SCL and NS.SCRs have shown good correlation with sympathetic arousal [33]–[35]. Note that the SCL and NS.SCRs can also be interpreted as the response of EDA in two different frequency bands, as the SCL comprises the slow changes (low frequency) and NS.SCRs represent rapid shifts (higher frequencies). We also tested the variability of EDA, from which we concluded that frequency-domain components are more reproducible than time-domain measures (number of SCRs and changes in SCL). In this study we found significant differences in SCL and NS.SCRs after postural stimulation when compared to the baseline. We found that the main drawbacks of these indices are their high variability (in the case of SCL) and the need for manual computing (to count NS.SCRs) (Tables 2 and 3). It is worth mentioning that there are many studies that have examined automatic ways to count spontaneous SCRs, extract amplitude or other measures of a single causal SCR, and deal with motion artifacts and superposition on the SCRs [29], [36]–[38]. There are also publically-available toolboxes for these tasks (pspm.sourceforge.net and www.ledalab.de). While these time-domain methods are reliable, the proposed EDASympn does not rely on either manual or automatic SCR detection, which is usually more complex and time consuming. Using PSD analysis on EDA signals, we were able to determine that EDASympn was significantly increased in healthy subjects, when they changed their posture from supine to standing. EDASympn exhibited lower variability, and can easily be implemented in an automated fashion for sympathetic function assessment under orthostatic stress.

The cold pressor stimulus has been increasingly used in clinical practice to evaluate autonomic function in cardiovascular regulation, because stressful cooling evokes an increase in sympathetic neurotransmissions [18]. The responses of HRV dynamics and EDA to cold stress are also poorly understood. In this study, no significant differences were found in HRVLF and HRVLFn between cold pressor and baseline. The reported results on HRVLF and HRVLFn in response to cold pressor are

not congruent. Although some studies reported increases [39], [40], decreases or insignificant changes are reported more often [41]–[44]. In this study we found non-significant decreases in HRVLF and HRVLFn.

Previous studies have tested EDA dynamics in response to the cold pressor test [45], [46]. Those works found increases in SCL and NS.SCRs in healthy subjects when cold stressor was applied. Consistently with those reports, we found significant differences in NS.SCRs and SCL indices when comparing cold pressor to baseline. Nonetheless, these indices showed higher variability on this test when compared to postural stimulation. Using PSD analysis of EDA signals, we found significant increases in EDASympn between cold pressor and baseline, with much less variability when compared to NS.SCRs and SCL.

Significant increases in the low-frequency components of HRV during Stroop tests have been previously reported [47]–[49]. We also found significant differences in HRVLF between Stroop tasks and baseline, but not in HRVLFn. The SCL and NS.SCRs indices were significantly higher during the Stroop test when compared to baseline. Besides the sensitivity of these indices, their variability was also high for this test. In frequency-domain analysis, not only the normalized index (EDASympn) was significantly increased, but the integral of sympathetic components (EDASymp) also exhibited a significant increase. The effect of the Stroop test on the power spectrum of EDA was a combined increase in the LF + HF1 (EDASymp) and VLF range, which influence the total power (Table 2).

While the number of subjects enrolled for this study was relatively low, significant differences between baseline and stimuli-induced conditions enabled the opportunity to examine if time- and frequency-domain indices can discriminate between the absence and presence of the specific stressor. We were also interested in further investigating the ability of SCL, NS.SCRs and EDASympn indices to discriminate whether the stressors (orthostatic, physical or cognitive) were present when the data were collected. To compare the indices' performance on these task stimuli, the Youden's index (J), the area under the ROC curve (AUC) and the maximum accuracy of the detector (Acc) were computed (Table 3). The EDASympn exhibited the best performance in detecting the induced cold pressor stimuli as measured by the Youden's index. However, both SCL and NS.SCRs performed better than EDASympn for

orthostatic and cognitive stress. It should be noted, however, that the EDASympn provided the lowest coefficient of variation values for all three stimuli conditions.

Even though SCL and NS.SCRs have been shown in the literature to be elevated by administration of dextroamphetamine, caffeine, and threatening instructions [33]–[35] (consistent with sympathetic arousal), they are only moderately positively correlated with each other and have relatively low within-subject variability (correlation of test-retest ranges from 0.50 to 0.70) and high variability between subjects [15]. We also found evidence of such high variability in this study, as SCL exhibited a coefficient of variability more than four times larger than the EDASympn index. The NS.SCRs also had a higher coefficient of variability. As for the consistency of the indices, although the SCL and NS.SCRs demonstrated a higher degree of consistency (ICC) than EDASympn (Table 3), all three indices presented a consistency beyond chance (> 0.75) [50].

Because of the high sensitivity to three different types of stimuli and relatively low variability, EDASympn can be recognized as a suitable index of sympathetic function during such stressors in healthy individuals. While there are many and varied approaches to directly measure the sympathetic response, due to high cost, or the invasiveness of the technique, or the inability to provide continuous monitoring, or the inaccurate assessment of the sympathetic dynamics, the widespread use of these techniques in practice is not practical.

3.4 Conclusion

In summary, the EDASympn index is a suitable discriminator of orthostatic, physical and cognitive stress, and has the potential to be used as a reliable marker of quantitative assessment of the sympathetic function. It was found to be more reliable and sensitive than the LF index of HRV, was consistent between the subjects, and exhibited a lower variability compared to the time-domain measures of EDA. Finally, the frequency bands of the sympathetic nervous activities can be defined to be within 0.045-0.25 Hz based on spectral analysis of EDA.

3.5 References

[1] K. H. Chon, B. Yang, H. F. Posada-Quintero, K. L. Siu, M. Rolle, P. Brink, A. Birzgalis, and L. C. Moore, “A novel quantitative method for diabetic cardiac autonomic neuropathy assessment in type 1 diabetic mice,” *J. Diabetes Sci. Technol.*, vol. 8, no. 6, pp. 1157–1167, Nov. 2014.

[2] G. Grassi and M. Esler, “How to assess sympathetic activity in humans,” *J. Hypertens.*, vol. 17, no. 6, pp. 719–734, Jun. 1999.

[3] Y. Bai, R. T. Mahon, J. C. White, P. R. Brink, and K. H. Chon, “Impairment of the autonomic nervous function during decompression sickness in swine,” *J. Appl. Physiol. Bethesda Md 1985*, vol. 106, no. 3, pp. 1004–1009, Mar. 2009.

[4] Y. Bai, N. Selvaraj, K. Petersen, R. Mahon, W. A. Cronin, J. White, P. R. Brink, and K. H. Chon, “The autonomic effects of cardiopulmonary decompression sickness in swine using principal dynamic mode analysis,” *Am. J. Physiol. - Regul. Integr. Comp. Physiol.*, vol. 305, no. 7, pp. R748–R758, Oct. 2013.

[5] M. Esler, G. Jennings, P. Korner, I. Willett, F. Dudley, G. Hasking, W. Anderson, and G. Lambert, “Assessment of human sympathetic nervous system activity from measurements of norepinephrine turnover,” *Hypertension*, vol. 11, no. 1, pp. 3–20, Jan. 1988.

[6] J. L. Rouleau, L. A. Moyé, J. de Champlain, M. Klein, D. Bichet, M. Packer, G. Dagenais, B. Sussex, J. M. Arnold, and F. Sestier, “Activation of neurohumoral systems following acute myocardial infarction,” *Am. J. Cardiol.*, vol. 68, no. 14, p. 80D–86D, Nov. 1991.

[7] D. J. Ewing and B. F. Clarke, “Diagnosis and management of diabetic autonomic neuropathy.,” *Br. Med. J. Clin. Res. Ed*, vol. 285, no. 6346, pp. 916–918, Oct. 1982.

[8] C. J. Mathias and R. Bannister, “Investigation of autonomic disorders,” in *Autonomic failure: a textbook of clinical disorders of the autonomic nervous system*, C. J. Mathias and R. Bannister, Eds. Oxford: Oxford University Press, 1999, pp. 169–195.

[9] Task Force of the European Society of Cardiology and the North American Society of Pacing and Electrophysiology, “Heart rate variability. Standards of measurement, physiological interpretation, and clinical use,” *Eur. Heart J.*, vol. 17, no. 3, pp. 354–381, Mar. 1996.

[10] W. Boucsein, D. C. Fowles, S. Grimnes, G. Ben-Shakhar, W. T. roth, M. E. Dawson, D. L. Filion, and Society for Psychophysiological Research Ad Hoc Committee on Electrodermal Measures, “Publication recommendations for electrodermal measurements,” *Psychophysiology*, vol. 49, no. 8, pp. 1017–1034, Aug. 2012.

[11] R. Freeman and M. W. Chapleau, “Testing the autonomic nervous system,” *Handb. Clin. Neurol.*, vol. 115, pp. 115–136, 2013.

[12] A. P. Colbert, K. Spaulding, A. Larsen, A. C. Ahn, and J. A. Cutro, “Electrodermal activity at acupoints: literature review and recommendations for reporting clinical trials,” *J. Acupunct. Meridian Stud.*, vol. 4, no. 1, pp. 5–13, Mar. 2011.

[13] H. D. Critchley, “Electrodermal responses: what happens in the brain,” *Neurosci. Rev. J. Bringing Neurobiol. Neurol. Psychiatry*, vol. 8, no. 2, pp. 132–142, Apr. 2002.

[14] R. Edelberg, “Electrical activity of the skin: Its measurement and uses in psychophysiology,” *Handb. Psychophysiol.*, vol. 12, p. 1011, 1972.

[15] A. Crider and R. Lunn, “Electrodermal lability as a personality dimension,” *J. Exp. Res. Personal.*, vol. 5, no. 2, pp. 145–150, 1971.

[16] J. J. Braithwaite, D. G. Watson, R. Jones, and M. Rowe, “A guide for analysing electrodermal activity (EDA) & skin conductance responses (SCRs) for psychological experiments,” University of Birmingham, UK, Technical, 2013.

[17] Y. Shimomura, T. Yoda, K. Sugiura, A. Horiguchi, K. Iwanaga, and T. Katsuura, “Use of frequency domain analysis of skin conductance for evaluation of mental workload,” *J. Physiol. Anthropol.*, vol. 27, no. 4, pp. 173–177, Jun. 2008.

[18] D. Robertson, G. A. Johnson, R. M. Robertson, A. S. Nies, D. G. Shand, and J. A. Oates, “Comparative assessment of stimuli that release neuronal and adrenomedullary catecholamines in man.,” *Circulation*, vol. 59, no. 4, pp. 637–643, Apr. 1979.

[19] R. J. Stroop, “Studies of interference in serial verbal reactions,” *J. Exp. Psychol.*, vol. 18, no. 6, pp. 643–662, 1935.

[20] M. E. Nygårds and L. Sörnmo, “Delineation of the QRS complex using the envelope of the e.c.g,” *Med. Biol. Eng. Comput.*, vol. 21, no. 5, pp. 538–547, Sep. 1983.

[21] C. Vidaurre, T. H. Sander, and A. Schlögl, “BioSig: the free and open source software library for biomedical signal processing,” *Comput. Intell. Neurosci.*, vol. 2011, p. 935364, 2011.

[22] K. O. McGraw and S. P. Wong, “Forming inferences about some intraclass correlation coefficients.,” *Psychol. Methods*, vol. 1, no. 1, p. 30, 1996.

[23] J. W. Williamson, R. McColl, and D. Mathews, “Evidence for central command activation of the human insular cortex during exercise,” *J. Appl. Physiol. Bethesda Md 1985*, vol. 94, no. 5, pp. 1726–1734, May 2003.

[24] W. Wieling, J. F. van Brederode, L. G. de Rijk, C. Borst, and A. J. Dunning, “Reflex control of heart rate in normal subjects in relation to age: a data base for cardiac vagal neuropathy,” *Diabetologia*, vol. 22, no. 3, pp. 163–166, Mar. 1982.

[25] J. W. Sacre, C. L. Jellis, T. H. Marwick, and J. S. Coombes, “Reliability of heart rate variability in patients with type 2 diabetes mellitus,” *Diabet. Med. J. Br. Diabet. Assoc.*, vol. 29, no. 7, pp. e33-40, Jul. 2012.

[26] G. D. Pinna, R. Maestri, A. Torunski, L. Danilowicz-Szymanowicz, M. Szwoch, M. T. La Rovere, and G. Raczak, “Heart rate variability measures: a fresh look at reliability,” *Clin. Sci. Lond. Engl. 1979*, vol. 113, no. 3, pp. 131–140, Aug. 2007.

[27] G. R. H. Sandercock, P. D. Bromley, and D. A. Brodie, “The reliability of short-term measurements of heart rate variability,” *Int. J. Cardiol.*, vol. 103, no. 3, pp. 238–247, Sep. 2005.

[28] P. H. Ellaway, A. Kuppuswamy, A. Nicotra, and C. J. Mathias, “Sweat production and the sympathetic skin response: Improving the clinical assessment of autonomic function,” *Auton. Neurosci.*, vol. 155, no. 1–2, pp. 109–114, Jun. 2010.

[29] M. Benedek and C. Kaernbach, “A continuous measure of phasic electrodermal activity,” *J. Neurosci. Methods*, vol. 190, no. 1–5, pp. 80–91, Jun. 2010.

[30] B. M. W. Illigens and C. H. Gibbons, “Sweat testing to evaluate autonomic function,” *Clin. Auton. Res.*, vol. 19, no. 2, pp. 79–87, Apr. 2009.

[31] C. Setz, B. Arnrich, J. Schumm, R. La Marca, G. Tröster, and U. Ehlert, “Discriminating stress from cognitive load using a wearable EDA device,” *IEEE Trans. Inf. Technol. Biomed. Publ. IEEE Eng. Med. Biol. Soc.*, vol. 14, no. 2, pp. 410–417, Mar. 2010.

[32] J. . Healey and R. W. Picard, “Detecting stress during real-world driving tasks using physiological sensors,” *IEEE Trans. Intell. Transp. Syst.*, vol. 6, no. 2, pp. 156–166, Jun. 2005.

[33] T. P. Zahn, J. L. Rapoport, and C. L. Thompson, “Autonomic effects of dextroamphetamine in normal men: implications for hyperactivity and schizophrenia,” *Psychiatry Res.*, vol. 4, no. 1, pp. 39–47, Feb. 1981.

[34] T. P. Zahn and J. L. Rapoport, “Autonomic nervous system effects of acute doses of caffeine in caffeine users and abstainers,” *Int. J. Psychophysiol. Off. J. Int. Organ. Psychophysiol.*, vol. 5, no. 1, pp. 33–41, May 1987.

[35] G. Bohlin, “Delayed habituation of the electrodermal orienting response as a function of increased level of arousal,” *Psychophysiology*, vol. 13, no. 4, pp. 345–351, Jul. 1976.

[36] D. R. Bach and K. J. Friston, “Model-based analysis of skin conductance responses: Towards causal models in psychophysiology,” *Psychophysiology*, vol. 50, no. 1, pp. 15–22, Jan. 2013.

[37] T. Chaspari, A. Tsiartas, L. I. Stein, S. A. Cermak, and S. S. Narayanan, “Sparse representation of electrodermal activity with knowledge-driven dictionaries,” *IEEE Trans. Biomed. Eng.*, vol. 62, no. 3, pp. 960–971, Mar. 2015.

[38] A. Greco, G. Valenza, A. Lanata, E. Scilingo, and L. Citi, “cvxEDA: a Convex Optimization Approach to Electrodermal Activity Processing,” *IEEE Trans. Biomed. Eng.*, Aug. 2015.

[39] M. A. Sanchez-Gonzalez, R. W. May, A. P. Koutnik, M. Kabbaj, and F. D. Fincham, “Sympathetic Vasomotor Tone Is Associated With Depressive Symptoms in Young Females: A Potential Link Between Depression and Cardiovascular Disease,” *Am. J. Hypertens.*, vol. 26, no. 12, pp. 1389–1397, Dec. 2013.

[40] E. S. Prakash, Madanmohan, K. R. Sethuraman, and S. K. Narayan, “Cardiovascular autonomic regulation in subjects with normal blood pressure, high-normal blood pressure and recent-onset hypertension,” *Clin. Exp. Pharmacol. Physiol.*, vol. 32, no. 5–6, pp. 488–494, May 2005.

[41] Y.-P. Liu, Y.-H. Lin, Y.-C. Chen, P.-L. Lee, and C.-S. Tung, “Spectral analysis of cooling induced hemodynamic perturbations indicates involvement of sympathetic activation and nitric oxide production in rats,” *Life Sci.*, vol. 136, pp. 19–27, Sep. 2015.

[42] L. D. DeBeck, S. R. Petersen, K. E. Jones, and M. K. Stickland, “Heart rate variability and muscle sympathetic nerve activity response to acute stress: the effect of breathing,” *Am. J. Physiol. Regul. Integr. Comp. Physiol.*, vol. 299, no. 1, pp. R80-91, Jul. 2010.

[43] Z. B. Moses, L. J. Luecken, and J. C. Eason, “Measuring task-related changes in heart rate variability,” *Conf. Proc. Annu. Int. Conf. IEEE Eng. Med. Biol. Soc. IEEE Eng. Med. Biol. Soc. Annu. Conf.*, vol. 2007, pp. 644–647, 2007.

[44] J. P. Florian, E. E. Simmons, K. H. Chon, L. Faes, and B. E. Shykoff, “Cardiovascular and autonomic responses to physiological stressors before and after six hours of water immersion,” *J. Appl. Physiol. Bethesda Md 1985*, vol. 115, no. 9, pp. 1275–1289, Nov. 2013.

[45] E. S. Mezzacappa, R. M. Kelsey, and E. S. Katkin, “Breast feeding, bottle feeding, and maternal autonomic responses to stress,” *J. Psychosom. Res.*, vol. 58, no. 4, pp. 351–365, Apr. 2005.

[46] G. H. Prystav, “Electrodermal, Cardiac, and Respiratory Activity to Repeated Cold Pressor Stimulation in Drug Addicts,” *J. Gen. Psychol.*, vol. 94, no. 2, pp. 259–270, Apr. 1976.

[47] A. Garafova, A. Penesova, E. Cizmarova, A. Marko, M. Vlcek, and D. Jezova, “Cardiovascular and sympathetic responses to a mental stress task in young patients with hypertension and/or obesity,” *Physiol. Res. Acad. Sci. Bohemoslov.*, vol. 63 Suppl 4, pp. S459-467, 2014.

[48] Z. Visnovcova, M. Mestanik, M. Javorka, D. Mokra, M. Gala, A. Jurko, A. Calkovska, and I. Tonhajzerova, “Complexity and time asymmetry of heart rate variability are altered in acute mental stress,” *Physiol. Meas.*, vol. 35, no. 7, pp. 1319–1334, Jul. 2014.

[49] J. P. Delaney and D. A. Brodie, “Effects of short-term psychological stress on the time and frequency domains of heart-rate variability,” *Percept. Mot. Skills*, vol. 91, no. 2, pp. 515–524, Oct. 2000.

[50] J. R. Landis and G. G. Koch, “The measurement of observer agreement for categorical data,” *Biometrics*, vol. 33, no. 1, pp. 159–174, Mar. 1977.

Chapter 4: Highly Sensitive Index of Sympathetic Activity based on Time-Frequency Domain Analysis of Electrodermal Activity

(Posada-Quintero, H. F., Florian, J. P., Orjuela-Canon, A. D., & Chon, K. H. (2016). Highly Sensitive Index of Sympathetic Activity based on Time-Frequency Spectral Analysis of Electrodermal Activity. American Journal of Physiology - Regulatory, Integrative and Comparative Physiology)

4.1 Introduction

Time-invariant frequency-domain analysis of EDA was explored in the previous chapter as a tool for sympathetic tone assessment and it was termed EDASympn [16]. The usefulness of EDASympn was demonstrated, with lower variability compared to time-domain measures of EDA, but the technique exhibited only acceptable consistency, with lower sensitivity for orthostatic (stand test) and cognitive stress compared to SCL and NS.SCRs.

Given that the sympathetic tone is time varying, especially when experiments are specifically designed to invoke its dynamics, we hypothesized that time-varying analysis of EDA may provide more sensitive results than the time-invariant frequency-domain analysis (42) and time-domain indices consisting of SCL and NS.SCRs. To this end, we performed time-frequency analysis of EDA signals to examine if we can obtain an even more sensitive and reliable index of sympathetic tone. Specifically, variable frequency complex demodulation (VFCDM), a time-frequency spectral (TFS) analysis technique that provides accurate amplitude estimates and one of the highest time-frequency resolutions [17] was employed in this study to develop an index of sympathetic tone. The time-varying EDA index of sympathetic control (TVSymp) was computed by using the mean spectral amplitudes in the frequency band associated with sympathetic tone of the EDA.

To test our hypothesis, we have computed TVSymp and a full set of EDA (SCL, NS.SCRs and EDASympn) and HRV (HRVLF and HRVLFn) indices of sympathetic control for subjects undergoing four

tests known to elicit sympathetic tone arousal: cold pressor test, 70° head-up tilt (HUT) test, stand test, and Stroop task. Sensitivity, consistency and variability of TVSymp were computed and compared gainst the time-domain and time-invariant spectral indices.

4.2 Materials and Methods

4.2.1 Protocol

Participants were asked to avoid caffeine and alcohol and to not exercise during the 24 hours preceding the test, and were instructed to fast for at least 3 hours before testing. Prospective subjects using psychoactive drugs, nicotine or other recreational drugs, and taking any medicine were asked to exclude themselves from the study. The experiments were carried out in a quiet, dimly lit room (ambient temperature, 26-27 °C). The study protocol was approved by the Institutional Review Board of The University of Connecticut and all volunteers provided written informed consent to participate in the experiment. ECG and EDA signals were simultaneously recorded throughout all tests (Hewlett-Packard HP 78354A and ADINSTRUMENTS GSR module, respectively). After preparing the skin with alcohol, ECG electrodes were placed to acquire Lead I, and EDA electrodes were placed on the index and middle finger for all subjects. Signals were digitized using a PowerLab system at 1 kHz, 12-bit resolution.

Twelve healthy volunteers (10 males, 2 female) of ages ranging from 19 to 36 years old (26.2 ± 6.1; mean ± SD), weight 64.6 ± 7 kg, and height 171.5 ± 9.6 cm, were enrolled in this study. No gender-related differences have been reported for EDA or sympathetic function. To induce a wide variety of sympathetic arousal types, subjects underwent four tests, in the following order: cold pressor (physical stress), 70° HUT, stand test (orthostatic stress) and Stroop task (cognitive stress). The order of tests was the same for all the subjects.

Before each test, subjects remained in the supine position for at least 5 minutes to ensure hemodynamic stabilization (end-point criteria was when the subject achieved a baseline level of heart rates). After the stabilization period, 5 minutes of resting baseline data were recorded with subjects in the supine

position before each test. For the cold pressor test, subjects were asked to immerse their left hand to the wrist level into a 0-1 °C water bath for a period of 3 minutes. For HUT, subjects were tilted from 0 to 70 degrees and remained tilted for 5 minutes. The stand test consisted of a 5-minute standing period in which subjects were asked not to move and not to actively contract their leg muscles. For the Stroop task, subjects were asked to speak a word which named a color. They were shown congruent (the word was written in the color it expressed) and incongruent (the word and the color it was printed in were different) combinations to induce cognitive stress [18]. The words and colors were "blue," "yellow," "green," "red," "purple" and "black". The background also changed to be randomly congruently or incongruently colored with the word. A computerized version of the original Stroop task was designed. The Stroop task was 5 minutes total, with the first minute used for training.

4.2.2 Signal processing

Time-frequency spectra (TFS) of EDA signals were used to quantify the elicited changes of the sympathetic nervous system due to the cold pressor test, HUT, stand test, and Stroop task. Prior to time-frequency analysis, EDA signals were down–sampled to 2 Hz and high-pass filtered (0.01 Hz) to remove any trends. The VFCDM technique has been described in detail previously [17], [19], and tested with different physiological signals [19]–[21], hence the technique will be only briefly summarized.

4.2.2.1 Variable Frequency Complex Demodulation Algorithm

The first step is to use complex demodulation (CDM) to obtain an estimate of the TFS. In CDM, a bank of low pass filters (LPFs) is used to decompose the signal into a suite of band-limited signals. The analytic signals that are obtained from these, through use of the Hilbert transform, then provide estimates of instantaneous amplitude, frequency, and phase within each frequency band. Consider a sinusoidal signal x(t) to be a narrow-band oscillation with a center frequency f0, instantaneous amplitude A(t), phase ϕ(t), and the direct current component dc(t) defined as:

$$x(t) = dc(t) + A(t)\cos(2\pi f_0 t + \phi(t)). \quad (1)$$

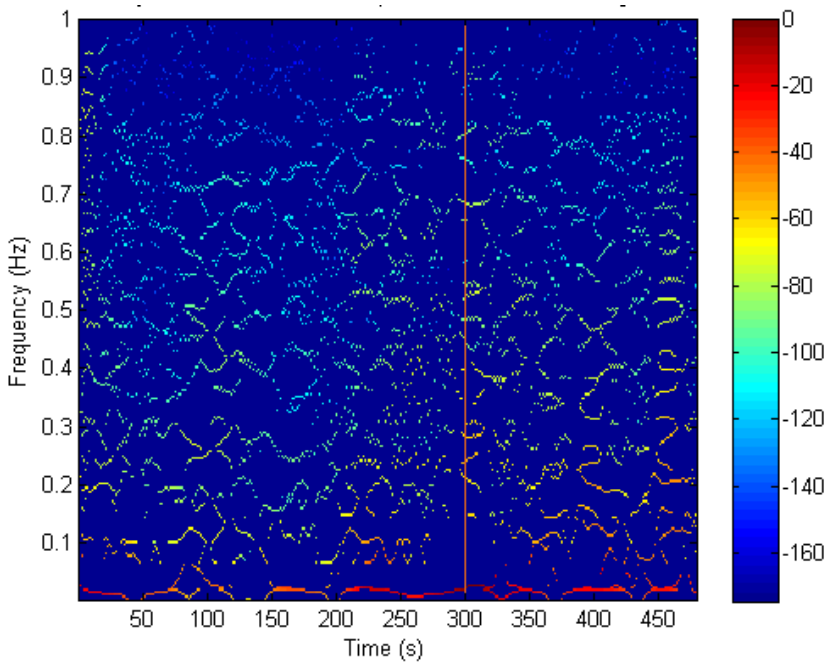

Figure 4.1 – Normalized amplitude time-frequency spectrum of an EDA signal, obtained via the complex demodulation method (VFCDM), for a given subject under cold pressor test.
Vertical line represents the start of the cold pressor. Color bar shows the logarithmic scale in dB.

For a given center frequency (or carrier), we can extract the instantaneous amplitude information A(t) and phase information ϕ(t) by multiplying x(t) by $e^{-j2\pi f_0 t}$, which results in the following:

$$z(t) = x(t)e^{-j2\pi f_0 t}$$

$$= dc(t)e^{-j2\pi f_0 t} + \left(\frac{A(t)}{2}\right)e^{j\phi t} + \left(\frac{A(t)}{2}\right)e^{-j(4\pi f_0 t + \phi(t))}. \quad (2)$$

A leftward shift by $e^{-j2\pi f_0 t}$ moves the center frequency f0 to zero frequency in the spectrum of z(t). If z(t) is subjected to an ideal LPF with a cutoff frequency fC < f0, then the filtered signal z1P(t) will contain only the component of interest, and we obtain

$$z_{1P}(t) = \left(\frac{A(t)}{2}\right)e^{j\phi(t)} \quad (3)$$

$$A(t) = 2\left|z_{1P}(t)\right| \quad (4)$$

$$\phi(t) = \tan^{-1}\left(\frac{\mathrm{Im}(z_{1P}(t))}{\mathrm{Re}(z_{1P}(t))}\right). \quad (5)$$

Consider a case when a modulating frequency is not fixed as described before but varies as a function of time. In this case, the signal x(t) can be written in the following form:

$$x(t) = dc(t) + A(t)\left(\int_0^t \cos(2\pi f(\tau)d\tau + \phi(t))\right). \quad (6)$$

Similar to the operations in (1) and (2), multiplying (6) by $e^{-j\int_0^t 2\pi f(\tau)d\tau}$ yields both instantaneous amplitude, A(t), and instantaneous phase, ϕ(t) [22], so that:

$$z(t) = x(t)e^{-j\int_0^t 2\pi f(\tau)d\tau} = dc(t)e^{-j\int_0^t 2\pi f(\tau)d\tau} + \frac{A(t)}{2}e^{j\phi(t)} + \frac{A(t)}{2}e^{-j\int_0^t 4\pi f(\tau)d\tau} \quad (7)$$

From (7), when z(t) is filtered with an ideal LPF with a cutoff frequency fC < f0, then the filtered signal z1P(t) will be obtained with the same instantaneous amplitude A(t) and phase ϕ(t) as provided in (4) and (5). The instantaneous frequency, as reported previously [23], is given by:

$$f(t) = f_0 + \frac{1}{2\pi}\frac{d\phi(t)}{dt} \quad (8)$$

For this study, x(t) corresponds to the EDA signal. The instantaneous frequency and amplitude of di can be calculated using the Hilbert transform [24]. The entire time-frequency spectrum can be obtained by the calculation of the Hilbert transform of the equation above for all time points for the obtained low-pass filtered frequency components. Therefore, by the combination of the CDM and Hilbert transform, a high TF resolution spectrum and accurate amplitude information can be obtained.

The procedure for the implementation of the CDM-based TFS is summarized next.

1. Design a finite-impulse response (FIR) LPF with the bandwidth and the length of the filter set to Fω and Nω, respectively. Set center frequencies as

$$f_{0i} = (i-1)(2F_\omega), \qquad i = 1,2,\ldots,\mathrm{int}\left(\frac{f_{\max}}{2F_\omega}\right) \quad (9)$$

where the bandwidth between neighboring center frequencies is 2Fω, and fmax represents the highest signal frequency.

2. Use the CDM to extract the dominant frequency within the confined bandwidth and repeat it over the entire frequency band (by incrementing f0i).
3. Decompose the signal into sinusoidal modulations via the CDM.
4. Calculate the instantaneous frequencies using (8) based on the phase (5) and the instantaneous amplitudes (4) of each sinusoidal modulation component using the Hilbert transform.
5. Obtain the TF representation of the signal using the estimated instantaneous frequencies and amplitudes.

4.2.2.2 Determining the relevant components for the sympathetic responses.

Once the TFS is obtained via the VFCDM method as described above (e.g. Figure 4.1), the resulting time-varying spectral amplitudes at each frequency interval are analyzed to examine whether they evolve in time in response to sympathetic stimulation. These spectral amplitudes are not rigid bands of frequency. Instead, they represent the evolution over time of a spectral amplitude that changes within a range of frequencies (see Figure 4.2). These frequencies depend on the sampling frequency (fs) and given that fs = 2 Hz was selected, the spectral frequencies are centered on 0.04 Hz, 0.12 Hz, 0.2 Hz, 0.28 Hz, 0.36 Hz, 0.44 Hz, 0.52 Hz, 0.6 Hz, 0.68 Hz, 0.76 Hz, 0.84 Hz and 0.92 Hz. Finer spectral resolution was explored. Since we were only interested in the sum of time-varying spectral amplitudes in the frequency range that may correspond to the sympathetic dynamics (e.g., 0.045-0.25 Hz), finer frequency resolution was not found informative.

The power contained in each frequency resolution band was computed for all subjects to determine sympathetic-relevant dynamics. Those powers that did not change from baseline to stimuli stage were considered insensitive to sympathetic control and subsequently considered irrelevant. The time-varying

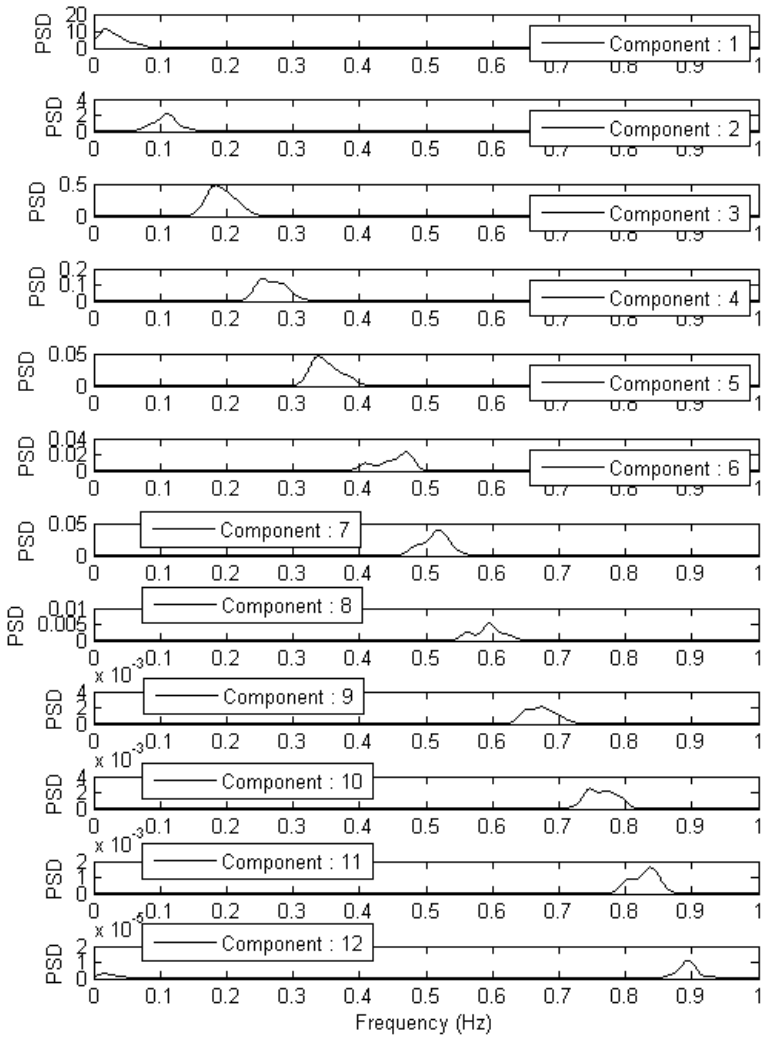

Figure 4.2 – Exemplification of the twelve resulting VFCDM components, shown in frequency domain. Sampling frequency is 2 Hz.

spectral powers with a low value (comprising less than 5% of the total spectral power) were also considered irrelevant. It was recently shown that ~5% of time-invariant spectral content of HRV is also enclosed in frequencies above HF (> 0.4 Hz) [16]. In the same study, the frequency bound of EDA associated with the sympathetic activity was largely confined to 0.045 Hz to 0.25 Hz, with about 5% of the power in the frequencies beyond 0.25 Hz.

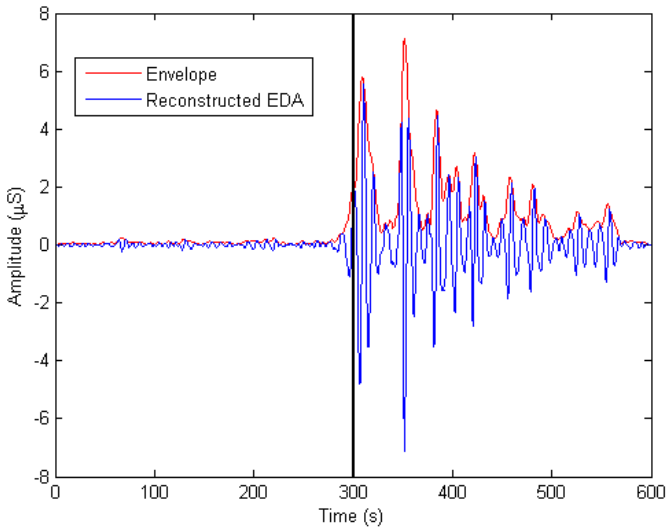

Figure 4.3 – Computed envelope for the sum of selected VFCDM backbones, for a given subject, during stand test.
Blue line is the reconstructed signal using the two components with the most power. Red line represents the envelope, estimated via instantaneous amplitude. Vertical black line represents the moment when the subject stood up.

4.2.2.3 Computing the index of sympathetic control.

Time-varying spectral amplitudes in the frequency bands that are considered to be responsive to sympathetic stimuli are summed together to obtain an estimated reconstructed EDA signal (X'(t)), which is then normalized to unit variance (divided by its standard deviation), and its instantaneous amplitude is computed using Hilbert transform [24], as follows

$$Y'(t) = \frac{1}{\pi} P \int_{-\infty}^{\infty} \frac{X'(\tau)}{t-\tau} d\tau \qquad (10)$$

where P indicates the Cauchy principal value. X'(t) and Y'(t) form the complex conjugate pair, so we can define an analytic signal, Z(t), as

$$Z(t) = X'(t) + iY'(t) = a(t)e^{j\theta(t)} \qquad (11)$$

in which

$$a(t) = \left[X'^2(t) + Y'^2(t)\right]^{1/2}, \qquad \theta(t) = \arctan\left(\frac{Y'(t)}{X'(t)}\right) . \qquad (12)$$

The resulting a(t) is considered the instantaneous amplitude of Z(t) (see Figure 4.3). The mean amplitude of a(t), termed TVSymp, was computed for the four tests for all subjects. This value constitutes our intended index of sympathetic tone. Notice that TVSymp is a dimensionless quantity as it was normalized to the standard deviation.

4.2.2.4 EDA indices

To extract the conductance level of EDA, a 10th-order low-pass FIR filter with a cut-off frequency of 0.0004 Hz was applied. The raw signal minus the conductance level was used to compute the NS.SCRs. The SCL index was computed using the mean of the conductance level over the two-minute period. NS.SCRs were obtained by visual inspection over the two-minute period, and averaged per minute. A threshold value of 0.05 μS was used to determine relevant SCRs [14]. In addition, when a second response occurred before completion of the prior response, the two responses were counted as two NS.SCRs even though they were overlapped.

The time-invariant frequency domain index of EDA, EDASympn, was also computed. Power spectral density analysis of EDA signals was performed on the same two-minute segments used to compute SCL and NS.SCRs. For this process, EDA signals were down–sampled to 2 Hz. Before down-sampling, the data were filtered with an 8th-order Chebyshev Type I low-pass filter (0.8 Hz). Down-sampling from 400 Hz to 2 Hz was performed in two steps (using consecutive down-sampling factors of 1/20 and 1/10, respectively). Finally, signals were high-pass filtered (0.01 Hz, Butterworth, 8th order) to remove any trend. The power spectra of EDA signals were calculated using Welch's periodogram method with 50% data overlap. A Blackman window (length of 128 points) was applied to each segment, the Fast Fourier Transform was calculated for each windowed segment, and the power spectra of the segments were averaged. EDASympn was computed as the normalized power within the frequency band of interest (0.045 to 0.25 Hz) [16].

4.2.2.5 HRV analysis

For HRV analysis, ECG signals were band-pass filtered (0.05-40 Hz) to reduce noise and motion artifacts. The R-waveform peaks were detected using a widely-used peak detection algorithm (57), and HRV series (from RR segments) were computed. The power spectra of HRV were calculated using Welch's periodogram method with 50% data overlap. The RR interval series were converted to an evenly time-sampled signal (4 Hz) by cubic spline interpolation. A Blackman window (length of 256 points) was applied to each segment and the Fast Fourier Transform was calculated for each windowed segment. Finally, the power spectra of the segments were averaged. The low-frequency index (HRVLF [ms2], 0.04 to 0.15 Hz) (67) and normalized LF index (HRVLFn = (HRVLF)/Total power, normalized units) were computed. Four minutes of clean ECG signals were used to compute HRV for HUT, the stand test, and the Stroop task, and three minutes for the cold pressor test given the extreme characteristics of this physical test. Within each test, the same data length was used consistently for baseline and test segments.

4.2.3 Statistics

Six indices of sympathetic control were computed, including one time-frequency domain index, TVSymp, two time-domain indices, SCL (μS) and NS.SCRs (#/min), and three frequency-domain indices, EDASympn (normalized units, n.u.), HRVLF (ms2) and HRVLFn (n.u.). All the statistical analysis was performed using MATLAB ®. The paired t-test was applied to test the null hypothesis that elicited responses to the cold pressor test, HUT testing, the stand test and Stroop task, as measured by each of the above-defined indices, are equal to the baseline values. A p value <= 0.05 was set to define statistical significance. These results are useful to evaluate the suitability of the indices to quantitatively assess sympathetic function in healthy subjects.

Measures from detection theory analysis were employed to assess sensitivity of the indices, including the receiver operating characteristic (ROC) curve (39), Youden's index (J = Sensitivity + Specificity – 1, to assess the performance of the detector) (62), the area under the ROC curve (AUC, the

probability that the index will assign to a positive instance a higher value than to a negative one) (25), and the maximum accuracy of the detector. The coefficient of variation (CV) (i.e. the standard deviation between all the measurements divided by the mean) and the intra-class correlation (ICC) (38) were computed for all the indices in order to assess inter-subject variability and degree of consistency of each index, respectively.

4.3 Results

Figure 4.2 illustrates how the time-varying spectral powers are distributed in the frequency domain. Notice how as frequency increases, the power decreases (note that y-axes are not equal). Table 4.1 shows the percentage of spectral power contained in three bands of frequencies throughout the subjects. The time-varying spectral amplitudes in the first band comprise most of the spectral content of the signal (> 60%) for any test. The percentage of spectral power at the very low frequencies (< 0.08 Hz) is usually reduced under testing conditions when compared to the baseline, because sympathetic dynamics become more pronounced with test stimuli [16]. Time-varying spectral components at frequencies between 0.08 and 0.24 Hz (2nd and 3rd center frequencies) are the ones that bear the most power and increase the most between baseline and tests. Although some of the remaining spectral power increased during testing at > 0.24 Hz, it was less than 5% of the power. For this reason, we have selected the spectral amplitudes in the 0.08 to 0.24 Hz range to compute the sympathetic index.

Table 4.1 Percentage of power for the resulting backbones of VFCDM.

	Cold Pressor		**70° Head-up Tilt**		**Stand Test**		**Stroop Task**	
Frequency range	**Baseline**	**Test**	**Baseline**	**Test**	**Baseline**	**Test**	**Baseline**	**Test**
0 to 0.08 Hz	88.3	67.7	86	83.8	91.1	81.8	89.4	81
0.08 to 0.24 Hz	6.9	19.5	8.4	7.5	5.4	10	6.5	11.4
0.24 to 1 Hz	2.2	4.3	1.7	2.9	0.7	1.9	2.2	2.3

Values are % of total power throughout the full set of subjects.

Table 4.2 shows the overall EDA and HRV response for cold pressor test, HUT, stand test, and Stroop task, along with the significance of differences found between baseline and stimuli for each index. All EDA measures (TVSymp, SCL, NS.SCRs and EDASympn) significantly increased between baseline and test stages. HRVLF only exhibited significant differences during the stand test and Stroop task. HRVLFn showed differences during HUT and the stand test, but not during cold pressor and Stroop task. Figure 4.4 shows 8 minutes (6 minutes in the case of cold pressor as this tests was shorter) of time evolution (mean ± standard deviation) of TVSymp for cold pressor, HUT, stand test and Stroop task. For all stimuli, TVSymp reaches a maximum value at ~2 minutes and then gradually decrease with time. However, the Stroop test differs from other stimuli in that the maximum values linger for long time durations and then gradually decrease to a baseline values. Note that before each test, subjects remained in the supine position for at least 5 minutes to ensure hemodynamics stabilization. This can be seen in Table 4.2 especially for TVSymp as its baseline values are nearly identical prior to stimuli.

Table 4.2 Results for EDA and HRV indices.

Index	Stage	Cold Pressor	70° Head-up Tilt	Stand Test	Stroop Task
TVSymp	**Baseline**	0.5 ± 0.3	0.3 ± 0.3	0.3 ± 0.3	0.2 ± 0.3
	Test	1.4 ± 0.7*	1.6 ± 0.7*	1.6 ± 0.7*	1.4 ± 0.7*
SCL (μS)	**Baseline**	0.8 ± 4.7	2.9 ± 6.2	4.1 ± 8.1	-1.3 ± 3.9
	Test	4.5 ± 7.5*	6.5 ± 8.4*	10.8 ± 7.5*	6.3 ± 4.0*
NS.SCR (#/min)	**Baseline**	2.7 ± 2.9	1.5 ± 2.3	1.8 ± 2	0.9 ± 1.5
	Test	4.9 ± 4.5*	3.6 ± 2.7*	6 ± 2.9*	9.8 ± 3.9*
EDASympn (n.u.)	**Baseline**	0.2 ± 0.2	0.2 ± 0.2	0.3 ± 0.2	0.3 ± 0.2
	Test	0.4 ± 0.2*	0.4 ± 0.2*	0.5 ± 0.2*	0.5 ± 0.2*
HRVLF (ms^2)	**Baseline**	7.1 ± 6.4	4.7 ± 3.9	3.8 ± 3.9	4.2 ± 3.4
	Test	4.8 ± 3.3	16 ± 21	36 ± 33*	6.1 ± 4.4*
HRVLFn (n.u.)	**Baseline**	0.3 ± 0.1	0.3 ± 0.1	0.2 ± 0.05	0.4 ± 0.1
	Test	0.3 ± 0.1	0.5 ± 0.2*	0.6 ± 0.2*	0.4 ± 0.1

Values are mean ± standard deviation

* represents significant difference compared to baseline stage (p<0.05)

TVSymp, Time-varying index of sympathetic tone; SCL, skin conductance level; NS.SCRs, non-specific skin conductance responses; EDASympn, normalized sympathetic component of the EDA; HRVLF, low frequency components of HRV; HRVLFn, normalized low frequency components of HRV

Table 4.3 Sensitivity analysis of sympathetic indices.

	Cold Pressor			70° Head-up Tilt			Stand Test			Stroop task		
Index	**J**	**AUC**	**Acc**	**J**	**AUC**	**Acc**	**J**	**AUC**	**Acc**	**J**	**AUC**	**Acc**
TVSymp	0.75	0.80	0.88	0.92	0.91	0.96	0.83	0.88	0.92	1.00	0.92	1.00
SCL	0.50	0.66	0.75	0.42	0.63	0.71	0.58	0.69	0.79	0.83	0.85	0.92
NS.SCR	0.33	0.61	0.67	0.50	0.73	0.75	0.83	0.87	0.92	0.92	0.92	0.96
EDASympn	0.58	0.70	0.79	0.50	0.66	0.75	0.50	0.63	0.75	0.42	0.69	0.71
HRVLF	0.25	0.42	0.63	0.38	0.59	0.69	0.75	0.80	0.88	0.50	0.55	0.75
HRVLFn	0.38	0.48	0.69	0.88	0.81	0.94	1.00	0.88	1.00	0.38	0.44	0.69

J is Youden's index, AUC is Area under the ROC curve, Acc is accuracy.
TVSymp, Time-varying index of sympathetic tone; SCL, skin conductance level; NS.SCRs, non-specific skin conductance responses; EDASympn, normalized sympathetic component of the EDA; HRVLF, low frequency components of HRV; HRVLFn, normalized low frequency components of HRV

Results for the analysis of sensitivity are shown in Table 4.3. TVSymp outperformed all the other indices (highest J) at detecting stress, with the only exception being HRVLFn which exhibited a higher performance (J=1 vs. J=0.83) during the stand test. NS.SCRs and TVSymp exhibited equal J values for the stand test. TVSymp also showed a higher probability to assign a higher value to a positive instance than to a negative one (highest AUC). NS.SCRs and HRVLFn equaled TVSymp on this measure for Stroop task and postural stimulation (stand test), respectively. Similar behavior was found for the accuracy, where TVSymp surpassed all the other indices, with the only exception being HRVLFn during the stand test (Acc = 1 vs. Acc = 0.92). Figure 4.5 includes ROC curves for the four tests. Notice how the TVSymp ROC curve is more pronounced towards the left top corner, with the only exception being the stand test curve, where HRVLFn curve is slightly higher.

As for the measures of variation and consistency, Table 4.4 shows how TVSymp exhibits higher variation during baseline, compared to the four tests. However, such variation is almost always lower than the variation of SCL and NS.SCRs. NS.SCRs were only less variable during the stand test baseline. That is consistent with studies that report high variability of SCL and NS.SCRs, a concern among researchers [15], impeding the widespread use of these indices for assessing the general state of activation of the sympathetic system. Compared to EDASympn, TVSymp exhibited similar CV, slightly lower for cold pressor and HUT, and higher for stand test and Stroop task baselines. HRVLF was one of the more variable

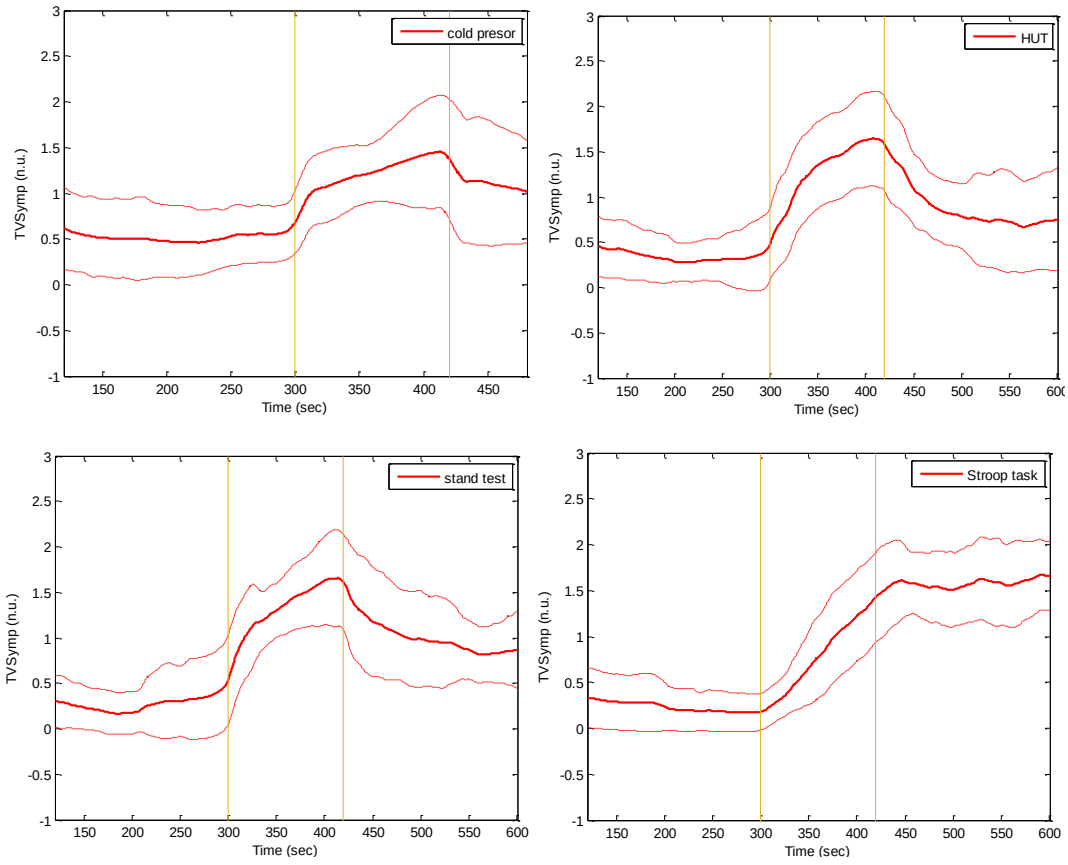

Figure 4.4 – Evolution (mean ± standard deviation) of TVSymp, Time-varying index of sympathetic tone, for the four tests: cold pressor, HUT (head-up tilt), stand test and Stroop task. TVSymp is at baseline levels before the test is performed.

indices, ranking third overall after SCL and NS.SCRs. In contrast, HRVLFn was the least variable index overall.

TVSymp was the most consistent index, as its intra-class correlation achieved a very high value of 0.96 with bounds between 0.9 and 0.99 for a level of significance of 0.05. Even though SCL's and NS.SCRs' consistencies were high, in agreement with previously reported values [16], their consistencies were not as high as those of TVSymp. The least consistent index was the EDASympn. HRVLF and HRVLFn proved to be moderately consistent indices.

Table 4.4 Coefficient of Variation and Intra-Class correlation results.

Indices	Cold Pressor		70° Head-		Stand Test		Stroop task		Average CV	Intra-class correlation (LB UB)
	BL	Test	BL	Test	BL	Test	BL	Test		
TVSymp	0.66	0.48	0.76	0.33	1.33	0.33	1.13	0.34	0.67	0.96 (0.9 0.99)
SCL	6.04	1.68	2.12	1.28	1.96	0.69	3.07	0.64	2.18	0.87 (0.67 0.97)
NS.SCR	1.09	0.91	1.50	0.76	1.11	0.48	1.56	0.40	0.98	0.92 (0.8 0.98)
EDASympn	0.68	0.47	0.90	0.45	0.59	0.48	0.72	0.37	0.58	0.81 (0.46 0.95)
HRVLF	0.90	0.69	0.82	1.32	1.02	0.91	0.85	0.69	0.90	0.84 (0.58 0.96)
HRVLFn	0.39	0.52	0.28	0.34	0.22	0.29	0.42	0.20	0.33	0.89 (0.72 0.97)

BL: baseline; LB and UB are upper and lower bounds, respectively, of the intra-class correlation with a level of significance of 0.05; TVSymp, Time-varying index of sympathetic tone; SCL, skin conductance level; NS.SCRs, non-specific skin conductance responses; EDASympn, normalized sympathetic component of the EDA; HRVLF, low frequency components of HRV; HRVLFn, normalized low frequency components of HRV

4.4 Discussion

The time-varying spectral EDA index of sympathetic control, TVSymp, was significantly higher during the cold pressor test, HUT, stand test and Stroop task, compared to baseline. TVSymp can be used as a noninvasive measure for assessing sympathetic function, as these induced stressors are known to invoke the sympathetic nervous system's response. Measures of detection theory showed that TVSymp is the most sensitive index of sympathetic arousal overall for the four stimuli experiments in the study, with the exception of the stand test where HRVLFn was slightly better. Furthermore, TVSymp exhibited lower variability (coefficient of variation) than did time-domain EDA indices (SCL and NS.SCRs), and higher consistency (intra-class correlation coefficient) than any other tested index of sympathetic control. Time-frequency analysis of EDA provides relevant information about sympathetic arousal in different scenarios, as all biological systems are time-variant, increasing the potential for an EDA signal to be used for detecting the onset and level of stress induced by various stimuli. However, more testing is needed to determine the method can be applied to diagnosis of the onset and progression of diseases that affect the autonomic nervous system.

Traditionally, techniques for sympathetic function assessment have involved hemodynamic measurements [25], [26], adrenergic and ganglionic pharmacological blockade [27]–[30], noradrenaline measurement in urine or plasma [3], [31], [32], microneurography [33], [34], plasma noradrenaline kinetics

[35], [36], HRV analysis [9], [37], [38] or imaging techniques [39]. However, hemodynamic measurements and pharmacological blockade are invasive and present limited reproducibility. Noradrenaline measurement provides only a 'static' picture of sympathetic function. Microneurography is the only method for directly and continuously recording efferent postganglionic muscle sympathetic nerve activity; however, it is an invasive technique. Imaging techniques, including positron emission tomography and single photon emission computed tomography scanning, have been applied to visualize the sympathetic innervation of human organs with good success, but neuroimaging techniques are costly and require specialized technical support.

HRV analysis has been widely employed because it is a low-cost noninvasive continuous method to evaluate cardiac sympathetic regulation. The low-frequency components of HRV (0.045-0.15 Hz) are commonly used as a marker of sympathetic control, even though such components are known to be influenced by both the sympathetic and parasympathetic nervous systems. Such influence reduces the accuracy of the technique. Time-domain analysis of EDA has also been used as a noninvasive marker of sympathetic nervous system regulation. The main advantage of EDA over HRV is that there is no parasympathetic innervation of eccrine sweat glands. However, a drawback to using time-domain measures of EDA is that they are highly variable between subjects [15].

A recent study suggests that sympathetic function influences the EDA spectrum mainly in the range from 0.045 to 0.25 Hz [16]. This is in agreement with what we found, specifically, that the spectral amplitudes with frequencies of 0.08 to 0.24 Hz are the most responsive to sympathetic control, with the improvement in consistency and sensitivity shown by the time-frequency index, the TVSymp. We also performed VFCDM decomposition using sampling frequencies of 1 Hz and 0.8 Hz (not shown), in order to explore the effect of a higher frequency resolution on the signal decomposition. This allowed us to compute the percentage of spectral power with higher spectral resolution and calculate the TVSymp index at frequencies between 0.04 and 0.08 Hz, which was part of the frequency-domain index in our previous study [16]. Although this frequency band comprised about 10 to 15% of the total power, it was not as responsive to induced stimuli in this study, and its inclusion in computing the TVSymp resulted in lower sensitivity

and performance of the index (assessed by signal detection theory). Performing time-invariant spectral density calculations on time-variant dynamics has been known to cause spectral distortion in the form of broadening of the spectral density [40], hence, we surmise that this may have caused the difference between the lower bound of the sympathetic dynamics found in this and our previous study [16]. We believe that fs = 2 Hz is the most suitable sampling frequency, and that TVSymp index based on the frequency band 0.08 to 0.24 Hz is the most appropriate for capturing the sympathetic dynamics.

The responses of HRV dynamics and EDA to cold stress are also poorly understood, however, this stimulus has been increasingly used in clinical practice to evaluate autonomic function in cardiovascular regulation, because stressful cooling evokes an increase in sympathetic neurotransmissions via activation of cold thermoreceptors and nociceptors [41]. HRVLF and HRVLFn are known to be insensitive detectors of stress induced by cold pressor, as various studies have reported increases [42], [43], decreases or insignificant changes [44]–[47]. This is in agreement with our results, as HRVLF and HRVLFn exhibited no differences between baseline and test for this stressor. Other studies found increases in SCL and NS.SCRs in healthy subjects when cold pressor was applied [48], [49]. Despite the high variability (CV) for this test, we also found significant differences in NS.SCRs and SCL indices when comparing cold pressor to baseline. EDASympn index also exhibited sensitivity to this test, as reported previously [16]. The time-frequency analysis index in this study, TVSymp, was able to discriminate between baseline and cold pressor. Indeed, although we observed that cold pressor was the most challenging test for detection, TVSymp performed the best among the various indices (highest J, AUC and Acc).

HUT testing has been widely used to elicit sympathetic activation, as evidenced by increases in the low frequency components of HRV, mainly in normalized units [47], [50]–[52]. We were in agreement, as we found significant differences only in the normalized index, HRVLFn. EDA data during HUT are scarce, as only one study has tested skin conductance during HUT [53], showing an increase in the SCL in the tilt-negative group. In addition to the increase in SCL and NS.SCRs, the novel findings for the current study were the EDASympn and TVSymp responses, both of which have never been tested during HUT. EDASympn was able to discriminate between supine baseline and HUT, and TVSymp not only showed

differences between baseline and HUT, but was the most sensitive, accurate and responsive index at detecting when the subjects were under orthostatic stress induced by HUT.

Sympathetic tone normally increases with postural stimulation (e.g. stand test) [5], [54], [55]. However, HRV has been shown to have poor reproducibility during an orthostatic challenge in healthy subjects, and even poorer reproducibility in a clinical population [56]. In the supine position, HRVLF and HRVLFn were shown to have poor relative reliability (i.e. high inter-subject variability). In this study we found significant differences in both HRV indices during the stand test. Indeed, HRVLFn showed the highest performance in distinguishing between supine and standing position. For its part, EDA has not

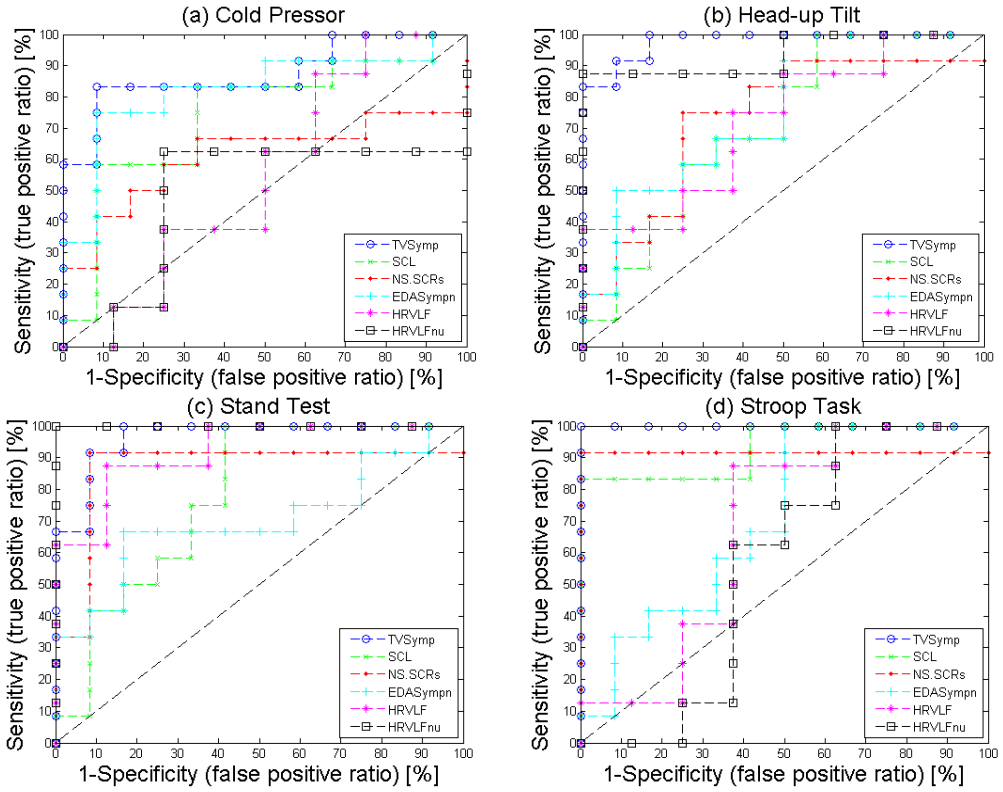

Figure 4.5 – ROC curves (sensitivity vs. 1-specificity) for the four tests, (a) cold pressor, (b) head-up tilt, (c) stand test and (d) Stroop task.
The indices of sympathetic control are: TVSymp, Time-varying index of sympathetic tone; SCL, skin conductance level; NS.SCRs, non-specific skin conductance responses; EDASympn, normalized sympathetic component of the EDA; HRVLF, low frequency components of HRV; HRVLFn, normalized low frequency components of HRV

been used often for assessing the stress induced in a stand test [14], [16]. In this study we found significant differences in SCL and NS.SCRs between supine and standing. EDASympn, the time-invariant frequency-domain index, was also different between body postures, with a much lower variability than SCL and NS.SCRs. The time-frequency domain index, TVSymp, was significantly different between supine and upright positions. Even though the best detector for stand test was the HRVLFn, TVSymp exhibited a similarly good performance.

Low-frequency components of HRV have been shown to increase significantly during Stroop task [57]–[59]. We found that HRVLF, but not HRVLFn, significantly increased between baseline and Stroop test. Regardless of their high variability during this test, SCL and NS.SCRs indices were significantly higher during the Stroop test when compared to baseline. EDASymp also exhibited a significant increase. The performance and sensitivity of the TVSymp index was nearly perfect for the Stroop task. Beyond the significant differences encountered between baseline and the induced cognitive stress, TVSymp detected such stress with the maximum possible accuracy (Acc = 1) and performance (J = 1).

As shown in Table 4.2, the greatest change in the EDA indices to induced stimuli occurred for the Stroop task for TVSymp, SCL and NS.SCR, which are then sequentially followed by stand and head-up tilt tests. For these three indices, the cold pressor stimuli induced the least change in their EDA responses. For HRVLF index, the greatest change was noted for the stand test followed by the Stroop test. While the EDASympn showed significant differences between the baseline and all stimuli, the induced changes in the amplitude of the EDA responses were similar for all tests. For TVSymp, SCL and NS.SCR indices, the EDA responses are most sensitive to cognitive followed by orthostatic and cold pressor tests. However, further studies are needed to quantify and validate these findings using direct measures of the sympathetic activity.

The SCL index and NS.SCRs are consistent with sympathetic arousal, as they are elevated by administration of dextroamphetamine, caffeine, and threatening instructions [60]–[62]. They also have relatively low within-subject variability (correlation of test-retest ranges from 0.50 to 0.70) but high variability between subjects [15]. In this study, we also found SCL to be a sensitive, but very highly variable

index. Although NS.SCRs are a consistent and fairly sensitive index, frequency-domain and time-frequency domain (EDASympn and TVSymp) indices do not rely on either manual or automatic SCR detection, which is usually more complex and time consuming. Because of its high sensitivity to four different types of stimuli and relatively low variability, the frequency-domain EDASympn index was recognized as a promising index of sympathetic function under multiple stressors in healthy individuals. However, it lacks consistency between subjects and has an inability to detect postural stimulation (stand test) and cognitive stress, compared to SCL and NS.SCRs. TVSymp uses time-varying dynamics, an inherent characteristic of all biological systems, hence, it was shown to be a highly sensitive index of the sympathetic autonomic nervous system activity.

Time-varying analysis of EDA not only overcomes the well-known lack of consistency limitation of traditional time-domain analysis of EDA, it was also shown to be highly sensitive measure of the sympathetic dynamics. Moreover, time-varying analysis of EDA was found to be more sensitive measure of the sympathetic dynamics than the low frequency component of the heart rate variability. While this work explored cognitive, physical and orthostatic stress, the time-varying analysis of EDA along with HRV could be extended to host of other studies to better characterize and discriminate dynamics of the autonomic nervous system that may be indicative of impending fatigue and stress. An accurate understanding of the autonomic nervous system's dynamics pertaining to the situation at hand can lead to better guidance and interventions to improve human health and performance.

4.5 Conclusion

The TVSymp index is a suitable discriminator of the stress induced by cold pressor, HUT, stand test, and Stroop task, and has the potential to be used as a reliable marker of quantitative assessment of sympathetic function. Although HRVLFn was slightly more sensitive to postural stimulation from the stand test, it was not as sensitive to HUT, cold pressor and Stroop task compared to TVSymp. Overall, TVSymp was found to be more reliable and sensitive than indices based on low-frequency components of HRV, was

highly consistent between subjects, and exhibited a lower variability compared to the time-domain measures of EDA. Finally, the frequency bands of the sympathetic nervous activities in healthy subjects can be defined to be most responsive in the frequencies between 0.08 and 0.24 Hz. More research is needed to determine whether these characteristics extend to patient populations.

4.6 References

[1] K. H. Chon *et al.*, "A novel quantitative method for diabetic cardiac autonomic neuropathy assessment in type 1 diabetic mice," *J. Diabetes Sci. Technol.*, vol. 8, no. 6, pp. 1157–1167, Nov. 2014.

[2] G. Grassi and M. Esler, "How to assess sympathetic activity in humans," *J. Hypertens.*, vol. 17, no. 6, pp. 719–734, Jun. 1999.

[3] M. Esler *et al.*, "Assessment of human sympathetic nervous system activity from measurements of norepinephrine turnover," *Hypertension*, vol. 11, no. 1, pp. 3–20, Jan. 1988.

[4] J. L. Rouleau *et al.*, "Activation of neurohumoral systems following acute myocardial infarction," *Am. J. Cardiol.*, vol. 68, no. 14, p. 80D–86D, Nov. 1991.

[5] D. J. Ewing and B. F. Clarke, "Diagnosis and management of diabetic autonomic neuropathy.," *Br. Med. J. Clin. Res. Ed*, vol. 285, no. 6346, pp. 916–918, Oct. 1982.

[6] C. J. Mathias and R. Bannister, "Investigation of autonomic disorders," in *Autonomic failure: a textbook of clinical disorders of the autonomic nervous system*, C. J. Mathias and R. Bannister, Eds. Oxford: Oxford University Press, 1999, pp. 169–195.

[7] P. Schwartz, M. La Rovere, and E. Vanoli, "Assessment: Clinical autonomic testing report of the Therapeutics and Technology Assessment Subcommittee of the American Academy of Neurology," *Neurology*, vol. 46, no. 3, pp. 873–880, Mar. 1996.

[8] V. Spallone, R. Morganti, T. Fedele, C. D'Amato, and M. R. Maiello, "Reappraisal of the diagnostic role of orthostatic hypotension in diabetes," *Clin. Auton. Res. Off. J. Clin. Auton. Res. Soc.*, vol. 19, no. 1, pp. 58–64, Feb. 2009.

[9] Task Force of the European Society of Cardiology and the North American Society of Pacing and Electrophysiology, "Heart rate variability. Standards of measurement, physiological interpretation, and clinical use," *Eur. Heart J.*, vol. 17, no. 3, pp. 354–381, Mar. 1996.

[10] R. Freeman and M. W. Chapleau, "Testing the autonomic nervous system," *Handb. Clin. Neurol.*, vol. 115, pp. 115–136, 2013.

[11] B. M. W. Illigens and C. H. Gibbons, "Sweat testing to evaluate autonomic function," *Clin. Auton. Res.*, vol. 19, no. 2, pp. 79–87, Apr. 2009.

[12] C. Setz, B. Arnrich, J. Schumm, R. La Marca, G. Tröster, and U. Ehlert, “Discriminating stress from cognitive load using a wearable EDA device,” *IEEE Trans. Inf. Technol. Biomed. Publ. IEEE Eng. Med. Biol. Soc.*, vol. 14, no. 2, pp. 410–417, Mar. 2010.

[13] J. . Healey and R. W. Picard, “Detecting stress during real-world driving tasks using physiological sensors,” *IEEE Trans. Intell. Transp. Syst.*, vol. 6, no. 2, pp. 156–166, Jun. 2005.

[14] W. Boucsein *et al.*, “Publication recommendations for electrodermal measurements,” *Psychophysiology*, vol. 49, no. 8, pp. 1017–1034, Aug. 2012.

[15] A. Crider and R. Lunn, “Electrodermal lability as a personality dimension,” *J. Exp. Res. Personal.*, vol. 5, no. 2, pp. 145–150, 1971.

[16] H. F. Posada-Quintero, J. P. Florian, A. D. Orjuela-Cañón, T. Aljama-Corrales, S. Charleston-Villalobos, and K. H. Chon, “Power Spectral Density Analysis of Electrodermal Activity for Sympathetic Function Assessment,” *Ann. Biomed. Eng.*, vol. 44, no. 10, pp. 3124–3135, Apr. 2016.

[17] K. H. Chon, S. Dash, and K. Ju, “Estimation of respiratory rate from photoplethysmogram data using time-frequency spectral estimation,” *IEEE Trans. Biomed. Eng.*, vol. 56, no. 8, pp. 2054–2063, Aug. 2009.

[18] R. J. Stroop, “Studies of interference in serial verbal reactions,” *J. Exp. Psychol.*, vol. 18, no. 6, pp. 643–662, 1935.

[19] H. Wang, K. Siu, K. Ju, and K. H. Chon, “A high resolution approach to estimating time-frequency spectra and their amplitudes,” *Ann. Biomed. Eng.*, vol. 34, no. 2, pp. 326–338, Feb. 2006.

[20] K. L. Siu, B. Sung, W. A. Cupples, L. C. Moore, and K. H. Chon, “Detection of low-frequency oscillations in renal blood flow,” *Am. J. Physiol. Renal Physiol.*, vol. 297, no. 1, pp. F155-162, Jul. 2009.

[21] Y. Zhong, K.-M. Jan, and K. H. Chon, “Frequency modulation between low- and high-frequency components of the heart rate variability spectrum may indicate sympathetic-parasympathetic nonlinear interactions,” *Conf. Proc. Annu. Int. Conf. IEEE Eng. Med. Biol. Soc. IEEE Eng. Med. Biol. Soc. Annu. Conf.*, vol. 1, pp. 6438–6441, 2006.

[22] H. Gasquet and A. J. Wootton, “Variable-frequency complex demodulation technique for extracting amplitude and phase information,” *Rev. Sci. Instrum.*, vol. 68, no. 1, pp. 1111–1114, Jan. 1997.

[23] A. Monti, C. Médigue, and L. Mangin, “Instantaneous parameter estimation in cardiovascular time series by harmonic and time-frequency analysis,” *IEEE Trans. Biomed. Eng.*, vol. 49, no. 12 Pt 2, pp. 1547–1556, Dec. 2002.

[24] N. E. Huang *et al.*, “The empirical mode decomposition and the Hilbert spectrum for nonlinear and non-stationary time series analysis,” *Proc. R. Soc. Lond. Math. Phys. Eng. Sci.*, vol. 454, no. 1971, pp. 903–995, Mar. 1998.

[25] J. Brod, V. Fencl, Z. Hejl, and J. Jirka, “Circulatory changes underlying blood pressure elevation during acute emotional stress (mental arithmetic) in normotensive and hypertensive subjects,” *Clin. Sci.*, vol. 18, pp. 269–279, May 1959.

[26] C. B. Thomas, J. A. Stanley, and M. A. Kendrick, “Observations on some possible precursors of essential hypertension and coronary artery disease. VII. The subjective reaction to the cold pressor test as expressed in the verbal response,” *J. Chronic Dis.*, vol. 14, pp. 355–365, Sep. 1961.

[27] G. Grassi *et al.*, “Heart rate as marker of sympathetic activity,” *J. Hypertens.*, vol. 16, no. 11, pp. 1635–1639, Nov. 1998.

[28] S. Julius, A. V. Pascual, and R. London, “Role of parasympathetic inhibition in the hyperkinetic type of borderline hypertension,” *Circulation*, vol. 44, no. 3, pp. 413–418, Sep. 1971.

[29] N. K. Hollenberg *et al.*, “Renal vascular tone in essential and secondary hypertension: hemodynamic and angiographic responses to vasodilators,” *Medicine (Baltimore)*, vol. 54, no. 1, pp. 29–44, Jan. 1975.

[30] B. Egan, R. Panis, A. Hinderliter, N. Schork, and S. Julius, “Mechanism of increased alpha adrenergic vasoconstriction in human essential hypertension.,” *J. Clin. Invest.*, vol. 80, no. 3, pp. 812–817, Sep. 1987.

[31] R. D. Hoeldtke, K. M. Cilmi, G. A. Reichard, G. Boden, and O. E. Owen, “Assessment of norepinephrine secretion and production,” *J. Lab. Clin. Med.*, vol. 101, no. 5, pp. 772–782, May 1983.

[32] I. J. Kopin, “Catecholamine metabolism: basic aspects and clinical significance,” *Pharmacol. Rev.*, vol. 37, no. 4, pp. 333–364, Dec. 1985.

[33] A. B. Vallbo, K. E. Hagbarth, H. E. Torebjörk, and B. G. Wallin, “Somatosensory, proprioceptive, and sympathetic activity in human peripheral nerves,” *Physiol. Rev.*, vol. 59, no. 4, pp. 919–957, Oct. 1979.

[34] W. Delius, K. E. Hagbarth, A. Hongell, and B. G. Wallin, “General characteristics of sympathetic activity in human muscle nerves,” *Acta Physiol. Scand.*, vol. 84, no. 1, pp. 65–81, Jan. 1972.

[35] G. L. Brown and J. S. Gillespie, “The output of sympathetic transmitter from the spleen of the cat,” *J. Physiol.*, vol. 138, no. 1, pp. 81–102, Aug. 1957.

[36] T. Bradley and P. Hjemdahl, “Renal extraction of endogenous and radiolabelled catecholamines in the dog,” *Acta Physiol. Scand.*, vol. 126, no. 4, pp. 505–510, Apr. 1986.

[37] S. Akselrod, D. Gordon, J. B. Madwed, N. C. Snidman, D. C. Shannon, and R. J. Cohen, “Hemodynamic regulation: investigation by spectral analysis,” *Am. J. Physiol.*, vol. 249, no. 4 Pt 2, pp. H867-875, Oct. 1985.

[38] A. Malliani, M. Pagani, F. Lombardi, and S. Cerutti, “Cardiovascular neural regulation explored in the frequency domain,” *Circulation*, vol. 84, no. 2, pp. 482–492, Aug. 1991.

[39] D. S. Goldstein, “Clinical assessment of catecholaminergic function,” *Stress Catecholamines Cardiovasc. Dis. N. Y. Oxf. Univ. Press*, pp. 234–286, 1995.

[40] S. L. Marple, *Digital Spectral Analysis: With Applications*. Englewood Cliffs, N.J: Prentice Hall, 1987.

[41] D. Robertson, G. A. Johnson, R. M. Robertson, A. S. Nies, D. G. Shand, and J. A. Oates, "Comparative assessment of stimuli that release neuronal and adrenomedullary catecholamines in man.," *Circulation*, vol. 59, no. 4, pp. 637–643, Apr. 1979.

[42] M. A. Sanchez-Gonzalez, R. W. May, A. P. Koutnik, M. Kabbaj, and F. D. Fincham, "Sympathetic Vasomotor Tone Is Associated With Depressive Symptoms in Young Females: A Potential Link Between Depression and Cardiovascular Disease," *Am. J. Hypertens.*, vol. 26, no. 12, pp. 1389–1397, Dec. 2013.

[43] E. S. Prakash, Madanmohan, K. R. Sethuraman, and S. K. Narayan, "Cardiovascular autonomic regulation in subjects with normal blood pressure, high-normal blood pressure and recent-onset hypertension," *Clin. Exp. Pharmacol. Physiol.*, vol. 32, no. 5–6, pp. 488–494, May 2005.

[44] Y.-P. Liu, Y.-H. Lin, Y.-C. Chen, P.-L. Lee, and C.-S. Tung, "Spectral analysis of cooling induced hemodynamic perturbations indicates involvement of sympathetic activation and nitric oxide production in rats," *Life Sci.*, vol. 136, pp. 19–27, Sep. 2015.

[45] L. D. DeBeck, S. R. Petersen, K. E. Jones, and M. K. Stickland, "Heart rate variability and muscle sympathetic nerve activity response to acute stress: the effect of breathing," *Am. J. Physiol. Regul. Integr. Comp. Physiol.*, vol. 299, no. 1, pp. R80-91, Jul. 2010.

[46] Z. B. Moses, L. J. Luecken, and J. C. Eason, "Measuring task-related changes in heart rate variability," *Conf. Proc. Annu. Int. Conf. IEEE Eng. Med. Biol. Soc. IEEE Eng. Med. Biol. Soc. Annu. Conf.*, vol. 2007, pp. 644–647, 2007.

[47] J. P. Florian, E. E. Simmons, K. H. Chon, L. Faes, and B. E. Shykoff, "Cardiovascular and autonomic responses to physiological stressors before and after six hours of water immersion," *J. Appl. Physiol. Bethesda Md 1985*, vol. 115, no. 9, pp. 1275–1289, Nov. 2013.

[48] E. S. Mezzacappa, R. M. Kelsey, and E. S. Katkin, "Breast feeding, bottle feeding, and maternal autonomic responses to stress," *J. Psychosom. Res.*, vol. 58, no. 4, pp. 351–365, Apr. 2005.

[49] G. H. Prystav, "Electrodermal, Cardiac, and Respiratory Activity to Repeated Cold Pressor Stimulation in Drug Addicts," *J. Gen. Psychol.*, vol. 94, no. 2, pp. 259–270, Apr. 1976.

[50] I. C. Cozza *et al.*, "Physical exercise improves cardiac autonomic modulation in hypertensive patients independently of angiotensin-converting enzyme inhibitor treatment," *Hypertens. Res. Off. J. Jpn. Soc. Hypertens.*, vol. 35, no. 1, pp. 82–87, Jan. 2012.

[51] Y. Takimoto, K. Yoshiuchi, T. Ishizawa, Y. Yamamoto, and A. Akabayashi, "Autonomic dysfunction responses to head-up tilt in anorexia nervosa," *Clin. Auton. Res. Off. J. Clin. Auton. Res. Soc.*, vol. 24, no. 4, pp. 175–181, Aug. 2014.

[52] E. Gil, M. Orini, R. Bailon, J. M. Vergara, L. Mainardi, and P. Laguna, "Time-varying spectral analysis for comparison of HRV and PPG variability during tilt table test," *Conf. Proc. Annu. Int. Conf. IEEE Eng. Med. Biol. Soc. IEEE Eng. Med. Biol. Soc. Annu. Conf.*, vol. 2010, pp. 3579–3582, 2010.

[53] A. McGrady, C. Kern-Buell, E. Bush, S. Khuder, and B. P. Grubb, "Psychological and physiological factors associated with tilt table testing for neurally mediated syncopal syndromes," *Pacing Clin. Electrophysiol. PACE*, vol. 24, no. 3, pp. 296–301, Mar. 2001.

[54] J. W. Williamson, R. McColl, and D. Mathews, “Evidence for central command activation of the human insular cortex during exercise,” *J. Appl. Physiol. Bethesda Md 1985*, vol. 94, no. 5, pp. 1726–1734, May 2003.

[55] W. Wieling, J. F. van Brederode, L. G. de Rijk, C. Borst, and A. J. Dunning, “Reflex control of heart rate in normal subjects in relation to age: a data base for cardiac vagal neuropathy,” *Diabetologia*, vol. 22, no. 3, pp. 163–166, Mar. 1982.

[56] G. R. H. Sandercock, P. D. Bromley, and D. A. Brodie, “The reliability of short-term measurements of heart rate variability,” *Int. J. Cardiol.*, vol. 103, no. 3, pp. 238–247, Sep. 2005.

[57] A. Garafova, A. Penesova, E. Cizmarova, A. Marko, M. Vlcek, and D. Jezova, “Cardiovascular and sympathetic responses to a mental stress task in young patients with hypertension and/or obesity,” *Physiol. Res. Acad. Sci. Bohemoslov.*, vol. 63 Suppl 4, pp. S459-467, 2014.

[58] Z. Visnovcova *et al.*, “Complexity and time asymmetry of heart rate variability are altered in acute mental stress,” *Physiol. Meas.*, vol. 35, no. 7, pp. 1319–1334, Jul. 2014.

[59] J. P. Delaney and D. A. Brodie, “Effects of short-term psychological stress on the time and frequency domains of heart-rate variability,” *Percept. Mot. Skills*, vol. 91, no. 2, pp. 515–524, Oct. 2000.

[60] G. Bohlin, “Delayed habituation of the electrodermal orienting response as a function of increased level of arousal,” *Psychophysiology*, vol. 13, no. 4, pp. 345–351, Jul. 1976.

[61] T. P. Zahn, J. L. Rapoport, and C. L. Thompson, “Autonomic effects of dextroamphetamine in normal men: implications for hyperactivity and schizophrenia,” *Psychiatry Res.*, vol. 4, no. 1, pp. 39–47, Feb. 1981.

[62] Y. Zhong *et al.*, “Autonomic nervous nonlinear interactions lead to frequency modulation between low- and high-frequency bands of the heart rate variability spectrum,” *Am. J. Physiol. Regul. Integr. Comp. Physiol.*, vol. 293, no. 5, pp. R1961-1968, Nov. 2007.

Chapter 5: Electrodermal Activity Suggests a Change in Frequencies of Sympathetic Control During Exercise

(Posada-Quintero, H. F., Reljin, N., Mills, C., Mills, I., Florian, J. P., VanHeest, J. & Chon, K. H. Electrodermal Activity Suggests a Change in Frequencies of Sympathetic Control During Exercise. American Journal of Physiology - Exercise. Submitted)

5.1 Introduction

Traditionally, two frequency bands are considered in the spectral analysis of HRV during stationary conditions: high frequency (HF) band (0.15 to 0.4 Hz), for which the parasympathetic nervous system activity is the major contributor [1], [2]; and low frequency (LF) band (0.045 to 0.15 Hz), whose interpretation is more complex, but it has been demonstrated that it reflects both sympathetic and parasympathetic influences [1], [3]. Intuitively the LF and HF bands should increase with exercises as the heart rates are higher, however, the precise frequency bandwidths are not well established. Previous studies have shown inconsistent results if the prescribed bands of frequencies associated with the ANS are kept unmodified during exercises [4]–[7]. Other studies have made attempts to characterize the sympathetic and parasympathetic dynamics during exercises, especially taking into account influences of higher respiratory rates and other physiological effects of physical activity [8]–[11]. In particular, adjustments to the original HF band were made, either by extending the upper frequency bound (originally 0.4Hz) to about 1.2Hz to 1.5Hz, or defining HF as a time-varying or constant bandwidth around respiratory frequency, but LF bandwidth was fixed at the stationary prescribed range [8], [9], [11]–[18]. The LF bandwidth during exercise is difficult to establish due to the nature of the HRV as it is not able to separate contributions of the sympathetic and parasympathetic dynamics.

We hypothesize that the frequency bandwidth of the sympathetic dynamics should also be modified under physical activity. Exploring this hypothesis has been technically difficult using only HRV because

the increase in the upper frequency bound of LF band can potentially result in the overlap of the frequencies associated with the parasympathetic tone in the HF portion of the HRV spectrum [19]. Moreover, given that the LF band consists of both parasympathetic and sympathetic tones, it is not clear if the frequency range needs to be adjusted to higher frequencies or remain the same for exercise conditions. Given these scenarios, a novel approach is needed to overcome these limitations of HRV.

Electrodermal activity (EDA) has recently garnered interest as an alternative to HRV for assessing sympathetic dynamics given that sweat glands are only innervated by sympathetic nerves. EDA as a reflection of autonomic innervation of sweat glands [20], has shown strong correlation to sweat production, and is thought to provide a quantitative functional measure of sudomotor activity [21], [22]. EDA is technically defined as a measure of the changes in electrical conductance of the skin. In a recent studies, we have used power spectral density (PSD) and time-varying spectral analysis of EDA to obtain information of sympathetic arousal. We found that dynamics of the sympathetic dynamics estimated from the EDA signal under non-exercise conditions were found to be in the low-frequency range, from 0.045 to 0.25 Hz, when subjects underwent stress invoking tests [23, p.], [24]. This frequency range is similar to HRV's LF band albeit the upper limit frequency of 0.25 Hz from EDA is higher than 0.15 Hz. Hence, to test the ANS under physical activity, specifically the possible shifting of the frequency band of sympathetic tone to higher frequencies, we conducted submaximal physical tests on a treadmill and data collection of both electrocardiogram and EDA signals from healthy subjects.

5.2 Materials and Methods

5.2.1 Protocol

Subjects for which exercise represents a low risk level, based on standardized guidelines from the American College of Sports Medicine (ACSM) [25], were asked to participate in the study. Eighteen healthy subjects, 11 males and 7 females, age 21 ± 3 years old were enrolled. Participants were asked to avoid caffeine and alcohol during the 48 hours preceding the test, and were instructed to fast for at least 3 h before testing. The study was conducted in a quiet, comfortable room (ambient temperature, 26-27 °C,

and a relative humidity between 30-50%). All participants signed a consent form approved by the Institutional Review Board of UConn.

Before the exercise test begun, the subjects were asked to lay in the supine position for 5 min to procure hemodynamic stabilization. ECG and EDA were measured simultaneously for each subject throughout the whole experiment. HP ECG monitor (HP 78354A) and GSR ADInstruments module were used. Three hydrogel Ag-AgCl electrodes were employed for ECG signals collection on the torso, placed on the shoulders and lower left rib. In addition, a pair of stainless steel electrodes were placed on index and middle fingers to collect EDA signal. The skin was cleaned with alcohol before placing the ECG and EDA electrodes. All leads were taped to subject's skin using latex-free tape, to avoid movement of the cables, which can corrupt the signals. All signals were acquired through the ADInstruments analog-to-digital converter, and a compatible PowerLab software, while sampling frequency was fixed to 400 Hz for all signals. Participants were asked to wear their own active wear/gym clothes during the protocol with the shirt covering the electrodes and cables during the experiment.

Experimental protocol resembles the procedure utilized in [8] (sketched in table 1). Notice that this study involves only moderate intensity physical activity, as the stopping criteria is achieving 85% of subjects' maximal heart rate (HRmax). Subjects were first monitored for 5 min at rest (supine, without any movement or talking) to measure resting heart rate (HR) and EDA. The subjects then performed an incremental test on a motorized treadmill (Life Fitness F3), reaching 85% of their HRmax, calculated from the equation [25]:

$$HR_{max} = 206.9 - (0.67 * age),$$

The incremental running began with an initial warm-up walking at 3mi/h (about 4.82 km/h). Then the speed was increased to 5 mi/h (about 8 km/h) and increased 0.6 mi/h (about 1 km/h) every minute until the subjects were stopped due to reaching 85% of their HRmax. Thereafter, subjects were required to remain running at 5mi/h (about 8 km/h) for another 4 min to start the recovering phase, followed by walking at 3mi/h (about 4.82 km/h) for 5 minutes and a final 10 min (or more if needed to achieve baseline HR) period

Table 5.1 Experimental protocol.

Action (details)	Speed	Duration
Rest (supine)		5 min
Warm up (walking)	3 mi/h (~4.82km/h)	5 min
Running	5 mi/h (~8 km/h)	1 min
Running (until the subjects stopped due to reaching 85% of their HRmax)	+ 0.6 mi/h (+ ~1km/h)	Every 1 min
Running (recovery starts)	5 mi/h (~8 km/h)	4 min
Recovery (walking)	3 mi/h (~4.82km/h)	5 min
Rest (supine)		10 min

in the supine position to procure adequate recovering. The duration of the experiment lasted approximately one hour.

5.2.2 Signal processing

Time-invariant and time-variant spectral analysis have been employed recently on EDA data [23, p.], [24]. The criteria to define the maximum frequency (Fmax) or the upper frequency bound of the sympathetic components of EDA is to find a frequency greater than Fmax such that the integration of the spectral power from it to Fs/2 (half of sampling frequency or the Nyquist's frequency) consists of less than 5% of the total power. Using this criterion, our previous time-invariant and time-varying analyses found that in the non-exercise conditions, the upper bound or Fmax was found to be 0.25 Hz. Similarly, in this study, we analyzed Fmax for all subjects, to test the effects of physical activity on the possible increase of spectral power for frequencies beyond 0.25 Hz.

We define six exercise stages of data collection: stage 1, subjects are lying down on their back, labeled "supine"; stage 2, the subject is asked to move to the treadmill, named "going-to-walk"; stage 3, subject starts moving on the treadmill, called "walking"; subject has been walking on the treadmill at 3 mi/h for three minutes, the "end-of-walking"; speed is set to 5 mi/h and the increasing test starts, labeled "running"; and finally subject is running "at-85%-HRmax". Two-minute segments of every stage were utilized for data analysis.

Using these various exercise stage signals, we tested how Fmax evolves under the exercise protocol using both time-invariant and time-varying approaches. The time-invariant power spectra of EDA signals were calculated using Welch's periodogram method with 50% data overlap. A Blackman window (length of 128 points) was applied to each segment, the Fast Fourier Transform was calculated for each windowed segment, and the power spectra of the segments were averaged.

To compute the time-frequency representation (TFR) of EDA we employed the variable frequency complex demodulation (VFCDM), a time-frequency spectral (TFS) analysis technique that provides accurate amplitude estimates and one of the highest time-frequency resolutions. The technique has been previously described [26], [27]. We used the instantaneous spectral estimate for every time point of the TFR to compute an Fmax series. We averaged the Fmax series over the time segments defined previously for the six stages.

To test the differences on Fmax between stages we have utilized the Dunn's test, a non-parametric pairwise multiple comparisons procedure based on rank sums, often used as a "post hoc" procedure

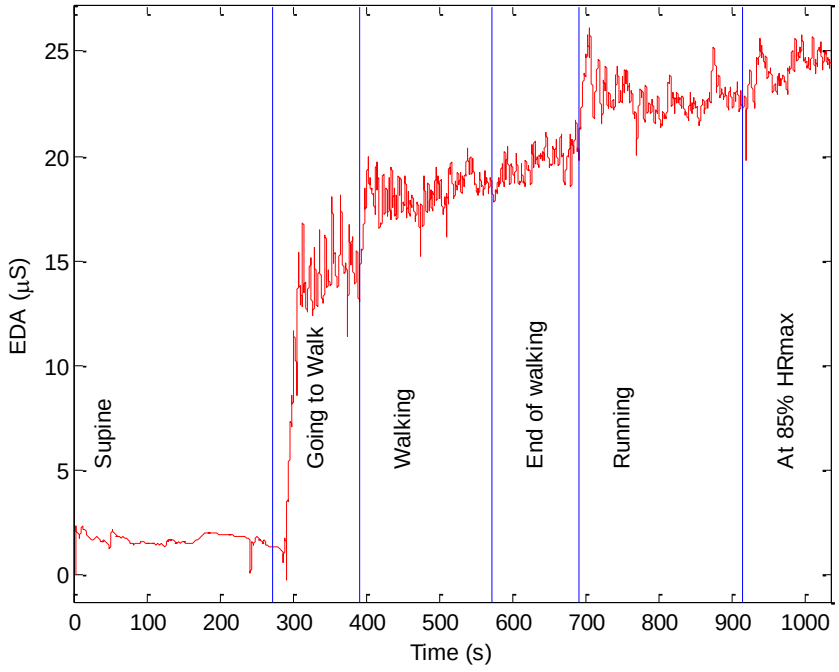

Figure 5.1 – Raw EDA signal for a given subject throughout different body positions and exercise conditions.

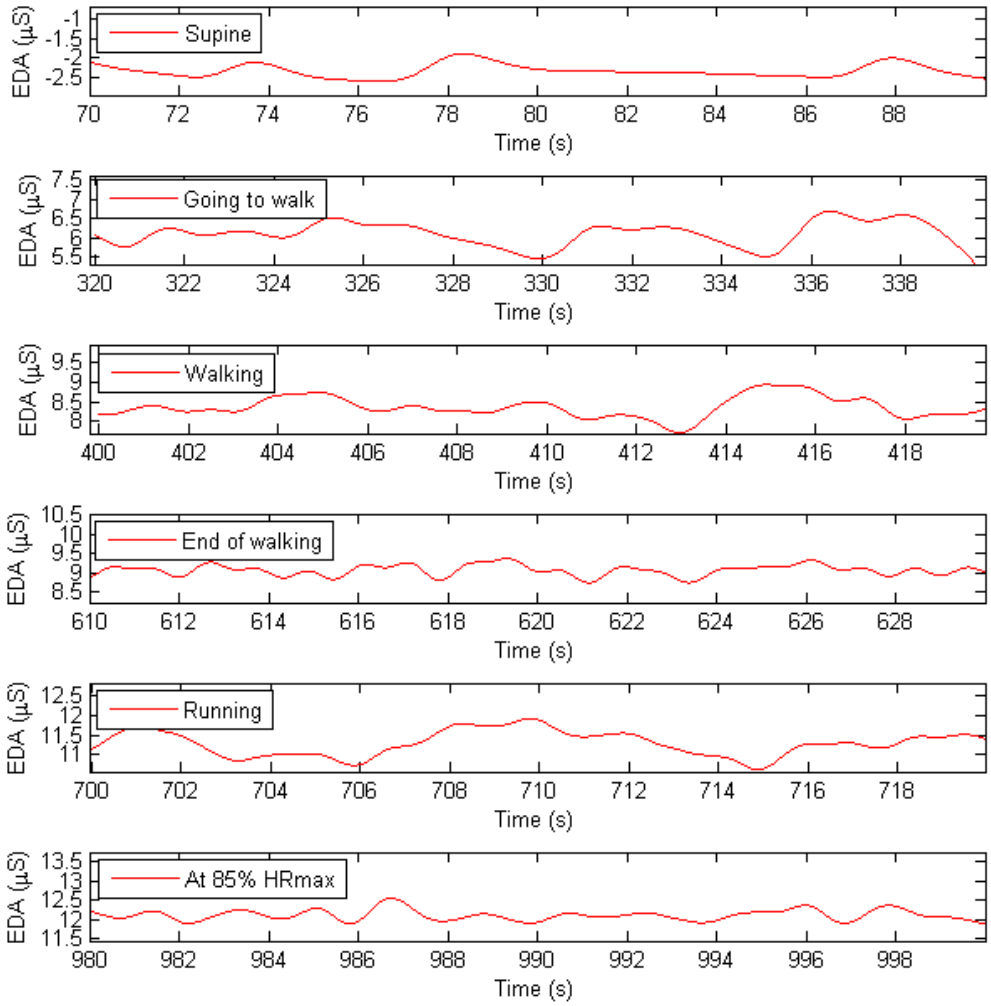

Figure 5.2 – Twenty seconds of raw EDA for a given subject during different events. Note the high-frequency oscillations increase with exercise intensity.

following rejection of a Kruskal–Wallis test. As such, it is a non-parametric analog to multiple pairwise t-tests following rejection of an ANOVA null hypothesis [28].

5.3 Results

This section comprises the results of this study, including a general description of the signals obtained during the experiment, their main characteristics, the parameter computed using spectral analysis, and the statistical analysis carried out to evaluate the significance of the results.

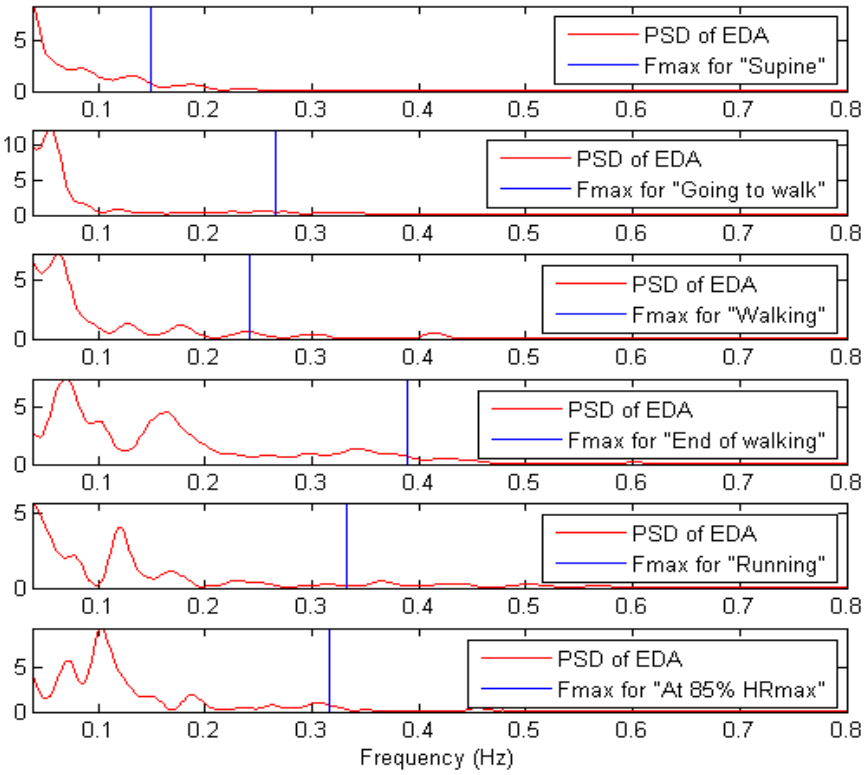

Figure 5.3 – Power spectral density of EDA for a given subject during different events and computed Fmax (to account for 95% of the total power). Fmax values increase concomitantly with exercise intensity.

Figure 5.1 shows the EDA signal for a representative subject, showing the time progression from lying on the table until the moment the heart rate reached 85% of HRmax. The EDA signal's dynamics as shown in Figure 5.1 were found to be similar for all subjects. Changes in the conduction levels of EDA, termed skin conductance level (SCL) in the literature [29], are seen with the progression of various exercise stages. For example, for this subject in the supine posture, the SCL is low, with an immense increase in conductance when the subject stood up to go to the treadmill. There is also a considerable increase in SCL when the subject started walking. The mean conductance level tends to increase during exercise (walking and running). Lines in the Figure 5.1 denote the time when the subject started walking and running, respectively.

Table 5.2 Fmax (Hz) for different stages.

	Time-invariant analysis	Time-varying analysis
Supine	0.11 ± 0.07	0.11 ± 0.07
Going to walk	0.16 ± 0.12	0.14 ± 0.08
Walking	0.22 ± 0.12	0.22 ± 0.08
End of walking	0.28 ± 0.09	0.27 ± 0.07
Running	0.27 ± 0.12	0.31 ± 0.12
At 85% HRmax	0.31 ± 0.15	0.37 ± 0.11

Values are mean ± standard deviation

In addition to the increase in conductance level, there is also an increase in high-frequency components, as shown in Figure 5.2. A good indicator of the quality of the EDA signals is the smoothness of the raw waveform [29]. These waves are called skin conductance responses (SCRs). Since these SCRs

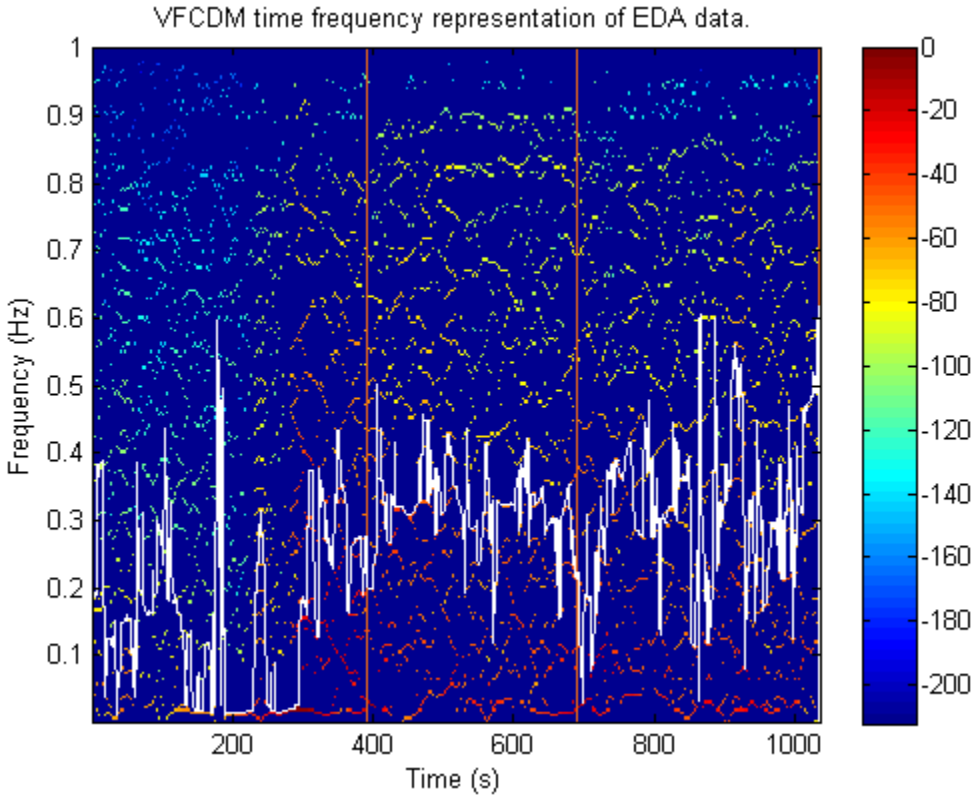

Figure 5.4 – Time-frequency representation of EDA for a given subject. Red lines demarcate when the subject started walking and running. Instantaneous Fmax (white line) is computed for each time point.

we obtain in this experiment are not due to any specific instantaneous stimuli, in contrast to startle-like experiments, they are called non-specific skin conductance responses (NS.SCRs). Note that the occurrence of NS.SCRs is more frequent when the intensity of the exercise is increased. Although NS.SCRs have been traditionally quantified in time domain, by counting them and providing an index of number of NS.SCR's per unit of time, these high-frequency oscillations have shown to be an even more sensitive index of sympathetic arousal when analyzed in the frequency or time-frequency domain [23], [24].

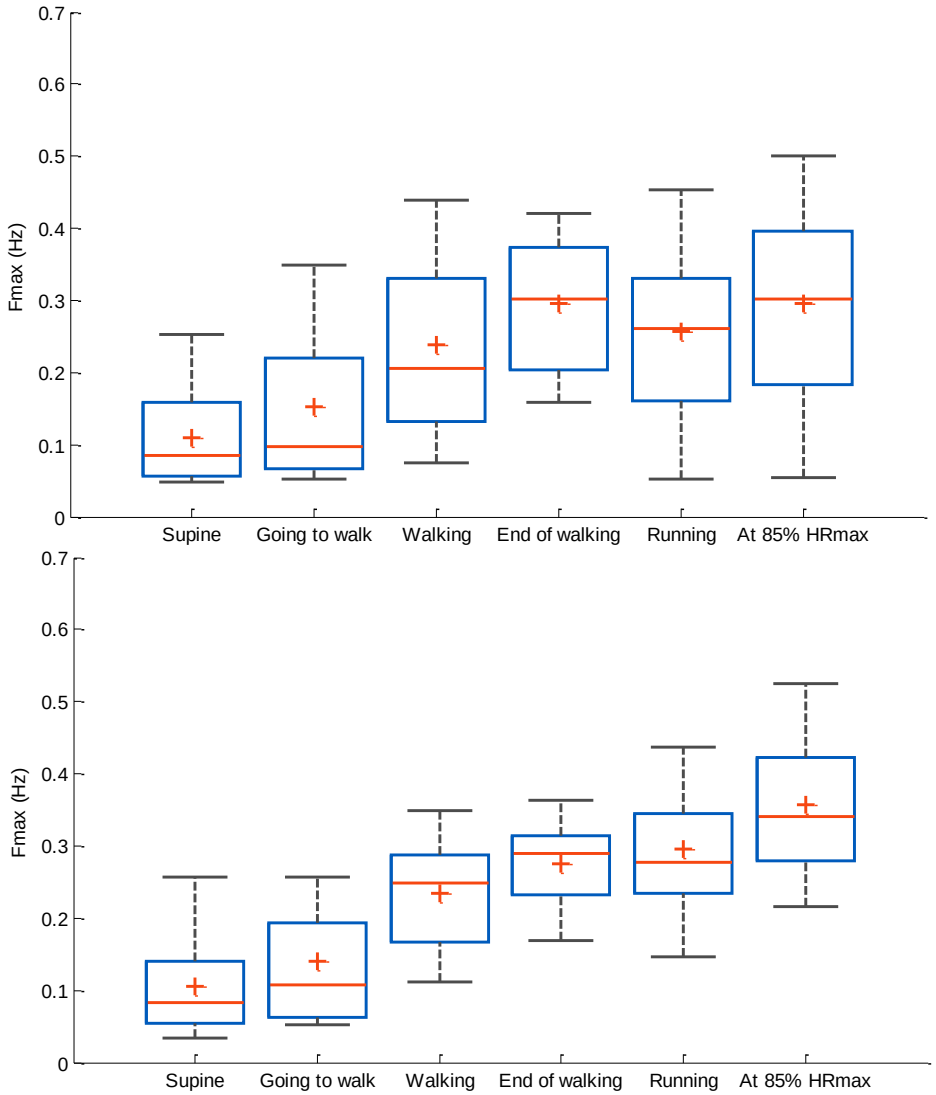

Figure 5.5 – Box plots for estimated Fmax for all exercise stages and subjects using time-invariant (top panel) and time-varying (bottom panel) approaches.

Table 5.3 Summary of Dunn's test for time-invariant and time-varying analysis

	Time-invariant					Time-variant				
	Going to walk	**Walking**	**End of walking**	**Running**	**At 85% HRmax**	**Going to walk**	**Walking**	**End of walking**	**Running**	**At 85% HRmax**
Supine	0	0	**1**	0	**1**	0	0	**1**	**1**	**1**
Going to walk	-	0	**1**	0	**1**	-	0	**1**	**1**	**1**
Walking	-	-	0	0	0	-	-	0	0	0
End of walking	-	-	-	0	0	-	-	-	0	0
Running	-	-	-	-	0	-	-	-	-	0

"1" indicates statistical significance $p < 0.05$. Left: results using time-invariant spectra (power spectral density); Right: results using time-varying analysis (time-frequency representation). Time-varying analysis provided a more clear difference on Fmax between the higher-intensity exercise and the lower levels of physical activity.

Power spectra of EDA signal segments were computed for all subjects and for every exercise stages. For each spectrum the Fmax was computed and is noted as the blue vertical line. Figure 5.3 includes representative results for one subject. For this representative subject, when the subject is at the supine posture, most of the spectral power is concentrated in the very-low frequency range. As the subject stands up (the second panel: "going to walk"), the Fmax is increased to about 0.25 Hz. After the subject has walked for about 5 minutes, spectral power shifts towards higher frequencies, reaching an Fmax value of about 0.35 Hz to 0.4 Hz; these frequencies do not shift higher for greater exercise intensities.

For the time-varying approach [27], instantaneous Fmax was computed for every time point. Figure 5.4 shows an example of how higher-frequency power is increased over time. Red and yellow lines are more visible as the subject undergoes to a walk and run, and the Fmax (shown as white line in Figure 5.4) moves upward.

Table II includes the results for Fmax for both time-invariant and time-varying analysis. Both approaches show an increase of Fmax for higher exercise intensities. The Fmax was lower during the running period when compared to the supine stage. Figure 5.5 consists of the box plot for the estimates of Fmax using time-invariant and time-varying approaches. Mean value of Fmax is stable for the first two

stages, then increases to a medium level when subjects start walking, and finally increases to a value between 0.3 to 0.4 Hz when subjects undergo higher-intensity exercises.

Table III shows the outcome of Dunn's test. These results suggest an increase in Fmax at higher intensities of exercise, starting when the subjects have walked for about 5 minutes, until the subjects are running at 85% of their HRmax. No statistical differences were found between stages one, two and three (supine, going to walk and walking) using either approach. PSD showed differences on Fmax between the time the subjects were walking before starting to run and the time the subjects were running at 85% of their HRmax, compared to the supine stage and right before subjects were going to walk. As mentioned, time-invariant PSD approach's estimated Fmax during the running stage is lower than the preceding stage (end of walking), resulting in non-significant difference when compared to end of walking stage.

The TFR approach was able to find differences more consistently for the three highest levels of physical activity, compared to the first two stages. This suggests that Fmax is significantly higher at the time the subjects have walked for about 5 minutes to any level of exercise, compared to the very low and

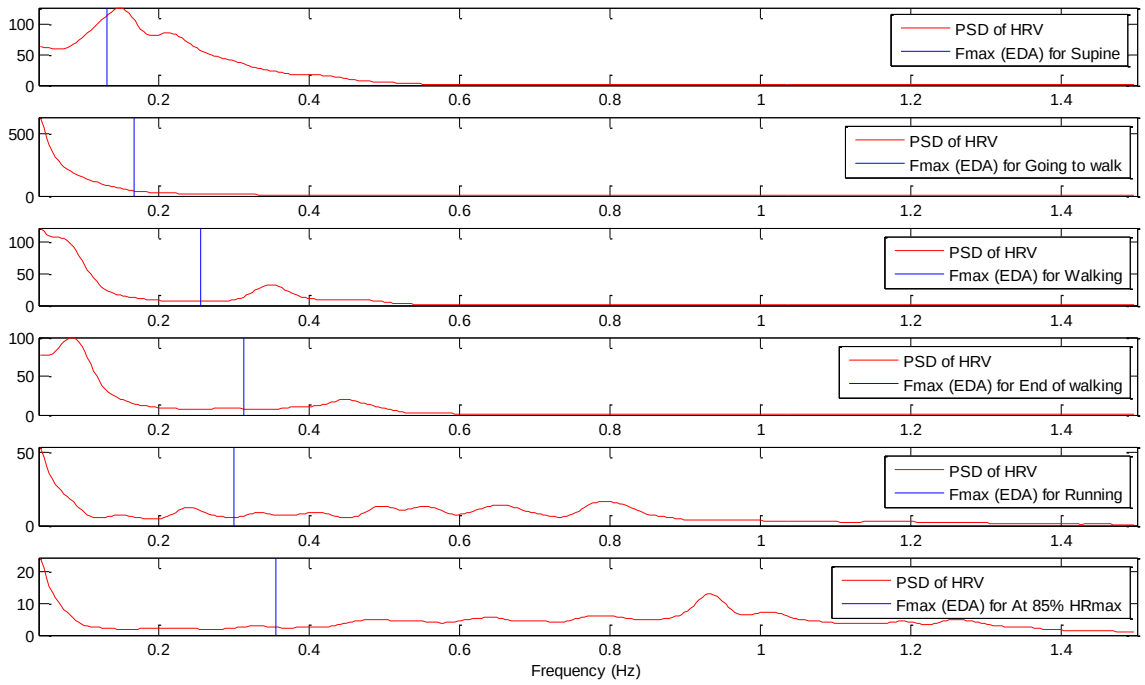

Figure 5.6 – Ensemble average of power spectral density of HRV during different events. Vertical lines are Fmax values computed via EDA. Note that Fmax is an estimation of the upper bound of LF band.

medium levels of exercise. The stage when the subject was starting to walk showed some increase on Fmax, but such increase was not significant.

Figure 5.6 shows averaged PSD of HRV derived from surface ECG obtained from 18 subjects during various body positions and exercise conditions. The vertical dotted lines in Figure 5.6 represent Fmax values determined from EDA. Note the shift of the respiratory rates to higher frequencies concomitant to the increased levels of exercise difficulty. When accounting for the respiratory frequencies in Figure 5.6, we observe that the Fmax demarcation lines are good approximations of the LF dynamics of the HRV derived from ECG. This result lends support to the following two observations. First, we observe that the sympathetic dynamics do shift to higher frequencies as the level of strenuous exercise increases. Second, the EDA derived upper frequency bounds, Fmax values, are good surrogate measures of the LF dynamics of the ECG derived HRV. Hence, when only the HRV values are available (e.g., no EDA data), our derived Fmax bounds from EDA may be confidently used as the demarcation of the upper limit of the sympathetic dynamics.

5.4 Discussion

We have found evidence of an increase of the maximum frequency of the sympathetic tone concomitant with the exercise intensities, termed Fmax, based on both time-invariant and time-varying spectral analysis of EDA, albeit more significant shifts were found with the latter approach. The implications of the current finding are twofold. First, the current practice of fixed frequency band of 0.04-0.15 Hz, termed, the low frequency via HRV analysis of RR intervals for all conditions can lead to inaccurate capture of the sympathetic dynamics especially during exercise conditions. Second, Fmax values obtained via EDA can be used as a good surrogate measure of the sympathetic dynamics even for HRV analysis. In other words, it is our view that even when EDA signals are not available, the derived Fmax from our study can be reliably used as the upper bound of the LF range of the HRV analysis based on RR intervals derived from electrocardiogram signals.

The relative role of the two branches of the ANS depends on the exercise intensity [30], [31]. In resting conditions, heart rate fluctuations are driven by homeostatic cardiovascular control systems [32]–[34]. On the contrary for the exercise condition, heart rate increases to a steady-state value due to both parasympathetic withdrawal and augmented sympathetic activity. However, HRV has shown to be an inconsistent means to assess sympathetic and parasympathetic tone especially during exercise conditions. For example, there have been reports of an unexpected decrease of HRVLF during exercise of high intensity [7], [10], [35], [36]. Some studies have proposed saturation of the sympathetic activity during physical activity of high intensity as a possible cause [36], [37]. In simulated data, a group of researchers indicated that the cause for the reduction of HRVLF and HRVHF with high-intensity exercise was likely due to the decrease of the mean heartbeat variability which would consequently result in decreased spectral power of HRV [38].

HRVHF (0.15 to 0.4 Hz) is widely accepted to be a measure of the parasympathetic activity at resting conditions [33]. Given that respiratory frequency is not restricted to the fixed frequency range during exercise, studies have been conducted to redefine the HRVHF band [8], [9], [11]–[18]. HRVHF band has been extended to include the entire physiologically relevant range of respiratory frequencies [39], [40], or centered on the respiratory frequency with a constant or time-dependent bandwidth [40], [41, p.], [42]–[44]. However, none of the referenced studies above, have adjusted HRVLF bound, mainly because HRV cannot separate dynamics of the sympathetic and parasympathetic dynamics in the low frequency range [19], [45]. The consequence of this is perhaps even greater inaccuracy of purported representation of the sympathetic dynamics in the LF as we show in Figure 5.3 and Figure 5.6, the sympathetic dynamics' upper frequency band does shift to higher frequencies with increasing exercise intensities.

In this study we used EDA to evaluate the sympathetic function under exercising conditions, as EDA represents only the sympathetic activity. We encountered no significant difference between the walking and the supine posture conditions. This is in agreement with the literature [31], because it has been reported that during mild exercise intensities heart rate rises primarily by a decrease on parasympathetic activity, whereas the increase in the sympathetic tone is minimal. With medium and high exercise intensity

the sympathetic tone also contributes to the cardiac acceleration [31]. We have found that such increase on the sympathetic tone, due to high-intensity exercise, is noticeable and statistically significant on the EDA signal.

The sympathetic dynamics' upper frequency bound shifted higher to 0.25 Hz when subject transitioned from supine to upright and started walking (Table II) stages. The walking stage corresponds to low-intensity exercise, where the main contribution of the ANS is the result of withdrawal of the parasympathetic tone. In our previous study using EDA, we found that the sympathetic control was confined to the range 0.045 to 0.25 Hz, when subject underwent cold pressor test, tilt table test, cognitive stress and orthostatic stress [23], [24]. It can be noted that low-intensity exercise produces similar sympathetic tone as seen with various stressor induced in our previous study [23]. When subjects undergo moderate stress, (e.g., after the subject was walking on the treadmill for 5 minutes), the increase of Fmax was found to be significant with respect to the first two stages (supine and going to walk). The upper frequency bound in this stage was located around 0.3 to 0.35 Hz. When the subjects went for running (not at 85% of HRmax), we did not observe Fmax shifting higher than 0.35 Hz. However, the mean Fmax increased to about 0.4 Hz when subjects were running at 85% of HRmax, but such increase was not significant compared to the previous two stages. These last three stages of moderate and high-intensity exercise are characterized by the increase of the sympathetic tone, however we found that the dynamics of the sympathetic tone also moved towards frequencies of 0.35 to 0.4 Hz.

The time-domain measures of EDA, e.g. SCL and NS.SCRs, are commonly utilized as markers of sympathetic arousal in response to tonic stimuli [29]. However, computing NS.SCRs relies on either manual or automatic SCR detection, which is usually more cumbersome and time consuming. Furthermore, these measures are highly variable and less sensitive than indices based on frequency or time-frequency analysis of EDA [23], [23], [24], [46]. More importantly, these measures do not provide dynamic characteristics of the ANS.

5.5 Perspectives and Significance

Spectral analysis of EDA can lead to a better understanding of the effect of physical exercise on humans and their autonomic nervous system. EDA, possibly along with HRV, could be extended to other studies to better characterize and discriminate dynamics of the autonomic nervous system that may be indicative of fatigue, stress or exercise intolerance. An accurate understanding of the autonomic nervous system's dynamics under exercise can lead to better guidance and interventions to improve human health and performance.

5.6 Conclusion

Previous studies have shown that in resting conditions most of the sympathetic spectral power of EDA is confined to a similar frequency band as that of HRVLF. In this study, we have found that when subjects undergo moderate to high-intensity exercises, the upper band of the sympathetic dynamics shift to 0.35 to 0.4 Hz. Moreover, we found that the low frequency bounds derived via EDA can be good surrogate measures of the sympathetic dynamics especially during moderate to high-intensity exercises, hence, the upper bound of HRVLF needs to shift to higher frequencies. The varying upper frequency band of the sympathetic dynamics to be taken into account to provide a better understanding on the functioning of the branches of autonomic nervous system especially under high-intensity physical activity.

5.7 References

[1] S. Akselrod, D. Gordon, F. A. Ubel, D. C. Shannon, A. C. Berger, and R. J. Cohen, "Power spectrum analysis of heart rate fluctuation: a quantitative probe of beat-to-beat cardiovascular control," *Science*, vol. 213, no. 4504, pp. 220–222, Jul. 1981.

[2] B. Pomeranz *et al.*, "Assessment of autonomic function in humans by heart rate spectral analysis," *Am. J. Physiol.*, vol. 248, no. 1 Pt 2, pp. H151-153, Jan. 1985.

[3] M. L. Appel, R. D. Berger, J. P. Saul, J. M. Smith, and R. J. Cohen, "Beat to beat variability in cardiovascular variables: noise or music?," *J. Am. Coll. Cardiol.*, vol. 14, no. 5, pp. 1139–1148, Nov. 1989.

[4] L. Bernardi *et al.*, “Evidence for an intrinsic mechanism regulating heart rate variability in the transplanted and the intact heart during submaximal dynamic exercise?,” *Cardiovasc. Res.*, vol. 24, no. 12, pp. 969–981, Dec. 1990.

[5] Y. Nakamura, Y. Yamamoto, and I. Muraoka, “Autonomic control of heart rate during physical exercise and fractal dimension of heart rate variability,” *J. Appl. Physiol. Bethesda Md 1985*, vol. 74, no. 2, pp. 875–881, Feb. 1993.

[6] O. Rimoldi *et al.*, “Analysis of neural mechanisms accompanying different intensities of dynamic exercise,” *Chest*, vol. 101, no. 5 Suppl, p. 226S–230S, May 1992.

[7] Y. Yamamoto, R. L. Hughson, and J. C. Peterson, “Autonomic control of heart rate during exercise studied by heart rate variability spectral analysis,” *J. Appl. Physiol. Bethesda Md 1985*, vol. 71, no. 3, pp. 1136–1142, Sep. 1991.

[8] R. Bailón, N. Garatachea, I. de la Iglesia, J. A. Casajús, and P. Laguna, “Influence of running stride frequency in heart rate variability analysis during treadmill exercise testing,” *IEEE Trans. Biomed. Eng.*, vol. 60, no. 7, pp. 1796–1805, Jul. 2013.

[9] R. Bailón, G. Laouini, C. Grao, M. Orini, P. Laguna, and O. Meste, “The integral pulse frequency modulation model with time-varying threshold: application to heart rate variability analysis during exercise stress testing,” *IEEE Trans. Biomed. Eng.*, vol. 58, no. 3, pp. 642–652, Mar. 2011.

[10] R. Perini, C. Orizio, G. Baselli, S. Cerutti, and A. Veicsteinas, “The influence of exercise intensity on the power spectrum of heart rate variability,” *Eur. J. Appl. Physiol.*, vol. 61, no. 1–2, pp. 143–148, 1990.

[11] M. P. Tulppo, T. H. Mäkikallio, T. Seppänen, R. T. Laukkanen, and H. V. Huikuri, “Vagal modulation of heart rate during exercise: effects of age and physical fitness,” *Am. J. Physiol.*, vol. 274, no. 2 Pt 2, pp. H424-429, Feb. 1998.

[12] A. Benítez *et al.*, “Ventilatory threshold prediction by spectral analysis of heart rate variability in incremental maximal tests,” in *Computing in Cardiology, 2010*, 2010, pp. 939–942.

[13] G. Blain, O. Meste, T. Bouchard, and S. Bermon, “Assessment of ventilatory thresholds during graded and maximal exercise test using time varying analysis of respiratory sinus arrhythmia,” *Br. J. Sports Med.*, vol. 39, no. 7, pp. 448-452-452, Jul. 2005.

[14] F. Cottin, C. Médigue, P. Lopes, P.-M. Leprêtre, R. Heubert, and V. Billat, “Ventilatory thresholds assessment from heart rate variability during an incremental exhaustive running test,” *Int. J. Sports Med.*, vol. 28, no. 4, pp. 287–294, Apr. 2007.

[15] M. J. Gaitan-Gonzalez, S. Carrasco-Sosa, R. Gonzalez-Camarena, and O. Yanez-Suarez, “Non-linear relationship between heart period and root mean square of successive differences during ramp exercise and early recovery,” in *Computers in Cardiology, 2005*, 2005, pp. 727–730.

[16] K. Martinmäki, K. Häkkinen, J. Mikkola, and H. Rusko, “Effect of low-dose endurance training on heart rate variability at rest and during an incremental maximal exercise test,” *Eur. J. Appl. Physiol.*, vol. 104, no. 3, pp. 541–548, Oct. 2008.

[17] O. Meste, G. Blain, and S. Bermon, “Analysis of the respiratory and cardiac systems coupling in pyramidal exercise using a time-varying model,” in *Computers in Cardiology, 2002*, 2002, pp. 429–432.

[18] E. F. Sierra-Alonso, L. M. Sepulveda-Cano, R. Bailon-Luesma, P. Laguna, and G. Castellanos-Dominguez, “Estimating respiratory frequency from HRV during treadmill exercise testing,” in *Computing in Cardiology Conference (CinC), 2013*, 2013, pp. 121–124.

[19] G. Baselli, A. Port, and G. Ferrari, “Models for the analysis of cardiovascular variability signals,” *Heart Rate Var.*, vol., no., pp. 135–145, 1995.

[20] H. D. Critchley, “Electrodermal responses: what happens in the brain,” *Neurosci. Rev. J. Bringing Neurobiol. Neurol. Psychiatry*, vol. 8, no. 2, pp. 132–142, Apr. 2002.

[21] P. H. Ellaway, A. Kuppuswamy, A. Nicotra, and C. J. Mathias, “Sweat production and the sympathetic skin response: Improving the clinical assessment of autonomic function,” *Auton. Neurosci.*, vol. 155, no. 1–2, pp. 109–114, Jun. 2010.

[22] M. Benedek and C. Kaernbach, “A continuous measure of phasic electrodermal activity,” *J. Neurosci. Methods*, vol. 190, no. 1–5, pp. 80–91, Jun. 2010.

[23] H. F. Posada-Quintero, J. P. Florian, A. D. Orjuela-Cañón, T. Aljama-Corrales, S. Charleston-Villalobos, and K. H. Chon, “Power Spectral Density Analysis of Electrodermal Activity for Sympathetic Function Assessment,” *Ann. Biomed. Eng.*, vol. 44, no. 10, pp. 3124–3135, Apr. 2016.

[24] H. F. Posada-Quintero, J. P. Florian, A. D. Orjuela-Canon, and K. H. Chon, “Highly Sensitive Index of Sympathetic Activity based on Time-Frequency Spectral Analysis of Electrodermal Activity,” *Am. J. Physiol. - Regul. Integr. Comp. Physiol.*, p. ajpregu.00180.2016, Jul. 2016.

[25] L. S. Pescatello, *ACSM’s Guidelines for Exercise Testing and Prescription*. Lippincott Williams & Wilkins, 2013.

[26] K. H. Chon, S. Dash, and K. Ju, “Estimation of respiratory rate from photoplethysmogram data using time-frequency spectral estimation,” *IEEE Trans. Biomed. Eng.*, vol. 56, no. 8, pp. 2054–2063, Aug. 2009.

[27] H. Wang, K. Siu, K. Ju, and K. H. Chon, “A high resolution approach to estimating time-frequency spectra and their amplitudes,” *Ann. Biomed. Eng.*, vol. 34, no. 2, pp. 326–338, Feb. 2006.

[28] G. Cardillo, *Dunn Test: a procedure for multiple, not parametric, comparisons*. MATLAB Central, MathWorks, Natick, MA, 2006.

[29] W. Boucsein *et al.*, “Publication recommendations for electrodermal measurements,” *Psychophysiology*, vol. 49, no. 8, pp. 1017–1034, Aug. 2012.

[30] C. Orizio, R. Perini, A. Comandè, M. Castellano, M. Beschi, and A. Veicsteinas, “Plasma catecholamines and heart rate at the beginning of muscular exercise in man,” *Eur. J. Appl. Physiol.*, vol. 57, no. 5, pp. 644–651.

[31] B. F. Robertson, S. E. Epstein, G. D. Beiser, and E. Braunwald, “Control of heart rate by the autonomic nervous system: studies in man on the interrelationship between baroreceptor mechanisms and exercise,” *Circ Res*, vol. 19, pp. 400–411, 1966.

[32] S. Akselrod, D. Gordon, J. B. Madwed, N. C. Snidman, D. C. Shannon, and R. J. Cohen, "Hemodynamic regulation: investigation by spectral analysis," *Am. J. Physiol.*, vol. 249, no. 4 Pt 2, pp. H867-875, Oct. 1985.

[33] Task Force of the European Society of Cardiology and the North American Society of Pacing and Electrophysiology, "Heart rate variability. Standards of measurement, physiological interpretation, and clinical use," *Eur. Heart J.*, vol. 17, no. 3, pp. 354–381, Mar. 1996.

[34] B. M. Sayers, "Analysis of heart rate variability," *Ergonomics*, vol. 16, no. 1, pp. 17–32, Jan. 1973.

[35] Y. Arai *et al.*, "Modulation of cardiac autonomic activity during and immediately after exercise," *Am. J. Physiol.*, vol. 256, no. 1 Pt 2, pp. H132-141, Jan. 1989.

[36] B. Casadei, S. Cochrane, J. Johnston, J. Conway, and P. Sleight, "Pitfalls in the interpretation of spectral analysis of the heart rate variability during exercise in humans," *Acta Physiol. Scand.*, vol. 153, no. 2, pp. 125–131, Feb. 1995.

[37] A. Malliani, M. Pagani, F. Lombardi, and S. Cerutti, "Cardiovascular neural regulation explored in the frequency domain," *Circulation*, vol. 84, no. 2, pp. 482–492, Aug. 1991.

[38] H.-W. Chiu, T.-H. Wang, L.-C. Huang, H.-W. Tso, and T. Kao, "The influence of mean heart rate on measures of heart rate variability as markers of autonomic function: a model study," *Med. Eng. Phys.*, vol. 25, no. 6, pp. 475–481, Jul. 2003.

[39] F. Cottin, C. Médigue, P.-M. Leprêtre, Y. Papelier, J.-P. Koralsztein, and V. Billat, "Heart rate variability during exercise performed below and above ventilatory threshold," *Med. Sci. Sports Exerc.*, vol. 36, no. 4, pp. 594–600, Apr. 2004.

[40] E. Toledo, O. Gurevitz, H. Hod, M. Eldar, and S. Akselrod, "Wavelet analysis of instantaneous heart rate: a study of autonomic control during thrombolysis," *Am. J. Physiol. Regul. Integr. Comp. Physiol.*, vol. 284, no. 4, pp. R1079-1091, Apr. 2003.

[41] R. Bailon, P. Laguna, L. Mainardi, and L. Sornmo, "Analysis of heart rate variability using time-varying frequency bands based on respiratory frequency," *Conf. Proc. Annu. Int. Conf. IEEE Eng. Med. Biol. Soc. IEEE Eng. Med. Biol. Soc. Annu. Conf.*, vol. 2007, pp. 6675–6678, 2007.

[42] R. Bailón, L. Mainardi, M. Orini, L. Sörnmo, and P. Laguna, "Analysis of heart rate variability during exercise stress testing using respiratory information," *Biomed. Signal Process. Control*, vol. 5, no. 4, pp. 299–310, Oct. 2010.

[43] F. Cottin, C. Médigue, and Y. Papelier, "Effect of heavy exercise on spectral baroreflex sensitivity, heart rate, and blood pressure variability in well-trained humans," *Am. J. Physiol. Heart Circ. Physiol.*, vol. 295, no. 3, pp. H1150–H1155, Sep. 2008.

[44] Y. Goren, L. R. Davrath, I. Pinhas, E. Toledo, and S. Akselrod, "Individual time-dependent spectral boundaries for improved accuracy in time-frequency analysis of heart rate variability," *IEEE Trans. Biomed. Eng.*, vol. 53, no. 1, pp. 35–42, Jan. 2006.

[45] Y. Zhong, K.-M. Jan, K. H. Ju, and K. H. Chon, “Quantifying cardiac sympathetic and parasympathetic nervous activities using principal dynamic modes analysis of heart rate variability,” *Am. J. Physiol. Heart Circ. Physiol.*, vol. 291, no. 3, pp. H1475-1483, Sep. 2006.

[46] A. Crider and R. Lunn, “Electrodermal lability as a personality dimension,” *J. Exp. Res. Personal.*, vol. 5, no. 2, pp. 145–150, 1971.

Chapter 6: Electrodermal Activity Can Track the Effects of Sleep Deprivation on Reactiveness and Vigilance

(Posada-Quintero, H. F., Bolkhovsky, J. B., Reljin, N. & Chon, K. H.. Electrodermal Activity Can Track the Effects of Sleep Deprivation on Reactiveness and Vigilance. To be published)

6.1 Introduction

This study analyzes the variations in electrodermal activity (EDA) and heart rate variability (HRV, see chapter 2) measures during a 24-hour period of sleep deprivation. Understanding the effects of sleep deprivation on humans' physiology is key to comprehending and mitigating the performance impairment produced by drowsiness. Human performance deterioration causes accidents in jobs like the military, health care, computer operations, and many more, that frequently require working long hours or late at night [1]. Occupational accidents result in a large social and economic cost [2], [3].

Drowsiness has a remarkable effect on the autonomic nervous system (ANS) [4]–[6]. The ANS compensates for increased levels of stress by modulating the balance between parasympathetic and sympathetic nervous system traffic within the body's regulatory network. A predominant sympathetic response to fatigue stressors is appropriate and beneficial. In contrast, a predominant parasympathetic response to the same fatigue stressor reflects an inappropriate response, indicating a progression toward a state of decompensation and failure of physiological function [5], [7]–[10]. Drowsiness induces such state of decompensation in humans. Given the high-sensitivity of ANS to drowsiness, the ANS is an attractive target for the development of an objective physiological measure of the effects of sleep deprivation.

Many studies have used indices of HRV to track the effects of sleep deprivation on humans [6], [11]–[18], with different levels of success. These studies suggest that HRV has the potential to track several effects of sleep deprivation. On the other hand, the effect of sleep deprivation on humans' EDA has been scarcely explored. However, recent studies suggested the important contribution of EDA and the

sympathetic function assessment to better understand the altered reactivity in sleep deprived persons [4], [19]. Surprisingly, those studies only looked at the very slow components of EDA, i.e., change in SCL, and did not explore the occurrence of rapid shifts, which are common in the EDA signal. We hypothesize that higher-frequency components of EDA contain valuable information to better understand the effects of sleep deprivation. We expect the changes found on the EDA and HRV due to prolonged sleep deprivation can be used to prevent the inconvenient (many times fatal) consequences of sleep deprivation. To test this, we have employed a simple yet robust test that requires the subject to maintain vigilance. We have collected measurements of HRV and EDA through a 24-hour sleep deprivation period, and deployed analysis on the results.

6.2 Materials and Methods

6.2.1 Subjects

Ten healthy volunteers (seven males and three females; ages ranging from 25 to 35) were enrolled in this study. Participants were asked to remain awake for at least 24 hours, and various precautions were taken to ensure the validity of this study as well as the safety of the participants (i.e., experimenter observation). Seven days prior to the experiment, participants were given a data sheet to record their sleep patterns, to indicate compliance and explain potential outliers.

6.2.2 Protocol

Participants were asked to halt all consumption of stimulants and depressants beginning 48 hours prior to the start of the experiment. Food was provided to ensure it adhered to the restrictions of this study. Within two hours of waking up participants arrived at the experimental facility located at the University of Connecticut. Participants remained in the building for approximately 25 hours to allow for the completion of all trials. Within the first hour of arrival participants completed a set of learning trials for the experimental task. They then proceeded to perform the task every other hour for the duration of the 24-hour period.

Five minutes before each task session, stainless steel electrodes were placed on the participants' middle and index fingers of their non-dominant hands to collect EDA signals. A set of three standard Ag/AgCl electrodes were placed on participant's chest for recording ECG. ECG and EDA signals were simultaneously recorded every run. An HP 78354A (Hewlett-Packard, FDA approved) and a GSR amplifier FE116 (fully isolated AC excitation and automatic zeroing low voltage amplifier, 22 mVrms @75 Hz, ADINSTRUMENTS) were used to collect ECG and EDA, respectively. No on-line filtering was applied during the signal recording. EDA device was adjusted to zero to assure a consistent level at the start of every run to avoid baseline differences in EDA that may arise from homeostatic and circadian processes [19], [20], allowing changes specific to the EAT to be isolated. The study protocol was approved by the Institutional Review Board of The University of Connecticut and all volunteers consented to be subjects for the experiment.

6.2.2.1 Error awareness task

To examine the effect of sleep deprivation on subjects' performance, we used the error awareness task (EAT). The EAT involves presenting a serial stream of single color words in congruent fonts, where each word is presented for 900 ms followed by a 600 ms inter-stimulus interval. Participants were trained to respond to each of the words with a single 'Go trial' button press and withhold this response ('No go trial') when either of two different circumstances arose. The first withhold condition occurred if the same word was present on two consecutive trials, while the second was caused if the word and color of the word did not match (see Figure 6.1) [21]. Notice that the latter situation utilizes the Stroop effect (using a keyboard in lieu of verbal responses), which induces cognitive stress to the subjects [22]. The two rules we induced to the subject brought about the need to be attentive rather than repetitive, because of the overlearned human behavior of reading the word over recognizing its color predisposed subjects to monitor for the repeat rather than the Stroop no-gos. In presence of these constrains, we have computed the 'Go trial' response time for every trial, as a measure of subjects' performance, to be able to examine the effects

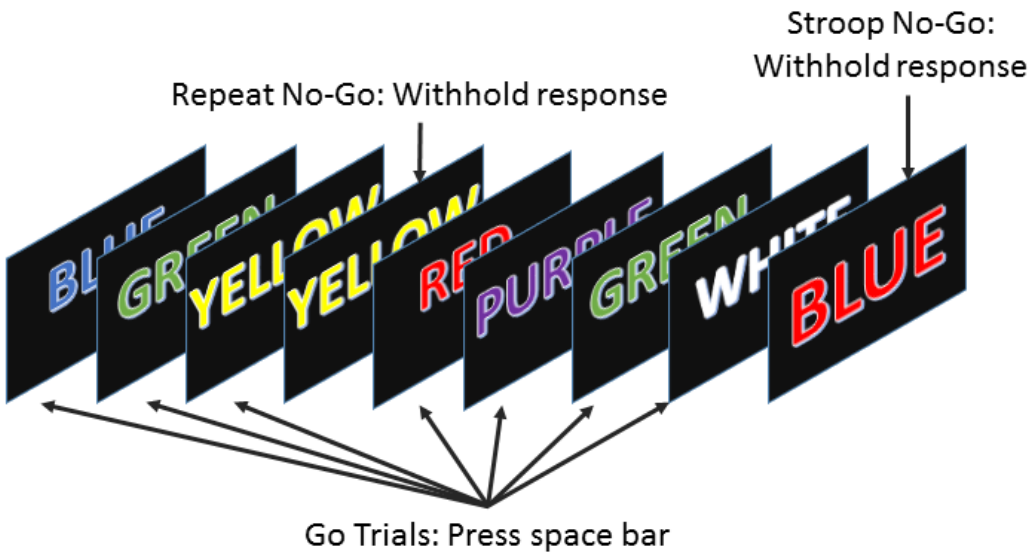

Figure 6.1 – The error awareness task (EAT).
EAT required subjects to respond pressing the space bar to a stream of color words and withhold their response when either a word was repeated on consecutive trials or the color and word were incongruous.

of sleep deprivation on such a simple measure and correlate with the various available physiological parameters.

6.2.3 Physiological indices of autonomic nervous system

Measures to assess the autonomic nervous system (ANS) based on analysis of HRV and EDA were computed using data collected while the subject was performing the EAT.

6.2.3.1 Indices of heart rate variability

For HRV analysis, ECG signals were band-pass filtered (0.05-40 Hz) to reduce noise and motion artifacts. The R-waveform peaks were detected using the detection algorithm that defines a delineation function based on the envelope of the ECG signal [23], [24]. All the segments were visually inspected to ensure that no beat was missed. After accounting for the missed R-wave beats, the HR time series were computed. The power spectra of HRV were then calculated using Welch's periodogram method with 50% data overlap. The RR interval series were converted to an evenly time-sampled signal (4 Hz) by cubic spline interpolation. A Blackman window (length of 256 points) was applied to each segment and the fast

Fourier transform was calculated for each windowed segment. Finally, the power spectra of the segments were averaged. The low-frequency index (HRVLF [ms2], 0.045 to 0.15 Hz), high-frequency index (HRVHF [ms2], 0.15 to 0.4 Hz), and normalized versions of these two (HRVLFn, HRVHFn, dividing by total power of HRV, in normalized units [n.u.]) were computed [25].

Four minutes of clean (subjects were asked to remain still) ECG signals were used to compute HRV indices. Indices from the LF range (HRVLF and HRVLFn) of HRV are used as indices of sympathetic control although they have proven parasympathetic influence, and indices from the HF power (HRVHF and HRVHFn) are used as indices of parasympathetic control, even though parasympathetic tone is present in both, the LF and HF range.

6.2.3.2 Indices of electrodermal activity

Indices of EDA were computed in time and frequency domain. In time domain, EDA signal is traditionally decomposed into two measures: skin conductance level (SCL) and skin conductance responses (SCRs) [26]. SCL (expressed in microsiemens, μS) is a measure related to the slow shifts of EDA, and specifically refers to the level of skin conductance. SCL was computed as the mean value of EDA taken during the given period. The skin conductance responses (SCRs) are the rapid transient events contained in the EDA signals. The non-specific SCRs (NSSCRs) is an index measured as the number of SCRs per minute [26]. In this study, for each run, two minutes of EDA was collected while the subject was performing the EAT, to compute SCL and NSSCRs.

The same two minutes of EDA extracted to compute time-domain indices were also used for spectral indices. The time-invariant spectra of EDA were calculated using Welch's periodogram method with 50% data overlap. A Blackman window (length of 128 points) was applied to each segment, the fast Fourier transform was calculated for each windowed segment, and the power spectra of the segments were averaged. The power spectral index of EDA, EDASymp [μS2], was computed by integrating the power in the range from 0.045 to 0.25 Hz, as it was found before to be sensitive to cognitive stress [27].

To compute the time-varying index of EDA, TVSymp, time-frequency representation (TFR) of EDA was computed using the variable frequency complex demodulation (VFCDM), a time-frequency spectral (TFS) analysis technique that provides accurate amplitude estimates and one of the highest time-frequency resolutions [28]. The components comprising the frequency power in the range from 0.08 to 0.24 Hz were used to compute TVSymp.

6.2.4 Statistics

The set of physiological indices tested in this study included: HRVLF, HRVLFn, HRVHF, HRVHFn, SCL, NSSCRs, EDASymp and TVSymp. As a measure of subjects' performance, average 'Go trial' reaction time (Go_RT), Stroop No-Go and Repeat No-Go accuracies (Stroop_NoGo_acc and Repeat_NoGo_acc, respectively) were computed for every run of every subject. Go_RT exhibits an inverse relationship to subjects' performance, as a higher reaction time represents lower performance. We explored the differences caused by the sleep deprivation on the physiological indices.

6.2.4.1 Changes on indices due to sleep deprivation

The impairment on participants' performance due to sleep deprivation was tested. In a similar manner, all the computed physiological indices of ANS were analyzed to test for significant differences due to sleep deprivation. In both cases (performance and physiological indices) we utilized the Dunn's test, a non-parametric pairwise multiple comparisons procedure based on rank sums, used as a "post hoc" procedure following rejection of a Kruskal–Wallis test. As such, it is a non-parametric analog to multiple pairwise t-tests following rejection of an ANOVA null hypothesis [29]. The analysis is meant to test the relationship between performance deterioration and changes to physiological indices, allowing us to understand the effect of prolonged wakefulness on subjects' EDA.

6.3 Results

For clarity and simplicity, we will refer to the run number to express the results, and the reader can easily abstract the relationship between run number and hours of sleep deprivation (hours of deprivation =

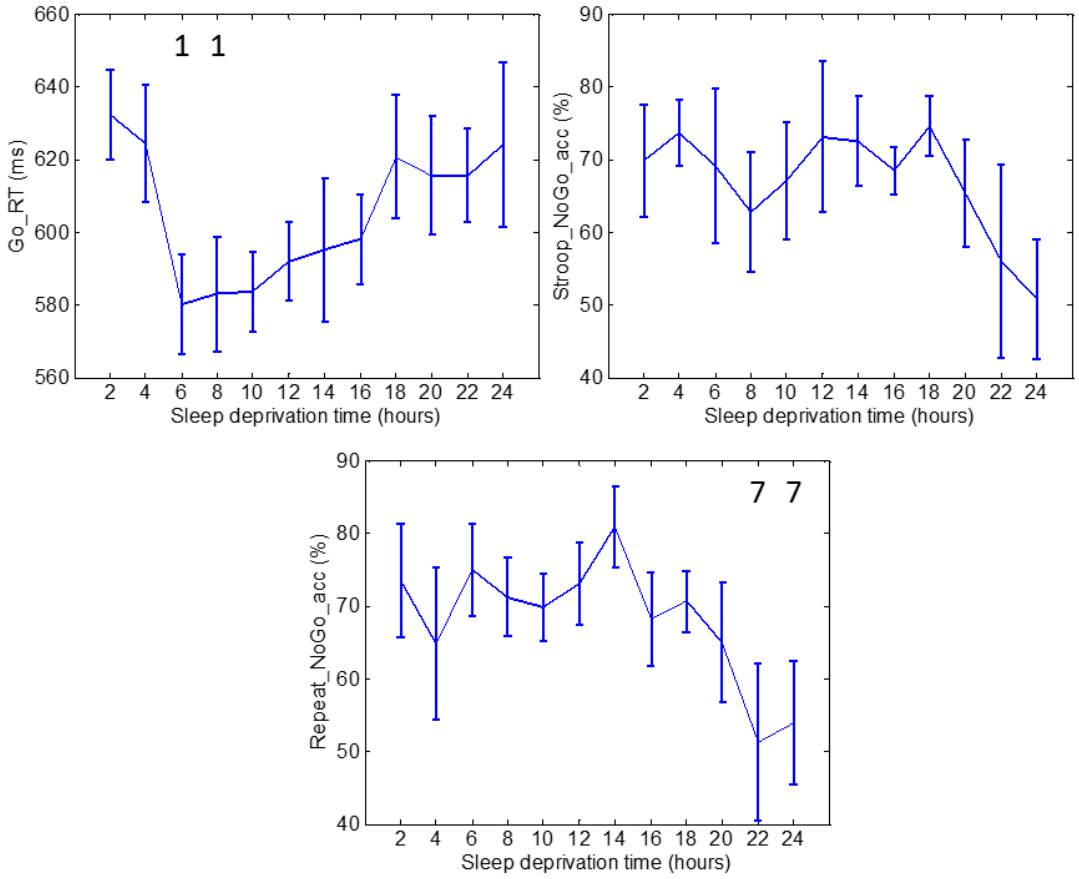

Figure 6.2 – Go_RT, Stroop_NoGo_acc and Repeat_NoGo_acc values through 24 hours of sleep deprivation.
Numbers on the figure represent the runs it was significantly different to. Whiskers account for one standard deviation.

2* run number). The changes in performance and ANS indices as a result of sleep deprivation are shown on Figure 6.2, Figure 6.3 and Figure 6.4. The figures display the results for Go_RT, HRV and EDA indices, respectively. Measures of Go_RT during run 3 and 4 were significantly different to the measurement during run 1. Measurements of Go_RT during runs 6 and 7 exhibited significantly lower values than those in run 2. The average reaction time increased after these two runs, but the increase was not significant. The results of Go_RT can be described in the following manner: the two runs performed during learning (2 hours) followed by the subjects reaching a plateau where the average reaction time stabilized for runs 3 through 8, ending in a final increase in average reaction time. Stroop_NoGo_acc and Repeat_NoGo_acc indices exhibited stable values for most of the test, followed by a sustained drop in value after 18 hours.

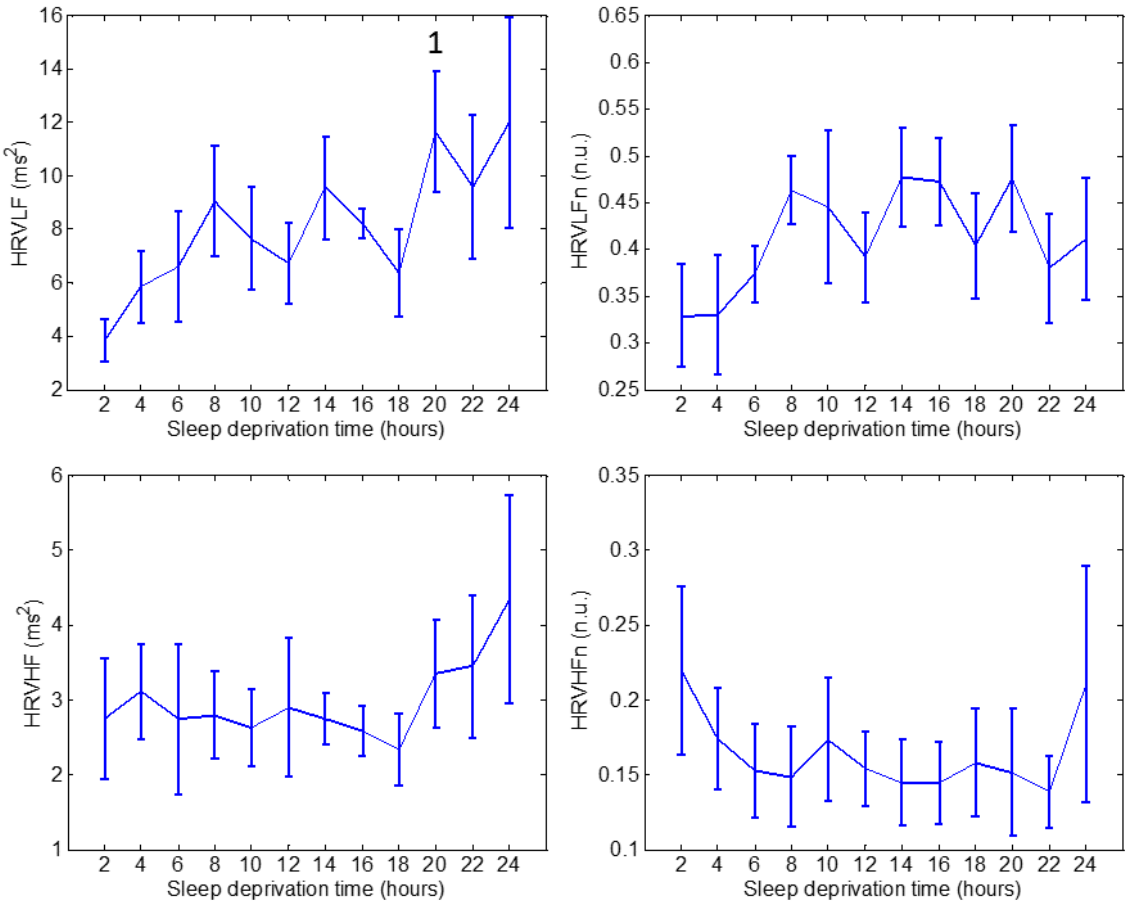

Figure 6.3 – Values through 24 hours of sleep deprivation for HRV indices: HRVLF (top left), HRVLFn (top right), HRVHF (bottom left) and HRVHFn (bottom right).
Numbers on the figure represent the runs it was significantly different to. Error bars account for one standard deviation.

Repeat_NoGo_acc showed a significant decrease in runs 11 and 12 compared to run 7; in this run Repeat_NoGo_acc exhibited a peak value. Differences in Stroop_NoGo_acc were not significant.

HRVLF exhibited a significant increase in run 10, compared to run 1. None of the other HRV indices, HRVLFn, HRVHF, and HRVHFn, showed a significant difference during the 24-hour period.

As for EDA measures, we found significant differences in SCL values during runs 5 and 8, compared to run 1. SCL profile looks similar to Go_RT for runs 1 through 8, in the sense that there are two runs similar to learning, followed by a plateau. The NSSCRs were significantly diminished on runs 9 and 11 compared to run 1 and 3. Values of the normalized EDASymp (EDASympn) were different at run

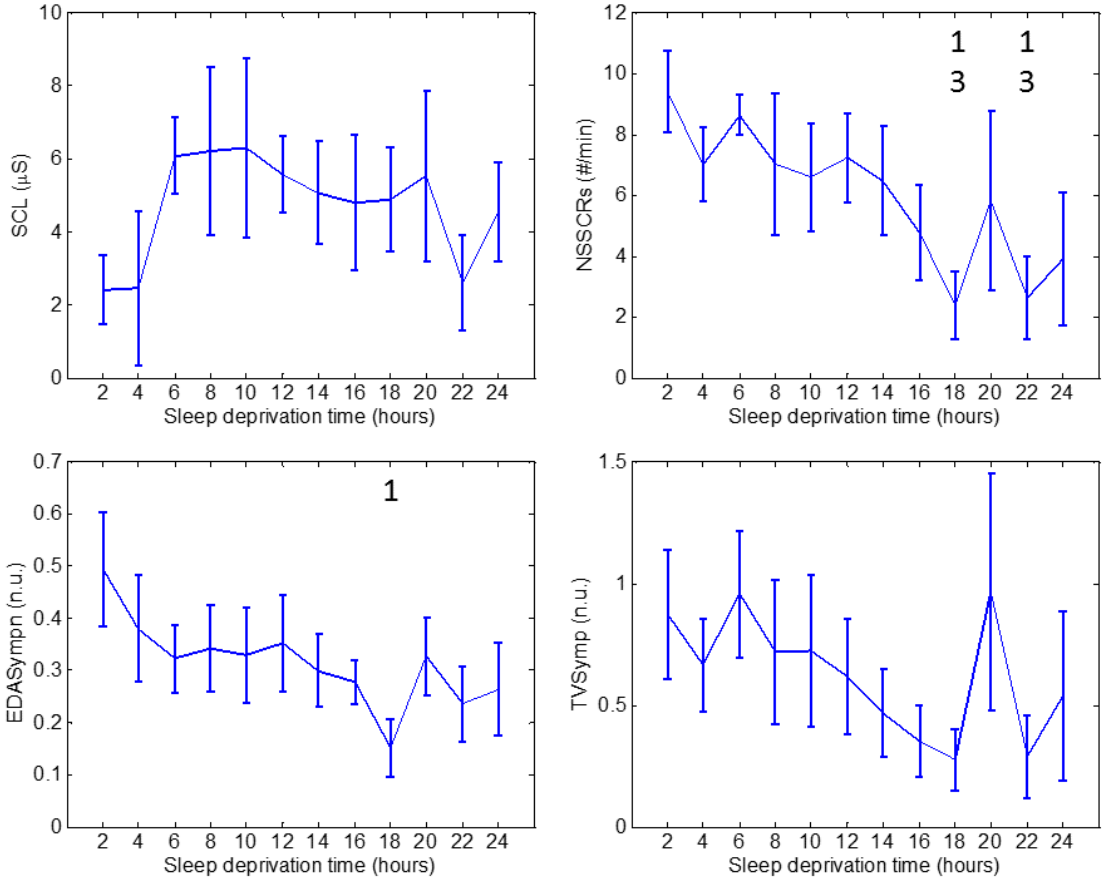

Figure 6.4 – Values through 24 hours of sleep deprivation for EDA indices: SCL (top left), NSSCRs (top right), EDASymp (bottom left) and TVSymp (bottom right).
Numbers on the figure represent the runs it was significantly different to. Whiskers account for one standard deviation.

9 compared to run 1. TVSymp, similarly to NSSCRs and EDAsympn, exhibited a continuous decrease in magnitude over time. However, that decrease was not significant for TVSymp at any point of time.

TVSymp was the only EDA index with differences between runs 2 and 1, which were found in the Go_RT index. Interestingly, this index exhibited more significant differences between runs than any other index. Values of runs 2, 5, 8 and 11 were significantly different to run 1, similar to the observed for HRVLF and HRVHFn indices. Runs 2, 5, 8 and 11 were different to runs 1, 4, 7 and 10, if the runs from the latter fall prior than those of the first set (e.g. run 5 was only different to 1 and 4). Values of run 4 were significantly different to run 2. Values of run 10 were different to runs 2, 5 and 8. During the 24-hour test,

there was a pattern of significant decrease on TVSymp every 3 runs (6 hours). Also, there were significant increases at runs 4 and 10 (8 and 20 hours).

6.4 Discussion

We have observed how indices accounting for higher frequencies of EDA follow a trend similar to indices of vigilance, measured by accuracy in performing an attention task, whereas the index that represents the slow changes of EDA resemblances more the changes in reactiveness, measured by reaction time. Our results suggest that indices of EDA can complement approaches using HRV, to predict the effect of sleep deprivation on humans' autonomic response and performance.

Many studies have studied the ANS using HRV under sleep deprivation. A group studied participants under 40-hour under constant routine conditions and determined that HRV was in general diminished during recovery sleep after sleep deprivation [18] . Analysis of these results revealed a decrease in HRV due to sleep deprivation, but with less intensity than during sleep. Another group found, in persons with over 36 h of sleep deprivation, a progressive increase during daytime in sympathetic, and a decrease in parasympathetic cardiac autonomic modulation [6]. This was demonstrated by reduced HRV values in the frequency domain for healthy participants while test persons performed a cognitive task repetitively. In contrast, another study could not find increased sympathetic drive expressed during daytime by diminished HRV values after one night of sleep deprivation [16]. Another investigation revealed a correlation of HRV spectral values with subjects' performance in a psychomotor vigilance test during sleep deprivation [11].

Information on the effect of sleep deprivation on humans' electrodermal activity is scarce. A classical review reported contradictory results on changes on SCL and SCRs during sleep deprivation [30]. However, that review highlighted that many of these studies suffered from methodological limitations (single case studies, measurements taken only once or twice during the test, or lack of statistical analysis). A study later reported an increased latency and reduced amplitude in event-related SCRs after 36 hours of sleep deprivation [31]. There are very few recent investigations. A study reported an increase of skin resistance level (inverse to SCL) that correlates with deterioration of reaction time, using a simple reaction

time test (mean correlation = 0.425) [19]. A recent study looked at the SCL to probe how the sympathetic nervous system might contribute to altered reactivity in sleep deprived persons [4]. Note that these two recent studies only analyzed the SCL, not including the information of the more rapid transients of EDA, where this signal has shown great sensitivity.

We found a significant reduction in Go_RT (learning effect) in runs 3 and 4 compared to run 1, and an increase after about 16 hours of sleep deprivation. Stroop_NoGo_acc and Repeat_NoGo_acc (indices of vigilance) were decreased towards the end of the 24-hour period. These results were expected, as human brain is able to maintain stable cognitive performance during certain period of time, but after prolonged wakefulness the level of arousal and performance tend to diminish [32]–[37]. In agreement to the affected level of arousal, indices of sympathetic control should ideally exhibit a decreasing trend. In this study, values of HRV indices of sympathetic control steadily increased with sleep deprivation (with some fluctuations), whereas NSSCRs, EDASymp and TVSymp tend to lower values by the end of the test.

EDAsymp exhibited a significant decrease in run 9 with respect to run 1, which coincided with an increase in mean Go_RT, and preceded the decrease in mean Stroop_NoGo_acc and Repeat_NoGo_acc noticeable in run 10. A similar peak in run 9 was also detected by NSSCRs index, with a repeated peak in run 11. The profiles of NSSCRs, EDASympn and TVSymp were similar, although EDASympn was somewhat smoother. In terms of significant change, it is noticeable that indices of higher-frequency components of EDA provide more information to understand and possibly predict the effects of sleep deprivation on the sympathetic nervous system.

There is an apparent relationship between the evolution of performance indices (Go_RT, Stroop_NoGo_acc and Repeat_NoGo_acc) and the indices of EDA. First, Go_RT and SCL showed a remarkable inverse relationship, showing a training period (the first two runs), a stable plateau for a long part of the test (top performance, when subjects learned the task), and a period where the indices went back close to training values. We hypothesize this final period, characterized by a drop in reactiveness (higher reaction time), is due to fatigue induced by sleep deprivation. This means that tonic SCL relates with subjects' reactiveness, which is in agreement with previous studies [4], [19], [38]. Second, the evolution

of indices that account for higher frequencies, NSSCRs, EDASymp and TVSymp, related to the measures of No-Go accuracy. These indices, Stroop_NoGo_acc and Repeat_NoGo_acc, which represent vigilance, remain stable for a part of the test (5 to 6 runs) then constantly degrade to low values. NSSCRs, EDASymp and TVsymp exhibited a behavior similar to the indices of vigilance, but at 20 hours they presented a large overshoot, followed by final return to low values. We believe that this high peak at the end of the test suggests that at such time subjects make an attempt to stay focused and vigilant. However, improved accuracy is not achieved. The results are in agreement with the classic studies that reported decrease in amplitude of SCRs after sleep deprivation [31], and with the classic report that related SCRs to attention, noting that such responses are sensitive to stimulus novelty [38].

The only available indices of parasympathetic control, HRVHF and HRVHFn indices, were stable throughout the test, with an increase in mean value towards the end of the 24 hours. These indices, especially HRVHFn, resembles the sleepiness of subjects at the start of the test, and the increased sleepiness by the end of the study.

6.5 Conclusion

We evaluated the effects of sleep deprivation on reactiveness, vigilance, HRV and EDA, every two hours during a 24-hour period. We found notable differences in the effects of sleep deprivation on lower and higher frequencies of EDA. Information confined to the higher frequency components of EDA relates to subjects' level of attention or vigilance. For its part, changes on tonic SCL, exhibited a relationship with subjects' reactiveness. This information can be utilized for developing tools to prevent the effects of prolonged wakefulness in jobs that require a high number of work hours, along with significant concentration to perform well, to assess and predict impaired cognitive performance.

6.6 References

[1] G. Costa, “The impact of shift and night work on health,” *Shiftwork*, vol. 27, no. 1, pp. 9–16, Feb. 1996.

[2] D. Leger, “The cost of sleep-related accidents: a report for the National Commission on Sleep Disorders Research,” *Sleep*, vol. 17, no. 1, pp. 84–93, Feb. 1994.

[3] J. M. Lyznicki, T. C. Doege, R. M. Davis, and M. A. Williams, “Sleepiness, driving, and motor vehicle crashes. Council on Scientific Affairs, American Medical Association,” *JAMA*, vol. 279, no. 23, pp. 1908–1913, Jun. 1998.

[4] J. C. J. Liu, S. Verhulst, S. A. A. Massar, and M. W. L. Chee, “Sleep deprived and sweating it out: the effects of total sleep deprivation on skin conductance reactivity to psychosocial stress,” *Sleep*, vol. 38, no. 1, pp. 155–159, Jan. 2015.

[5] E. Michail, A. Kokonozi, I. Chouvarda, and N. Maglaveras, “EEG and HRV markers of sleepiness and loss of control during car driving,” *Conf. Proc. Annu. Int. Conf. IEEE Eng. Med. Biol. Soc. IEEE Eng. Med. Biol. Soc. Annu. Conf.*, vol. 2008, pp. 2566–2569, 2008.

[6] X. Zhong *et al.*, “Increased sympathetic and decreased parasympathetic cardiovascular modulation in normal humans with acute sleep deprivation,” *J. Appl. Physiol. Bethesda Md 1985*, vol. 98, no. 6, pp. 2024–2032, Jun. 2005.

[7] A. Baharav *et al.*, “Fluctuations in autonomic nervous activity during sleep displayed by power spectrum analysis of heart rate variability,” *Neurology*, vol. 45, no. 6, pp. 1183–1187, Jun. 1995.

[8] W. H. Cooke *et al.*, “Heart rate variability and its association with mortality in prehospital trauma patients,” *J. Trauma*, vol. 60, no. 2, p. 363–370; discussion 370, Feb. 2006.

[9] G. D. Furman, A. Baharav, C. Cahan, and S. Akselrod, “Early detection of falling asleep at the wheel: A Heart Rate Variability approach,” in *2008 Computers in Cardiology*, 2008, pp. 1109–1112.

[10] R. J. Winchell and D. B. Hoyt, “Analysis of heart-rate variability: a noninvasive predictor of death and poor outcome in patients with severe head injury,” *J. Trauma*, vol. 43, no. 6, pp. 927–933, Dec. 1997.

[11] E. C.-P. Chua *et al.*, “Heart Rate Variability Can Be Used to Estimate Sleepiness-related Decrements in Psychomotor Vigilance during Total Sleep Deprivation,” *SLEEP*, Mar. 2012.

[12] D. L. Fogt, W. H. Cooke, J. E. Kalns, and D. J. Michael, “Linear Mixed-Effects Modeling of the Relationship Between Heart Rate Variability and Fatigue Arising from Sleep Deprivation,” *Aviat. Space Environ. Med.*, vol. 82, no. 12, pp. 1104–1109, Dec. 2011.

[13] D. L. Fogt, J. E. Kalns, and D. J. Michael, “A comparison of cognitive performance decreases during acute, progressive fatigue arising from different concurrent stressors,” *Mil. Med.*, vol. 175, no. 12, pp. 939–944, Dec. 2010.

[14] M. Glos, I. Fietze, A. Blau, G. Baumann, and T. Penzel, “Cardiac autonomic modulation and sleepiness: physiological consequences of sleep deprivation due to 40 h of prolonged wakefulness,” *Physiol. Behav.*, vol. 125, pp. 45–53, Feb. 2014.

[15] T. Nakano, K. Araki, A. Michimori, H. Inbe, H. Hagiwara, and E. Koyama, “Temporal order of sleepiness, performance and physiological indices during 19-h sleep deprivation,” *Psychiatry Clin. Neurosci.*, vol. 54, no. 3, pp. 280–282, Jun. 2000.

[16] M. Pagani *et al.*, “Hemodynamic, autonomic and baroreflex changes after one night sleep deprivation in healthy volunteers,” *Auton. Neurosci. Basic Clin.*, vol. 145, no. 1–2, pp. 76–80, Jan. 2009.

[17] J. Vicente, P. Laguna, A. Bartra, and R. Bailón, “Drowsiness detection using heart rate variability,” *Med. Biol. Eng. Comput.*, vol. 54, no. 6, pp. 927–937, Jun. 2016.

[18] A. U. Viola, L. M. James, S. N. Archer, and D.-J. Dijk, “PER3 polymorphism and cardiac autonomic control: effects of sleep debt and circadian phase,” *Am. J. Physiol. Heart Circ. Physiol.*, vol. 295, no. 5, pp. H2156-2163, Nov. 2008.

[19] E. Miró, M. C. Cano-Lozano, and G. Buela-Casal, “Electrodermal activity during total sleep deprivation and its relationship with other activation and performance measures,” *J. Sleep Res.*, vol. 11, no. 2, pp. 105–112, Jun. 2002.

[20] M. W. Miller and C. Gronfier, “Diurnal variation of the startle reflex in relation to HPA-axis activity in humans,” *Psychophysiology*, vol. 43, no. 3, pp. 297–301, May 2006.

[21] R. Hester, J. J. Foxe, S. Molholm, M. Shpaner, and H. Garavan, “Neural mechanisms involved in error processing: A comparison of errors made with and without awareness,” *NeuroImage*, vol. 27, no. 3, pp. 602–608, Sep. 2005.

[22] J. R. Stroop, “Studies of interference in serial verbal reactions.,” *J. Exp. Psychol.*, vol. 18, no. 6, p. 643, 1935.

[23] M. E. Nygårds and L. Sörnmo, “Delineation of the QRS complex using the envelope of the e.c.g,” *Med. Biol. Eng. Comput.*, vol. 21, no. 5, pp. 538–547, Sep. 1983.

[24] C. Vidaurre, T. H. Sander, and A. Schlögl, “BioSig: the free and open source software library for biomedical signal processing,” *Comput. Intell. Neurosci.*, vol. 2011, p. 935364, 2011.

[25] Task Force of the European Society of Cardiology and the North American Society of Pacing and Electrophysiology, “Heart rate variability. Standards of measurement, physiological interpretation, and clinical use,” *Eur. Heart J.*, vol. 17, no. 3, pp. 354–381, Mar. 1996.

[26] W. Boucsein *et al.*, “Publication recommendations for electrodermal measurements,” *Psychophysiology*, vol. 49, no. 8, pp. 1017–1034, Aug. 2012.

[27] H. F. Posada-Quintero, J. P. Florian, A. D. Orjuela-Cañón, T. Aljama-Corrales, S. Charleston-Villalobos, and K. H. Chon, “Power Spectral Density Analysis of Electrodermal Activity for Sympathetic Function Assessment,” *Ann. Biomed. Eng.*, vol. 44, no. 10, pp. 3124–3135, Apr. 2016.

[28] K. H. Chon, S. Dash, and K. Ju, “Estimation of respiratory rate from photoplethysmogram data using time-frequency spectral estimation,” *IEEE Trans. Biomed. Eng.*, vol. 56, no. 8, pp. 2054–2063, Aug. 2009.

[29] G. Cardillo, *Dunn Test: a procedure for multiple, not parametric, comparisons*. MATLAB Central, MathWorks, Natick, MA, 2006.

[30] J. A. Horne, “A review of the biological effects of total sleep deprivation in man,” *Biol. Psychol.*, vol. 7, no. 1–2, pp. 55–102, Sep. 1978.

[31] M. E. McCarthy and W. F. Waters, “Decreased attentional responsivity during sleep deprivation: orienting response latency, amplitude, and habituation,” *Sleep*, vol. 20, no. 2, pp. 115–123, Feb. 1997.

[32] P. Franco *et al.*, “Decreased Arousals Among Healthy Infants After Short-Term Sleep Deprivation,” *Pediatrics*, vol. 114, no. 2, pp. e192–e197, Aug. 2004.

[33] J. Kaplan, J. Ventura, A. Bakshi, A. Pierobon, J. R. Lackner, and P. DiZio, “The influence of sleep deprivation and oscillating motion on sleepiness, motion sickness, and cognitive and motor performance,” *Auton. Neurosci. Basic Clin.*, Aug. 2016.

[34] G. Legault, A. Clement, G. P. Kenny, S. Hardcastle, and N. Keller, “Cognitive consequences of sleep deprivation, shiftwork, and heat exposure for underground miners,” *Appl. Ergon.*, vol. 58, pp. 144–150, Jan. 2017.

[35] I. Lorenzo, J. Ramos, C. Arce, M. A. Guevara, and M. Corsi-Cabrera, “Effect of total sleep deprivation on reaction time and waking EEG activity in man,” *Sleep*, vol. 18, no. 5, pp. 346–354, Jun. 1995.

[36] T. Porkka-Heiskanen, R. E. Strecker, M. Thakkar, A. A. Bjørkum, R. W. Greene, and R. W. McCarley, “Adenosine: A Mediator of the Sleep-Inducing Effects of Prolonged Wakefulness,” *Science*, vol. 276, no. 5316, pp. 1265–1268, May 1997.

[37] N. D. Volkow *et al.*, “Sleep Deprivation Decreases Binding of [11C]Raclopride to Dopamine D2/D3 Receptors in the Human Brain,” *J. Neurosci.*, vol. 28, no. 34, pp. 8454–8461, Aug. 2008.

[38] J. Hochberg, J. W. Kling, and L. A. Riggs, *Woodworth & Schlosberg’s experimental psychology*. New York: Holt, Rinehart, & Winston, 1971.

Chapter 7: Low Impedance Carbon Adhesive Electrodes with Long Shelf Life

(Posada-Quintero, H., Reyes, B., Burnham, K., Pennace, J., & Chon, K.. Low Impedance Carbon Adhesive Electrodes with Long Shelf Life. Annals of BME, 2374-2382 (2015))

7.1 Introduction

The electrocardiogram (ECG) provides a graphical representation of the electrical activity of the heart, and to properly monitor the cardiac health of a patient, it is crucial to obtain an ECG signal with a high signal-to-noise ratio (SNR). In a typical ECG setup, depending on the particular application, three to twelve signal receptive electrodes are attached to the patient's body. These electrodes are able to measure minute changes in potential that occur as a consequence of the propagation of electrical signal from atria to ventricles during each heartbeat cycle, thus rendering it possible to produce the characteristic ECG waveforms that can then be used for diagnostic purposes. The ECG can also be further quantified by computing the heart rate variability (HRV) indices, as these have been shown to provide a good estimate of the dynamics of the autonomic nervous system[1]. To ensure optimal signal strength of the electrode, it is imperative to minimize the impedance of the electrode-skin interface by lowering the impedance of the electrode. High impedance levels at the skin-electrode interface can result in significant loss in signal strength and low SNR, which will lead to poor quality ECG waveforms.

The current industry gold standard for electrodes is the Silver/Silver Chloride (Ag/AgCl) wet (hydrogel) electrode, which has been proven to provide accurate ECG waveforms[2]. These electrodes consist of a layer of silver chloride, often in the form of a paste-like hydrogel surrounding a silver disc. While the hydrogel layer significantly improves the signal quality by effectively lowering the impedance that exists at the electrode-skin interface, it is also the principal reason behind the relatively short shelf life of these electrodes. The hydrogel layer that exists in the skin-electrode interface degrades with time as it dehydrates, producing high impedance. This leads to a loss of signal quality [3] and an increased incidence of motion artifacts and noise in the ECG[4]. Moreover, the electrodes need to be carefully packaged to

ensure prolonged retention of the hydrogel layer. Due to finite shelf life and electrode dehydration, these electrodes can only be used to record signals for a few days at maximum[5]. Also, Ag/AgCl electrodes are limited to short-term use because they are known to cause irritation to the skin especially after their removal. Moreover, Ag/AgCl electrodes are also relatively expensive since silver is an expensive commodity. For these reasons, dry electrodes have been developed in recent years to substitute traditional wet Ag/AgCl electrodes [4], [6], [7].

A novel type of electrode that does not require a hydrogel layer has been developed to address the issue of dehydration with the current industry gold standard electrodes. The new dry electrodes are designed by combining a visco-elastic polymeric adhesive[8], [9] with carbon black powder and a quaternary salt. This mixture is potentially much more economical than Ag/AgCl. The objective of this paper is to demonstrate and detail the fabrication process of our new Carbon/Salt/Adhesive (CSA) electrodes and compare their ECG morphologies to the standard Ag/AgCl wet electrodes.

First, a brief description of the fabrication of the CSA electrodes is provided. After the CSA electrodes are fabricated, they need to be activated by a procedure known as electrophoresis[10]. Once activated, the electrodes must meet the Association for the Advancement of Medical Instrumentation (AAMI) requirement for defibrillation overload recovery & impedance. The AAMI states that for electrodes such as hydrogel, the average post-activation impedance must remain equal to or below 2 kΩ, and no single electrode pair can have impedance greater than 3 kΩ after activation.

To ensure that dry CSA electrodes meet the AAMI standard for electrodes, we designed and implemented an activation circuit which is capable of providing various levels of activation voltage and amperage with varying discharge times. This allowed us to obtain the best parameters required for the activation. This procedure was also used to discern the optimal concentration of carbon by measuring pre- and post-activation impedance values.

Once the activation parameters as well as the carbon concentration were determined, several comparisons between CSA and Ag/AgCl electrodes were carried out. First, electrode-skin contact impedance was measured for each type of electrode. Subsequently, simultaneous ECG data acquisition

was performed using the two electrode types on human subjects in order to ensure similarities in the ECG waveforms. Finally, heart rate variability analyses were performed with the hypothesis that the CSA will provide statistically similar indices as that of the Ag/AgCl electrodes.

7.2 Materials and Methods

7.2.1 Carbon/Salt/Adhesive electrode fabrication

The base material used is a .001" thick polyester film with a conductive carbon ink coating on one surface which gives approximately 100 Ohms per square of measured surface resistivity. Silver/silver chloride coatings (which are commonly used in hydrogel based electrodes to provide electro-chemical stability) are not needed due to the characteristics of the waterless adhesive. Using a polar organo salt is a way to introduce into the adhesive composition a very polar molecule (electro-physically aligns with the applied electric filed) that orientates with a time varying signal, which can be alternating current, ramped, pulsed DC, mixed waveform or ECG. The salt in this case is a quaternary ammonium salt [hydrogenated tallowalkyl (2-ethylhexyl) dimethyl ammonium methylsulfate] that exhibits excellent compatibility with the chosen waterless adhesive by virtue of its organic functionality.

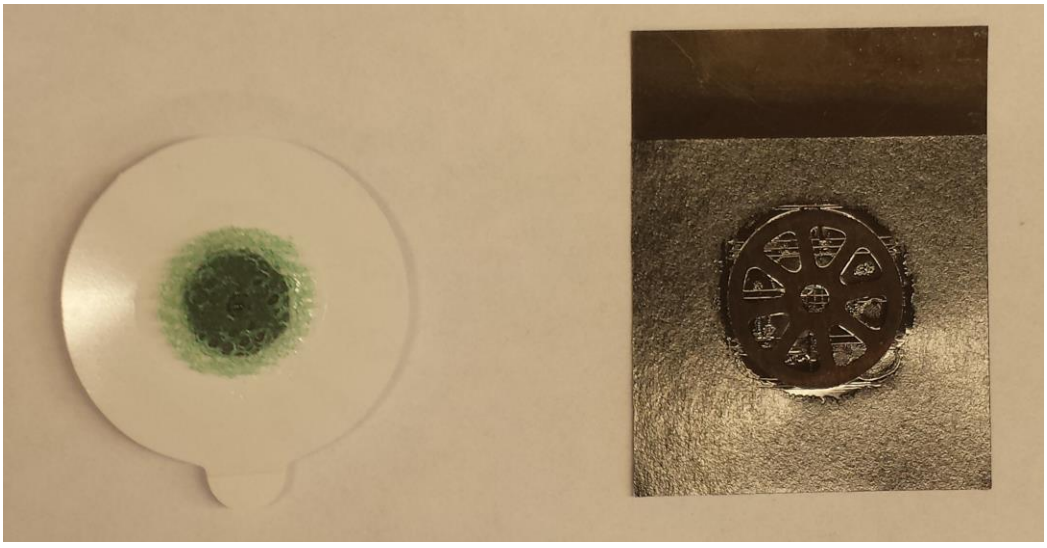

Figure 7.1 – Hydrogel Ag/AgCl electrode (left) and Carbon/Salt/Adhesive electrode (right). The circular piece of carbon in the center is the conductivity enhancing feature (bridge).

Table 7.1 Variable parameters for electrode activation.

Parameter	Values to test	Units
Voltage (DC)	5, 20, 45, 75, 120, 200	V
Current	1, 2, 5, 10, 20, 50, 100	mA
Frequency	DC, 60, 1000	Hz
Time	1, 10, 100, 1000	ms

Since the adhesive is not in a very polar solvent (like water) to stabilize its disassociated ions (the solvent here instead being an acrylic polymer), there is little ionic formation and thus it does not contribute much (if any) ionic conductivity. The alignment response of the polar salt molecule to an applied electric field facilitates a displacement current which is a different mechanism than the ionic current arising from the movement of dissociated salt ions. The greater that the concentration of the polar salt is, the greater the number of available parallel current pathways there are, thus leading to lower impedance. By contrast, salts (such as NaCl) in a hydrogel composition break down to Na +and Cl- (hydrolytic stabilized disassociated ions). It is the formation of these ions that is the basis for ionic conductivity in hydrogels but not in the waterless adhesive used here. Thus, there is no similarity in the mechanism of signal detection between the salt in a hydrogel and the salt used in the CSA electrode.

To create electrodes, 30 g total of the dopant and the visco-elastic polymeric adhesive are added to a beaker. The amount of carbon and salt added is dependent on the percent to be used out of 30 g. A magnetic mixer is used for 40 minutes to stir the adhesive and dopant. The mixture is spread onto a liner using a 12 mil spreading tool, and then placed into a 160° F oven for 10 minutes. The dried adhesive is covered with a 2nd liner and is cut into 4.45 cm wide pieces, the Carbon electrode film is cut into 5.08 cm wide pieces and the adhesive is placed onto the film, leaving a small amount of carbon film exposed. Electrodes were cut to a size of 4.45cm X 3.81cm.

A feature for enhancing surface conductivity is then applied. The conductivity enhancing feature (the bridge) is a low impedance electrically conductive material that produces a lower electrode ohm value by connecting in parallel multiple isolated Z direction (out of plane) conductive pathways in the adhesive.

This can be described by 1/Rtotal = (1/R1)+(1/R2)+1/R3)+....(1/Rn) where R represents each isolated Z direction pathway. The bridge is specifically designed to balance electrical, mechanical and electrode adhesion properties: its conductive loading level provides electrical conductivity, its polymeric content and thinness provide mechanical flexibility, and its large open area pattern minimizes reduction in adhesive bonding.

In general higher salt concentration leads to higher conductance, but it would also increase the risk of eliciting a reaction in subjects' skin. For the purposes of this study, salt concentration was fixed to 25%, given that such concentration produced very low to minimal skin irritation. A representative CSA electrode is shown on the right panel of Figure 7.1 and the left panel shows a standard Ag/AgCl ECG electrode.

7.2.2 Carbon black concentration

The ideal concentration of carbon powder in CSA electrodes was determined by minimizing post activation impedance. The carbon concentration ranged from 2% to 12% loading levels with an increment of 2% and we measured pre-activation and post-activation impedance using an impedance meter. Initially, for each carbon load level, 5 different sample electrodes were used. Subsequently, for the 3 carbon levels with the lowest post-activation impedance, 30 additional samples for each level were further analyzed. Impedance measurements were taken at 10 Hz as reference because this is within the ECG frequency range of interest.

7.2.3 Activation process

An activation device with variable parameters was designed and built in order to determine the best parameters to activate the electrodes. The test parameters are listed in Table 7.1. All permutations of parameter values were tested, in order to determine the optimum activation (i.e., lowest impedance). The design of the activation circuit was determined based on the AAMI standard defibrillation overload circuit. In order to vary parameters as listed in Table 7.1, dip switches were used to change values of resistors and capacitors. The power supply used provides an AC voltage from 0-240 Volts, but the circuit based on the

AAMI standards is typically used with a DC voltage. In order to address this, a diode rectifier was designed at the input to the circuit to convert the voltage from AC to DC.

Activation was obtained by applying electrophoresis through the Z direction of each electrode. Carbon columns formed in the Z-direction were an indication that the activation was successful which was verified in many samples using the scanning electron micrograph (see Figure 7.2). A voltage meter was applied across the activation capacitor to examine if the electrode pair was shorted during application of the two electrode adhesives. The electrodes were then removed and two impedance testing clips from a Hiroki IM 3570 were attached to the activation points of the material. The electrode's impedance was tested at 10 Hz by using a 1 V amplitude signal from the impedance testing device. The impedance of each electrode pair was measured before and after activation. In order to meet the Association for the Advancement of Medical Instrumentation (AAMI) standards, the average post-activation impedance is required to be under 2kΩ with no single value over 3kΩ.

7.2.4 Electrode-skin contact impedance measurements

The study protocol was approved by the Institutional Review Board of Worcester Polytechnic Institute and all volunteers consented to be subjects for the experiment.

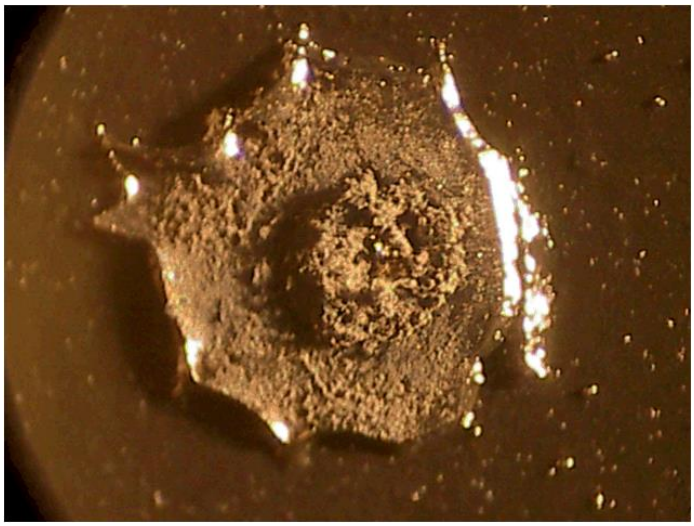

Figure 7.2 – Scanning electron micrograph image of an activated electrode.
Notice that in the depletion zone the carbon particles moved in from the surrounding area and form vertical columns in the Z-direction.

Activated CSA electrodes were used to carry out over-skin impedance measurements and compare to Ag/AgCl electrodes. The skin of the test subject was cleaned before each measurement by wiping with a 2%-alcohol impregnated cotton pad, which was allowed to evaporate before applying the electrodes. Two electrodes were mounted on the right forearm, one on the palm side of the wrist, and the second 5 cm apart from the first but situated towards the elbow. These electrodes were connected to the Hiroki IM3570 impedance analyzer, and each measurement is the result of averaging 20 measurements. The signal voltage amplitude was set to 1 V and the frequency range from 4 to 100 KHz, as used in previous studies [4], [11]. N = 7 pairs of electrodes were used. To keep skin properties as constant as possible, all measurements were performed in a single day.

7.2.5 Collection of electrode comparison data

A simultaneous set of 3 CSA (post-activation and optimal-mixture) and wet Ag/AgCl electrodes was used to collect ECG signals from 17 healthy subjects (12 males, 5 females, 28 ± 5 years old). An electrode was placed on xiphoid process (ground), a second one in the center of the manubrium (1−), and the third under the left pectoral near V6 electrode position (1+). These placements mimics lead II ECG configuration [12]. Subjects were seated for 7 minutes followed by standing for the same duration (Rozinn® Holter @ 180 Hz). The ECG signals were band-pass filtered (0.05-40 Hz) offline to reduce noise and motion artifacts. Throughout all the experiments for this study, the skin area was cleaned with 70% isopropyl alcohol prior to each measurement.

7.2.6 HRV indices

Heart Rate Variability (HRV) series were obtained from the ECG signals. The R-waveform peaks were detected using a widely-used peak detection algorithm[13]. Time and frequency domain HRV indices were then calculated from the HRV series.

7.2.6.1 Time domain indices.

Temporal measures of the HRV considered in this study were: mean RR interval (millisecond units), SDNN (standard deviation of all RR intervals; millisecond units), RMSSD (square root of the mean of the sum of the squares of differences between adjacent RR intervals; millisecond units), NN50 count (number of pairs of adjacent RR intervals differing by more than 50 ms in the entire recording; unitless), and pNN50 (NN50 count divided by the total number of all RR intervals; percentage).

7.2.6.2 Frequency domain indices.

The power spectra of HRV were calculated using Welch's periodogram method with 50% data overlap. The RR interval series were converted to an evenly time sampled signal by cubic spline interpolation. A Blackman window was applied to each segment and the Fast Fourier Transform was calculated for each windowed segment. Finally, the power spectra of the segments were averaged. From spectral analysis, two frequency bands were considered: low frequency (LF) band (0.045 to 0.15 Hz) and high frequency (HF) band (0.15 to 0.4 Hz)[1]. The very low frequency (VLF) band was not taken into account because the physiological correlates are still unknown[1].

Spectral powers were designated as the Total, LF, HF, LF/HF ratio and are presented as the absolute (square milliseconds, ms2) units. The spectral contents of the LF and HF are known to reflect dynamics of the autonomic nervous system. Parasympathetic nervous system activity is the major contributor to the HF component[14], [15]. The interpretation of the LF component is more difficult, but previous works have demonstrated that it reflects both sympathetic and parasympathetic dynamics[14], [16]. Consequently, the LF/HF ratio is considered as a reasonable estimate of the sympatho-vagal balance[1]. The paired t-test was used to compare all of the obtained parameters.

7.2.7 ECG morphology comparison

Out of the group of 17 subjects, 5 were enrolled to collect 5-lead ECG signals in order to perform ECG morphology (lead I, HP 78354A ECG) comparison between CSA and Ag/AgCl electrodes; data were

sampled at 1000 Hz for 2 minutes. With the subjects standing still, either a set of Ag/AgCl or CSA electrodes were placed and ECG signals were collected. Upon immediately after data collection involving a set of electrodes, a second set of electrodes which were not previously used were placed in the same exact position and ECG signals were acquired. The skin area was cleaned with 70% isopropyl alcohol prior to each measurement.

7.2.8 Motion artifacts

One of the disadvantages of dry electrodes compared to gel electrodes is the lack of flexible contact provided by the gel. This produces variations in contact during motion, and tend to introduce motion artifacts to the ECG signal. We presume that Z-direction formation of carbon columns after activation provides a better reaction to shifting against skin, as the electrodes should be less sensitive to X- and Y-direction potentials. Same 5 subjects enrolled for ECG morphology comparison were used to perform a motion artifacts evaluation (lead I, Chroma® Holter @512 Hz sampling rate). Subjects were requested to perform horizontal movements (HM; torso rotations), vertical movements (VM; squats-like up and down movements) and random walking (RW). Each subjects wore both types of electrodes (Ag/AgCl and CSA) and simultaneous ECG measurements were collected using two Holter monitors.

7.3 Results

7.3.1 Optimum carbon concentration

Table 7.2 shows three different levels of carbon powder concentration from a sample size of 35. As shown in Table 7.2, the most consistent results (e.g., smallest standard deviation values) were obtained for carbon loads at 10% and 12%. According to AAMI standards, the mean post activation impedance is required to be under 2 kΩ and no single electrode pair can have impedance greater than 3 kΩ. Based on this criterion, only the 10% and 12% carbon concentration levels meet the AAMI criterion. Note that 2%, 4% and 6% carbon concentration data are not shown because their post-activation impedance values were significantly higher than 2 kΩ.

Table 7.2 Electrode impedance test results

Carbon Load	Pre-activation impedance (MΩ)	Post-activation impedance (Ω)
8%	10.5 ± 6.01	1,170 ± 1,170
10%	2.09 ± 2.79	256 ± 51.4
12%	3.96 ± 2.39	286 ± 56.5

Values are expressed as mean ± standard deviation.

In order to verify that the data gathered for pre-activation and post-activation impedances are statistically significant, two-tailed t-tests were performed using MATLAB. Only the 12% and 10% carbon concentrations were found to be comparable. Given that there was no statistical difference between 10% and 12% carbon powder concentration, we selected the former as the optimal value. Notice that a slightly higher carbon loading of 15% would be comparable to 10% & 12%.

7.3.2 Activation Parameters

Pre-activation and post-activation impedances were recorded for 840 electrodes. Each parameter value shown in Table 7.1 was permuted with the other parameters to determine the optimal activation of electrodes. Table 7.3 details the mean and standard deviation values of the pre- and post-activation

Table 7.3 Electrode impedance test results

Parameters				
Voltage	Capacitance	Current	Pre-Activation [MΩ]	Post-Activation [kΩ]
200V	.1µF	20mA	18.83 ± 3.70	3.68 ± 1.87
200V	.1µF	100mA	17.17 ± 8.40	6.04 ± 6.67
200V	1µF	10mA	20.86 ± 2.34	2.41 ± 1.34
120V	1µF	10mA	7.82 ± 9.83	1.24 ± 0.26
200V	**1µF**	**100mA**	**20.71 ± 2.77**	**0.443 ± 0.189**
120V	1µF	100mA	20.63 ± 3.32	0.829 ± 0.296
200V	10µF	10mA	21.57 ± 3.22	1.67 ± 0.49
200V	10µF	20mA	15.64 ± 8.89	1.19 ± 2.16
120V	10µF	20mA	21.09 ± 1.96	1.05 ± 1.51

Values are expressed as mean ± standard deviation.

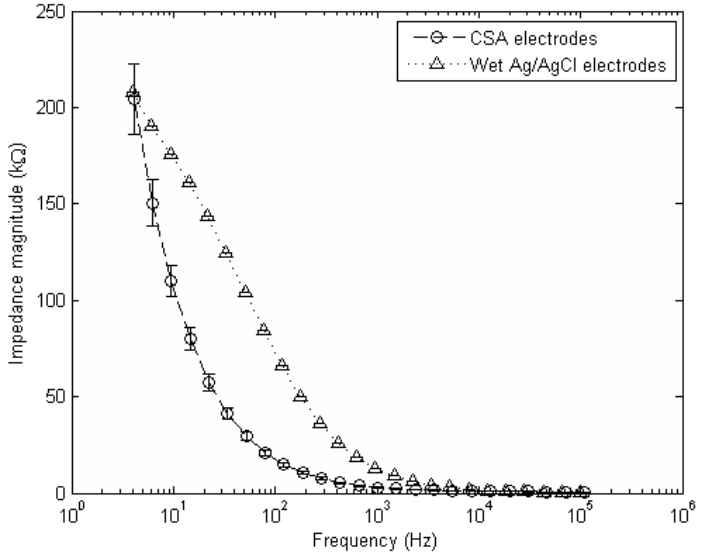

Figure 7.3 – Impedance of Carbon/Salt/Adhesive and Ag/AgCl electrodes.

impedances based on some of the chosen voltage, capacitance and current parameter values. We only show those data with the lowest post-activation impedance values.

As shown in Table 7.3, the optimum activation parameters are 200 V, 1 μF and 100 mA since this choice provides the lowest post-activation impedance. The post-activation values are well under the AAMI requirements of the mean value being no more than 2 kΩ and no single impedance exceeding 3 kΩ.

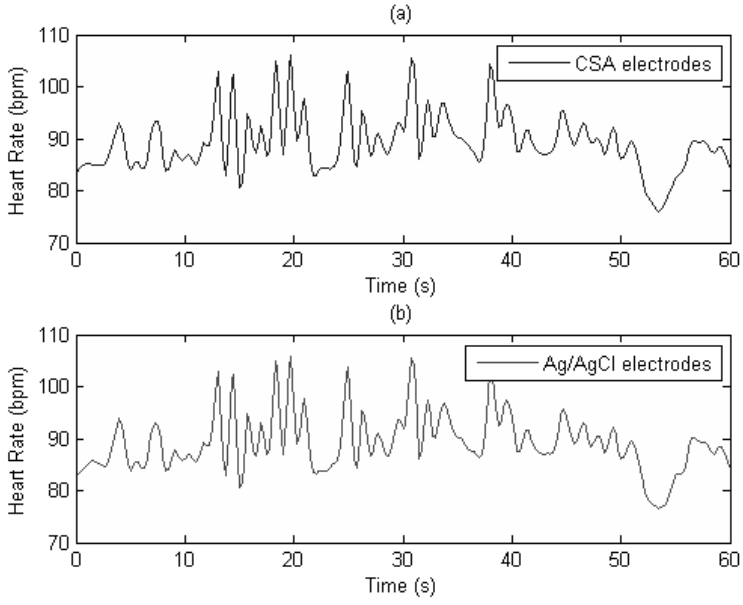

Figure 7.4 – Segment of interpolated HR time series signal from ECG signals acquired by using Ag/AgCl (a) and Carbon/Salt/Adhesive electrodes (b).

7.3.3 Electrode-skin contact Impedance

Figure 7.3 shows the comparison of skin impedance between Ag/AgCl and CSA electrodes as a function of varying frequencies. As shown, activated CSA electrodes exhibit much lower electrode-skin contact impedance than Ag/AgCl electrodes for the frequency band of 4 to 100 KHz.

Note that the measured Ag/AgCl impedance shown in Figure 7.3 is in agreement with previously reported studies[4].

7.3.4 HRV indices

For quantitative HRV analysis, R-wave peak detection was applied[13] and the resultant RR segments were used to calculate time- and frequency-domain indices were calculated, for sitting and standing positions. A summary of time- and frequency domain indices is presented in Table 7.4. Figure 7.4 shows a short duration HR time series obtained by both media.

Table 7.4 HRV indices

Time domain				
	Sitting		Standing	
	Carbon/Salt/Adhesive	Ag/AgCl	Carbon/Salt/Adhesive	Ag/AgCl
meanNN (ms)	1186.103 ± 205.9*	1186.11 ± 205.8*	1330.76 ± 238*	1330.77 ± 238*
SDNN (ms)	100.5 ± 62.2	99.9 ± 60.2	107.1 ± 41.3	106.9 ± 40.6
RMSSD (ms)	30.38 ± 48.24	30.003 ± 46.75	26.08 ± 34.14	25.77 ± 33.13
NN50	61.5 ± 126.3	61.5 ± 126.6	41.6 ± 67.6	41.6 ± 67.1
pNN50	0.039 ± 0.077	0.039 ± 0.07	0.025 ± 0.040	0.025 ± 0.040
Frequency domain				
	Sitting		Standing	
	Carbon/Salt/Adhesive	Ag/AgCl	Carbon/Salt/Adhesive	Ag/AgCl
LF (ms2)	2701 ± 2149	2696 ± 2150	3981 ± 3153	3983 ± 3154
HF (ms2)	3151 ± 8179	3040 ± 7716	1463 ± 1956	1438 ± 1846
Total (ms2)	12208 ± 21116	11921 ± 19957	11074 ± 10979	10958 ± 10520
LF/HF	2.80 ± 2.57	2.82 ± 2.62	4.59 ± 3.84	4.61 ± 3.87

Values are expressed as mean ± standard deviation.
*Statistically significant difference.

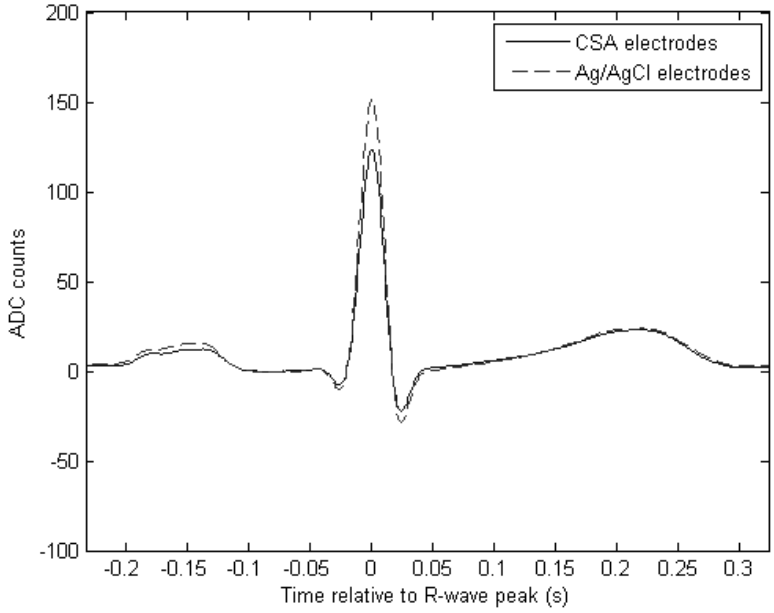

Figure 7.5 – Averaged ensembles of ECG signals acquired using Ag/AgCl and Carbon/Salt/Adhesive electrodes, for the same subject.

These indices are similar to those reported by the HRV task force[1]. Non-significant differences were found for all indices except for the mean NN interval index for both body positions. While the mean NN interval index is significantly different, the actual difference is quite small and it is physiologically insignificant.

7.3.5 ECG morphology comparison

Figure 7.5 represents the average of an ensemble template of ECG aligned by the R-wave peak, using the two media in the same body locations (not simultaneous measurement, however), for a given subject. Such ECG ensemble was computed for each subject during sitting and standing positions. Note the similarity in the morphologies of the ECG waveforms between the two media. The R-wave peak amplitude, ST-segment elevation and QT interval duration time were computed for each ensemble and two-tail paired t-test was performed to compare between CSA and Ag/AgCl results. Table 7.5 includes these results. We found only the R-wave peak amplitude of the Ag/AgCl electrodes showed significantly higher

Table 7.5 ECG morphology measurements over ensemble averages

	CSA	Ag/AgCl
R-peak amplitude [ADC counts]	151.2 ± 37.6*	165.99 ± 13.06
ST segment elevation [ADC counts]	0.45 ± 6.12	-0.17 ± 4.97
QT time segment [s]	0.24 ± 0.02	0.24 ± 0.018

Values are expressed as mean ± standard deviation.
*Statistically significant difference.

value than the CSA electrodes. There was no significant difference in the ST-segment elevation and QT interval time duration between the two electrode media.

7.3.6 Motion artifacts

Figure 7.6 shows an example of the data collected during introduction of motion artifacts. Data from both types of electrodes were simultaneously collected using 2 Holter monitors for each subject. Note that motion artifacts affect differently to CSA and Ag/AgCl electrodes. For comparison of motion artifacts on both types of electrodes, the R-wave peak amplitude misdetections were computed. Table 7.4 shows the percentage of R-wave peak misdetections found for each type of motion. In general, we found that CSA electrodes exhibited a similar performance to the wet Ag/AgCl electrodes in terms of miss-detected R-wave peak.

7.4 Discussion

Novel CSA electrodes were developed and their characteristics were compared to the standard Ag/AgCl electrodes. It was found that our dry electrodes are comparable to the industry gold standard

Table 7.6 R-wave peak misdetection percentage for CSA and Ag/AgCl electrodes in the presence of motion artifacts.

	No movement N = 249 beats		Torso rotation N = 261 beats		Vertical movement N = 267 beats		Random walking N = 255 beats	
	CSA	Ag/AgCl	CSA	Ag/AgCl	CSA	Ag/AgCl	CSA	Ag/AgCl
R-wave peak misdetection %	0%	0%	1%	3.43%	6.67%	3%	9.06%	7.91%

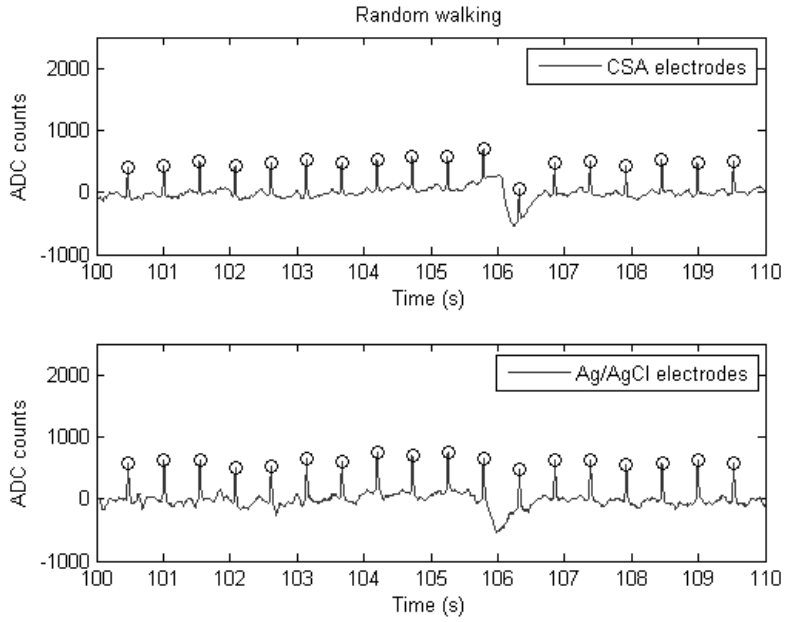

Figure 7.6 – Simultaneous ECG signals to show CSA and Ag/AgCl electrodes' motion artifact response.

Ag/AgCl electrodes in terms of impedance and ECG morphological characteristics. The optimal mixture to fabricate electrodes was determined to be 10% carbon when combined with 90% visco-elastic polymeric adhesive. This mixture resulted in the lowest post-activation impedance, which also meets AAMI requirements. These electrodes need to be activated prior to use in order to reduce their impedance; pre-activation impedance is in the range of mega ohms. Once the electrodes are activated, they are permanent. The optimal activation parameters were found to be 200 V, 100 mA current and a 100 ms discharge time using 1μF capacitor. CSA electrodes address two of Ag/AgCl electrode's issues: dehydration and high cost. The CSA electrodes are theoretically more economical than Ag/AgCl electrodes since carbon is cheaper than silver. Further, the CSA electrodes have an infinite shelf life whereas the Ag/AgCl electrodes dry out and the standard practice is to discard them after 1 month of storage. Finally, our CSA electrodes meet all AAMI requirements.

Electrode-skin impedance measurements showed much lower values for CSA electrodes when compared to wet Ag/AgCl electrodes. Moreover, the impedance of our CSA electrodes is even lower than those reported for carbon nanotube-polydimethylsiloxane (CNT-PDMS) flexible electrodes [5].

All HRV indices derived from the CSA electrodes were found to be no different than Ag/AgCl derived indices. Statistically significant differences were found only for the mean NN interval index for both body positions. However, the differences are minimal and not physiologically significant.

ECG morphological waveforms are well captured with CSA electrodes. ST segment elevation and QT segment time showed no significant differences. However, statistically significant differences in R-wave peak amplitudes were found between ECG signals collected using CSA and Ag/AgCl electrodes. Although CSA electrodes exhibited lower impedance than Ag/AgCl, amplitude and morphology of the ECG signals seem to be influenced by capacitive components of the impedance. The elimination of such reduction is an aim for future generations of CSA electrodes. During stable conditions (no movement), such amplitude reduction did not affect the R-wave peak detection (see Table 7.6).

We examined the quality of both types of electrodes during body movements. Specifically, we examined miss-detection of R-wave peak amplitudes during various body movements consisting of side-to-side and up-and-down torso movements as well as ECG data collection during normal walking condition. In general, CSA electrodes performed comparably to the wet Ag/AgCl electrodes in correct identification of R-wave peaks. During torso rotations, CSA electrodes presented less problems for R-wave peak detection. For vertical movements and random walking, CSA electrodes produced more misdetections than Ag/AgCl electrodes, but such differences were not dramatic. These findings involving CSA show better results with respect to other dry electrodes, which have been reported to have poor performance in comparison to Ag/AgCl in the presence of motion artifacts [4]–[7], [17]. However, more thorough side-by-side comparison of CSA to other dry electrodes will be needed to make such definitive claim.

Based on 30 minutes of exposure to CSA electrodes, none of the 17 subjects showed any negative reactions to electrode-skin contact. Further, in our previous study involving development of hydrophobic ECG electrodes based on a mixture of carbon-black powder and polydimethylsiloxane (CBPDMS), it was shown that CB/PDMS electrodes are not cytotoxic to L929 connective tissue fibroblasts or neonatal human keratinocytes [11]. Given that our current electrodes are also composed of carbon, we do not expect that they are cytotoxic to skin. Certainly, further experiments will need to be performed to determine the long-

term biocompatibility of the CSA electrodes. Moreover, CSA electrodes will need to be tested in the future for their sensitivity to moisture as it is well known that perspiration can lead to degradation of the quality of ECG signals. While we have not tested our electrodes after storing them for more than a year, we have found no ECG signal degradation with 2-month old CSA electrodes (not shown). For future work, we aim to test CSA electrodes after storing them for more than 1 year.

7.5 Conclusion

In summary, we demonstrated that dry ECG electrodes can be fabricated from a mixture of carbon powder, salt, and visco-elastic polymeric adhesive. All ECG morphological waveforms and HRV indices were found to be nearly identical to Ag/AgCl electrodes. Moreover, the CSA electrodes can also be applicable for defibrillation usage but the main advantage is their infinite shelf life which lowers both supply chain handling costs and scrap costs when compared to Ag/AgCl electrodes since the latter have a shelf life of only a month. Hence, our CSA electrodes have the potential to be a viable and cost-effective alternative to standard Ag/AgCl electrodes.

7.6 References

[1] Task Force of the European Society of Cardiology and the North American Society of Pacing and Electrophysiology, "Heart rate variability. Standards of measurement, physiological interpretation, and clinical use," *Eur. Heart J.*, vol. 17, no. 3, pp. 354–381, Mar. 1996.

[2] J. Webster, *Medical Instrumentation: Application And Design, 3Rd Ed*. Wiley India Pvt. Limited, 2009.

[3] A. Searle and L. Kirkup, "A direct comparison of wet, dry and insulating bioelectric recording electrodes," *Physiol. Meas.*, vol. 21, no. 2, pp. 271–283, May 2000.

[4] A. Gruetzmann, S. Hansen, and J. Müller, "Novel dry electrodes for ECG monitoring," *Physiol. Meas.*, vol. 28, no. 11, pp. 1375–1390, Nov. 2007.

[5] H.-C. Jung, J.-H. Moon, D.-H. Baek, J.-H. Lee, Y.-Y. Choi, J.-S. Hong, and S.-H. Lee, "CNT/PDMS composite flexible dry electrodes for long-term ECG monitoring," *IEEE Trans. Biomed. Eng.*, vol. 59, no. 5, pp. 1472–1479, May 2012.

[6] J.-Y. Baek, J.-H. An, J.-M. Choi, K.-S. Park, and S.-H. Lee, "Flexible polymeric dry electrodes for the long-term monitoring of ECG," *Sens. Actuators Phys.*, vol. 143, no. 2, pp. 423–429, May 2008.

[7] G. Ruffini, S. Dunne, L. Fuentemilla, C. Grau, E. Farrés, J. Marco-Pallarés, P. C. P. Watts, and S. R. P. Silva, “First human trials of a dry electrophysiology sensor using a carbon nanotube array interface,” *Sens. Actuators Phys.*, vol. 144, no. 2, pp. 275–279, Jun. 2008.

[8] I. Benedek, *Pressure-Sensitive Formulation*. VSP, 2000.

[9] I. Benedek, *Pressure-Sensitive Adhesives and Applications*. CRC Press, 2004.

[10] K. L. Lerner and B. W. Lerner, *The Gale Encyclopedia of Science*. Cengage Gale, 2008.

[11] B. A. Reyes, H. F. Posada-Quintero, J. R. Bales, A. L. Clement, G. D. Pins, A. Swiston, J. Riistama, J. P. Florian, B. Shykoff, M. Qin, and K. H. Chon, “Novel electrodes for underwater ECG monitoring,” *IEEE Trans. Biomed. Eng.*, vol. 61, no. 6, pp. 1863–1876, Jun. 2014.

[12] M. K. Delano and C. G. Sodini, “A long-term wearable electrocardiogram measurement system,” in *2013 IEEE International Conference on Body Sensor Networks (BSN)*, 2013, pp. 1–6.

[13] C. Vidaurre, T. H. Sander, and A. Schlögl, “BioSig: the free and open source software library for biomedical signal processing,” *Comput. Intell. Neurosci.*, vol. 2011, p. 935364, 2011.

[14] S. Akselrod, D. Gordon, F. A. Ubel, D. C. Shannon, A. C. Berger, and R. J. Cohen, “Power spectrum analysis of heart rate fluctuation: a quantitative probe of beat-to-beat cardiovascular control,” *Science*, vol. 213, no. 4504, pp. 220–222, Jul. 1981.

[15] B. Pomeranz, R. J. Macaulay, M. A. Caudill, I. Kutz, D. Adam, D. Gordon, K. M. Kilborn, A. C. Barger, D. C. Shannon, and R. J. Cohen, “Assessment of autonomic function in humans by heart rate spectral analysis,” *Am. J. Physiol.*, vol. 248, no. 1 Pt 2, pp. H151-153, Jan. 1985.

[16] M. L. Appel, R. D. Berger, J. P. Saul, J. M. Smith, and R. J. Cohen, “Beat to beat variability in cardiovascular variables: noise or music?,” *J. Am. Coll. Cardiol.*, vol. 14, no. 5, pp. 1139–1148, Nov. 1989.

[17] L.-F. Wang, J.-Q. Liu, B. Yang, and C.-S. Yang, “PDMS-Based Low Cost Flexible Dry Electrode for Long-Term EEG Measurement,” *IEEE Sens. J.*, vol. 12, no. 9, pp. 2898–2904, Sep. 2012.

Chapter 8: Assessment of Carbon/Salt/Adhesive Electrodes for Surface Electromyography Measurements

8.1 Introduction

Orthopedics, rehabilitation, sports medicine, stress assessment and neurology are some of the many fields where electromyography (EMG) measurements are employed. EMG aims to measure muscle activity by assessing the electrical activity elicited during muscle contraction. EMG measurements can be acquired directly on the muscle fibers through needle electrodes, but most EMG signals are collected by the use of superficial electrodes applied on the skin, corresponding to the part of the muscle that is of interest. This type of EMG measure is normally called surface electromyography (sEMG).

The current industry gold standard for sEMG is the Silver/Silver Chloride (Ag/AgCl) wet (hydrogel) electrode. These electrodes consist of a layer of silver chloride, often in the form of a paste-like hydrogel surrounding a silver disc. While the hydrogel layer significantly improves the signal quality by effectively lowering the impedance that exists at the electrode-skin interface, it also degrades with time as it dehydrates, producing high impedance. This leads to a loss of signal quality [1] and an increased incidence of motion artifacts and noise. Ag/AgCl electrodes have a number of other disadvantages: they need to be carefully packaged to ensure prolonged retention of the hydrogel layer; they are limited to short-term use because they are known to cause irritation to the skin with prolonged use, especially after their removal [2]; they are also relatively expensive since silver is an expensive commodity.

FLEXcon has developed a novel electrode that does not require a hydrogel layer, to address the issue of dehydration with most of the current industry gold standard electrodes. The new dry electrodes are

designed by combining a viscoelastic polymeric adhesive [3] with carbon black powder and a quaternary salt. This mixture is potentially much more economical than Ag/AgCl. We recently demonstrated and detailed the fabrication process of our new Carbon/Salt/Adhesive (CSA) electrodes and compared their performance to the standard Ag/AgCl electrodes' when acquiring electrocardiographic morphologies [4].

The purpose of this study was to assess the surface electromyography (sEMG) measuring capabilities of the newly-developed CSA electrodes compared to traditional Ag/AgCl electrodes. First, a brief description of the fabrication of the CSA sEMG electrodes is provided. Then the experimental protocol is explained. The experimental protocol, which covered measurements on muscles of various sizes, was meant to compare the impedance of CSA and Ag/AgCl EMG electrodes, evaluate how well the CSA electrodes can replicate Ag/AgCl electrodes for the task of sEMG signal collection, and evaluate the quality of sEMG signals obtained using each media. Measures related to sEMG signals, like "linear envelope" estimation, RMS value, on and off contraction times, and power spectral density were used to evaluate the interchangeability of EMG signals acquired with CSA and Ag/AgCl electrodes. Quality assessment, noise power, motion-artifact corruption, sensitivity to EMG activity and distortion were evaluated using previously-reported and validated indices.

8.2 Materials and Methods

8.2.1 sEMG CSA electrode fabrication

To create the testable CSA sEMG electrodes, the conductive base layer, the adhesive, and the bridge were prepared beforehand. Details about preparation of those components are provided below. After that, a description of the CSA electrode assembly process is included.

8.2.1.1 Conductive Base layer

A polyethylene foam carrier is coated with an electrically conductive material consisting of a polymeric binder loaded with conductive fillers. The conductive coating consists of 50% polymeric binder and 50% conductive filler based on the total solids weight of the mixture. The wet coating is prepared by

weighing out the desired amounts of each component and smoothly blending them together for about 10 minutes until a uniform appearance is obtained. The wet mixture is then coated onto the carrier using a #60 Mayer rod, and then placed into a 71.1 °C oven for 10 minutes to dry. The electrical conductivity of the dried coating is easily checked by measuring its surface resistance to confirm that approximately 150 Ohms per square has been achieved.

8.2.1.2 Adhesive

A releasable carrier is coated with a doped adhesive such as an acrylic pressure sensitive type loaded with conductive carbon filler & a quaternary ammonium salt. The wet adhesive mixture is prepared by weighing out the desired amounts of each component and smoothly blending together for about 10 minutes until a uniform appearance is obtained. The resulting wet mixture is then coated onto a release liner using a # 18 gap drawdown blade and then placed into a 71.1 °C air flow oven for 10 minutes to dry. The dried adhesive is covered with a second liner to facilitate easy handling.

8.2.1.3 Bridge

A releasable carrier is coated with an electrically-conductive material such as a polymeric binder loaded with conductive fillers. The conductive coating consists of 50% polymeric binder and 50% conductive filler based on the total solids weight of the mixture. The wet coating mixture is prepared by

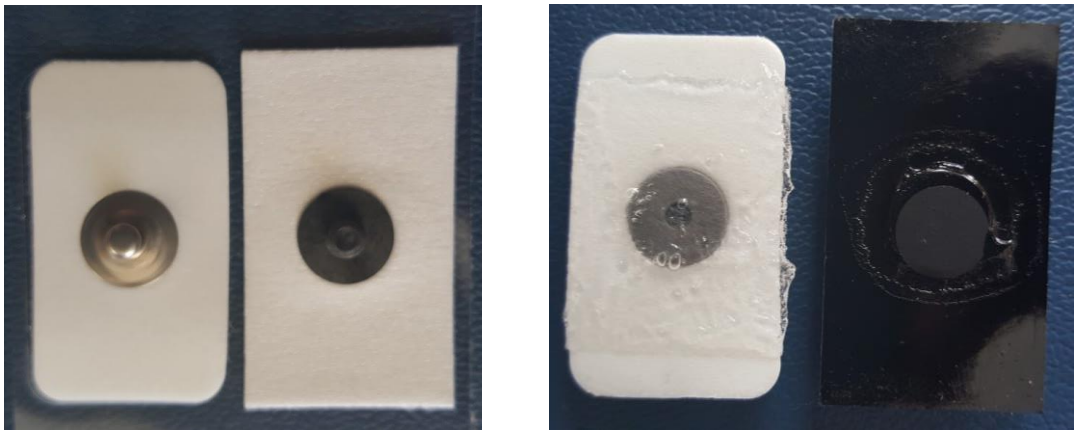

(a) (b)

Figure 8.1 – Connector and contact sides of Ag/AgCl (left) and CSA (right) sEMG electrodes. (a) Connection side; (b) Contact side.

(a) (b) (c) (d)

Figure 8.2 – Sample images of where the electrodes were placed for each muscle-contraction test. Note that the electrodes presented in these images were not the ones that were used for the actual tests. (a) Biceps brachii; (b) Triceps brachii (long head); (c) Tibialis anterior; (d) Quadriceps femoris (rectus femoris).

weighing out the desired amounts of each component and smoothly blending together for about 10 minutes until a uniform appearance is obtained. The wet mixture is then coated onto the carrier using a #60 Mayer rod, and then placed into a 71.1 °C oven for 10 minutes to dry. The electrical conductivity of the dried coating is easily checked by measuring surface resistance to confirm that approximately 150 Ohms per square has been achieved. Discs of the conductive bridge (3/8" diameter) coating/carrier are cut out using a die punch.

8.2.1.4 Electrode Assembly and Activation

A 2 mm round die is used to punch holes in the base layer material every 1-1/2". The bottom half of an electrode snap is inserted through the hole from the side with the conductive coating. The top half of the snap is assembled to the bottom half using sufficient pressure so that the snap halves are securely mated. After removing one release carrier from the adhesive, the adhesive layer is laminated to the conductive base layer so that it covers the bottom halves of the electrode snaps. The remaining release carrier is removed. The discs of conductive bridge coating/carrier are applied to the adhesive with the bridge against the adhesive so that each snap is covered by a bridge. The bridge's release carrier is removed. The lamination

is then applied to a release carrier to facilitate easy handling. The lamination is trimmed into 1-1/2" x 7/8" electrodes to complete the process. After the CSA electrodes are fabricated, they are activated by electrophoresis [5]. This produces multiple isolated Z direction (out of plane) conductive pathways in the adhesive. The resulting test electrodes were used for all testing described.

8.2.2 Electrode-skin contact impedance measurements

CSA-EMG electrodes were used to carry out electrode-skin impedance measurements and were compared to Ag/AgCl EMG electrodes (GS28 Solid Gel - Foam Electrode - 7/8" X 1-1/2", low impedance, disposable Ag/AgCl sensors). Figure 8.1 shows the Ag/AgCl and CSA electrodes used in this study. The skin of the test subject was cleaned before each measurement by wiping with a 2%-alcohol impregnated cotton pad, which was allowed to evaporate before applying the electrodes. Two CSA electrodes were mounted on the left forearm, one on the palm side of the wrist, and the second 5 cm apart from the first but situated towards the elbow. These electrodes were connected to a Hioki IM3570 impedance analyzer, and each measurement was the result of averaging 20 measurements. The signal voltage amplitude was set to 1 V and the frequency range from 4 to 2 KHz. N = 7 pairs of CSA electrodes were used. Once the testing of CSA electrodes were completed, we performed the same experiments as described above using only one pair of Ag/AgCl electrodes. To keep skin properties as constant as possible, all measurements were performed in a single day.

8.2.3 Protocol

N = 20 subjects were enrolled to take part in this test. The experiments were carried out in a quiet, comfortable room (ambient temperature 26-27 °C, relative humidity between 30-50%). To ensure accurate comparison between the electrodes, simultaneous measurements were recorded. To do this, CSA and Ag/AgCl (GS28) electrodes were placed side-by-side. sEMG measurements are largely dependent on location, since proximity to the muscle has a great effect on signal strength. Hence, to eliminate any benefit from being on either side, the CSA and the Ag/AgCl electrodes were assigned a lateral position (left or

right on the same muscle) that alternated from subject to subject. This should have reduced any error resulting from one of the side-by-side positions having a stronger sEMG signal than the other.

We had subjects lift a weight of 3 lb. (1.36 kg) for testing triceps brachii and tibialis anterior muscles. For biceps brachii and quadriceps femoris, they used a weight of 6 lb. (2.72 kg). These weights were chosen considering the size of the muscles and to ensure effective stress on the muscle during contraction time. Before performing every test, we made sure that the locations where the electrodes were placed did not exhibit excessive hair and had been wiped with alcohol and then allowed to dry. If the subject presented thick or abundant hair, they were provided with a disposable razor and asked to shave the hair from the site where the electrodes were placed. Figure 8.2 shows the areas where the electrodes were placed, for each muscle. The electrodes were placed with the subjects in resting condition. Surface EMG measurements of the biceps brachii, triceps brachii (long head), tibialis anterior, and quadriceps femoris (rectus femoris) were recorded while subjects performed four muscle contraction maneuvers during the experiment, one for each muscle. These specific muscles were chosen based on their variance in size. It has been observed that muscles of varying sizes will produce sEMG signals of varying amplitudes.

EMG signals were acquired using a dual-channel bioelectric amplifier (Nikon Kohden) and digitized through an ADInstruments analog-to-digital converter, with a sampling frequency of 1 kHz, and we used compatible PowerLab software.

The completion order of the four maneuvers should not influence the results because the muscles are independent, so for this study they were performed in an arbitrary numerical order that we assigned. While different motions and weights were involved for each muscle, the same time limit for each maneuver was followed for EMG signal recording (Figure 8.3). The contraction maneuvers were kept as clear of motion artifacts as possible by allowing the subject 2 seconds to perform the required movement. Subjects practiced the maneuvers prior to every test until they felt comfortable with the procedure. This was important given the time constraint for the movements in the tests. A visual tool with timing signals was used to guide the subjects throughout the tests.

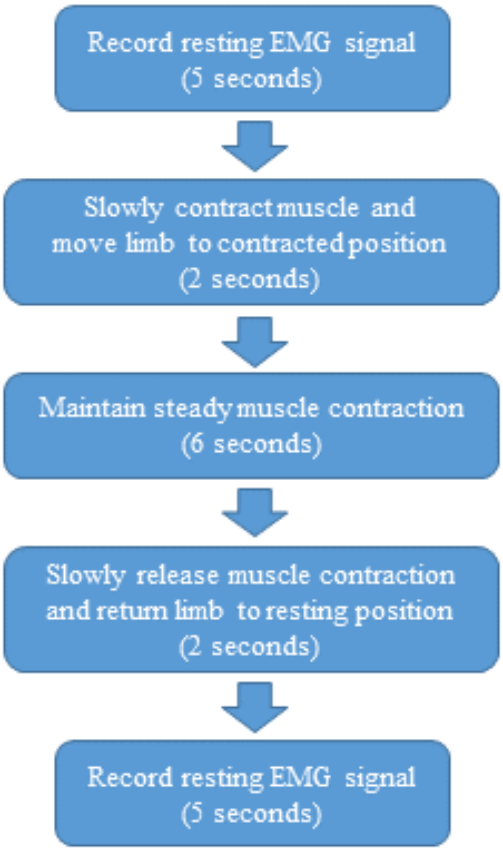

Figure 8.3 – Time frame for movements while recording EMG signal.

Subjects were asked to perform these maneuvers: 1) to contract their biceps, bringing the elbow to a 90 degree angle, with the forearm in supination; 2) to contract their triceps and extend their elbow joint so that the weight was suspended backwards; 3) to contract their tibialis anterior muscle and lift the weight off the floor without extension of the great toe; and 4) to lift their leg up (extend their knee) to procure contraction of the quadriceps. The protocol was approved by the Institutional Review Board of the University of Connecticut.

8.2.4 Signal processing

In the acquisition device the sEMG signals were filtered using an analog bandpass filter (5-300 Hz) and a Notch filter at 60 Hz. We also processed the signals offline to quantify their quality and to compare the performance of the CSA EMG electrodes to the Ag/AgCl EMG electrodes. Several time- and

frequency-domain indices of correlation and the sEMG signals' quality were computed. In the time domain, the linear envelope of each sEMG signal was computed using rectification and a low pass filter (7th-order Chebyshev, cut-off frequency = 16.66 Hz), and an RMS approach was also applied. From the linear envelope, on and off contraction times were estimated.

For frequency domain analysis, the power spectral density (PSD) of each sEMG signal was calculated using Welch's periodogram method with 50% data overlap. A Blackman window (length of 256 data points) was applied to each segment and the Fast Fourier Transform (FFT) was calculated for each windowed segment. Finally, the power spectra of the segments were averaged. An FFT segment size of 1024 data points was used. PSD correlation was computed between CSA and Ag/AgCl signals. Time- and frequency-domain correlations, along with the interchangeability of on- and off-time measures, were intended to prove whether or not CSA electrodes are able to match the functionality of Ag/AgCl electrodes in the task of sEMG signal collection.

To measure quality of the collected sEMG signals, signal-to-noise (SN) ratio (SNR), signal-to-motion (SM) ratio, the spectrum maximum-to-minimum drop in power (DP ratio) density and the power spectrum deformation (Ω ratio) indices were computed. All computations, including the statistical analyses of these indices, are explained below.

8.2.4.1 Time domain measures

8.2.4.1.1 Linear envelope

sEMG signals are rectified (by taking their absolute value), low-pass filtered at 10 Hz, and down-sampled to 41.66 Hz (a rate that is closer to motion frequencies) to get a linear envelope. The resulting envelope is an estimate of the standard deviation of the sEMG signal, which is in turn a measure of the muscles' power. The Pearson's correlation between CSA and Ag/AgCl electrodes' sEMG envelopes was computed, for each muscle and in the overall, to test the similarity between the two simultaneously-acquired signals. Correlation gives us an index of similarity, independent of the amplitude of the signals which were collected with the two types of electrodes side by side.

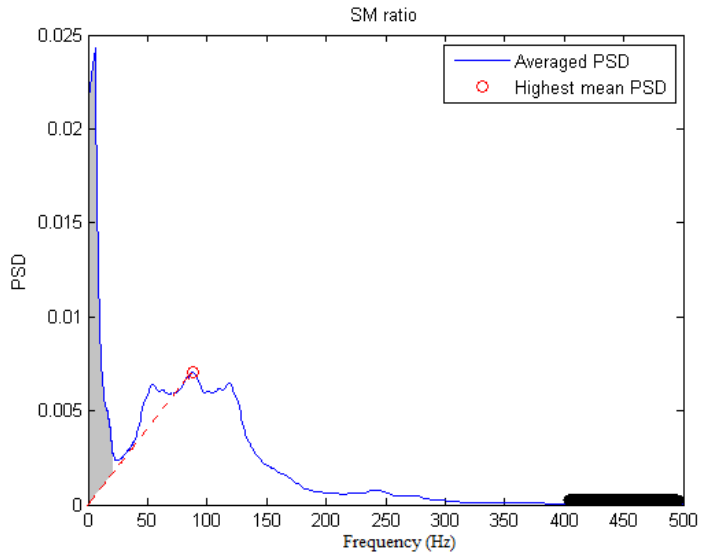

Figure 8.4 – Illustration of SM ratio and SN ratio estimation.
Gray area corresponds to motion artifact. Power on the thick black line (upper 20% of the range) is considered noise.

8.2.4.1.2 Amplitude

Mean value of the linear envelope was computed as an amplitude estimation of sEMG signals. This index was computed for relaxation and contraction stages, to evaluate the statistical differences in amplitude between the signals obtained using CSA and Ag/AgCl electrodes.

8.2.4.1.3 RMS value

The sEMG signals were divided into multiple windows of 25 ms [6]. RMS values were computed from the signals before rectification since the values have both negative and positive values. As with the linear envelope, the Pearson's correlation between CSA and Ag/AgCl electrodes' sEMG RMS values was computed, for each muscle and in the overall.

8.2.4.1.4 On- and off-time

Muscles' on and off contraction times were estimated using the linear envelope of sEMG signals. On and off detection is based on determining the times at which the envelope of the signal exceeds a threshold. In this study the threshold was calculated by:

$$Threshold = \mu + J\sigma \quad \textbf{(1)}$$

Where μ and σ are the mean and standard deviation of the linear envelope during a period of inactivity, and J is a constant. J was fixed to 3 [7] and it was required that the mean of the points in a sliding window of 25 ms exceed the threshold to label a point as an on- or off-time [8]. This approach provides a suitable on- and off-time detection. Agreement between the on and off estimations using CSA and Ag/AgCl sEMG signals was evaluated using Bland and Altman analysis and the Pearson's correlation.

8.2.4.2 Frequency domain measures

8.2.4.2.1 PSD correlation

The raw sEMG data were used to perform frequency domain analysis. To test the similarity between CSA and Ag/AgCl sEMG signals in the frequency domain, the Pearson's correlation coefficient of PSD representations was computed.

8.2.4.2.2 SN Ratio

This index takes into account all kinds of noisy disturbances as well as low signal levels. In this case, noise is defined as any signal of unrecognizable source present in the high-frequency range of the PSD [9]. For the SN ratio calculation we assumed that noise had a constant power density over the frequency region of interest in sEMG recordings and that no muscular activity-related power was present above 400 Hz (upper 20% of the frequency range). So, first, the power for the frequency range above 400 Hz was calculated. The predicted total power of the noise is this power summed over the whole frequency range. The SN ratio was then calculated as the ratio of the total sEMG power to the total power of the noise.

8.2.4.2.3 SM Ratio

For this study, motion artifacts are defined as low-frequency fluctuations of the signal induced by mechanical alteration of the electrode-skin interface. Use of the SM ratio is based mainly on two assumptions: 1) the frequency of motion-induced artifacts of the signal stays well below 20 Hz, and 2) the shape of the non-contaminated sEMG power spectrum is fairly linear between 0 and 20 Hz [10]. As a

consequence, the motion artifacts' spectral power will be mixed in with the true signal dynamics at frequencies between 0 to 20 Hz. According to Sinderby et al., the motion artifacts' power (grey area in Figure 8.4) can be reasonably estimated by summing the PSD area below 20 Hz that exceeds a straight line between the origin and the highest mean power density. The highest mean power density (the red dot in the averaged spectral plot of Figure 8.4) was defined as the largest mean spectral value within a window length of 12.7 Hz starting from 35 Hz to 500 Hz. Finally, the sum of the area under the PSD for all frequencies divided by motion artifact power was computed to obtain the SM ratio.

8.2.4.2.4 DP ratio

The spectrum maximum-to-minimum drop in power (DP ratio) was obtained by computing the quotient between the highest and lowest mean PSD values. The mean PSD is obtained by averaging a spectral window length of 12.7 Hz (13 consecutive points). The DP ratio is an indicator of whether the spectral frequency contents of interests are adequately peaked and is sensitive to the signal's amplitude and can detect the absence of sEMG activity. DP ratio is not sensitive to power below 35 Hz (in contrast to the SN ratio) and will not provide falsely high values because of the power induced by motion artifacts. A higher DP ratio is desirable.

8.2.4.2.5 Ω ratio.

The spectral deformation is computed in terms of spectral moments, as follows:

$$\Omega = (M_2/M_0)^{\frac{1}{2}}/(M_1/M_0), \quad \textbf{(2)}$$

where

$$M_n = \sum_{i=0}^{i_{max}} power\ density_i \cdot frequency_i^n \quad \textbf{(3)}$$

Ω ratio is sensitive to changes in symmetry and peaking of the PSD and to additive disturbances in the high- and low-frequency regions [9]. This index identifies all dynamics of spectral changes except those caused by pure translations along the frequency axis. In this manner it adapts to myoelectric changes

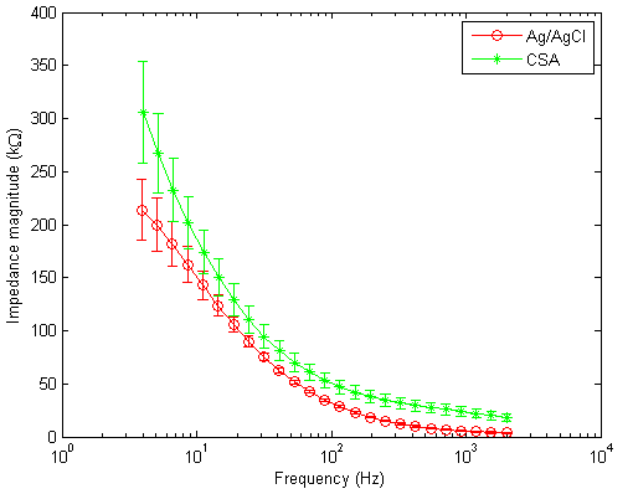

Figure 8.5 – Electrode-skin contact impedance measurements for CSA and Ag/AgCl electrodes.

due to muscle fatigue but not to additive disturbances. The feature is also sensitive to motion artifacts, which give an excess of low-frequency power. A lower Ω is desirable.

The SN, SM and DP ratios are presented in decibels, and the Ω ratio is unitless. These four indices obtained for CSA and Ag/AgCl electrodes were compared for each muscle and in the overall, by testing for statistically significant differences, to check whether there is an electrode media that collects the signal with lower noise power, lower motion-artifact corruption, more sensitivity to EMG activity and lower distortion, respectively. Quality indices were computed using a myoelectric signal processing toolbox developed by Chan and Green [11].

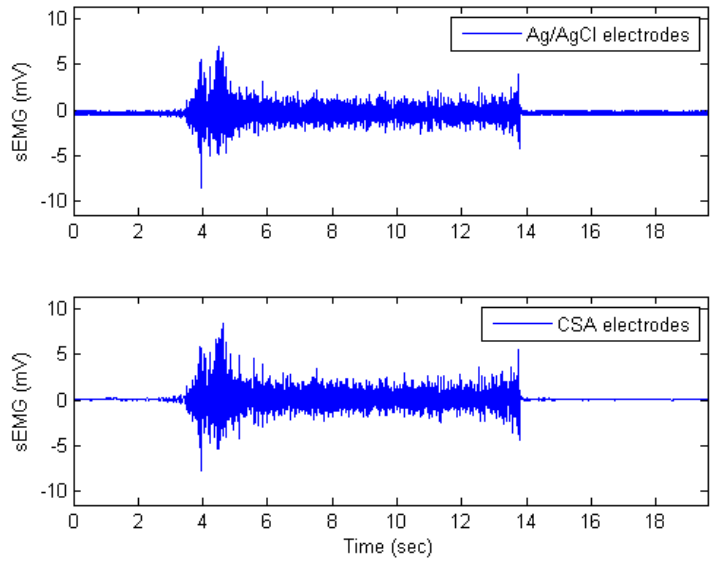

Figure 8.6 – Sample sEMG measures using Ag/AgCl (top) and CSA electrodes (bottom).

8.3 Results

Results for electrode-skin contact measurements are presented in Figure 8.5. Ag/AgCl sEMG electrodes exhibited lower impedance compared to CSA sEMG electrodes throughout the range of frequencies of interest (4 Hz to 2 kHz). Representative sEMG signals acquired with Ag/AgCl and CSA electrodes are shown in Figure 8.6. It is clearly evident that on the Figure 8.6 (biceps of a given subject),

Table 8.1 Results for evaluation of signals' interchangeability

Index	Stage	Biceps	Triceps	Tibialis	Quadriceps	Overall
Amplitude Ag/AgCl (V)	Relaxation	0.16 ± 0.17	0.42 ± 0.27	0.064 ± 0.101	0.072 ± 0.068	0.18 ± 0.22
	Contraction	0.99 ± 0.42	1.47 ± 0.53	0.98 ± 0.7	0.72 ± 0.36	1.04 ± 0.58
Amplitude CSA (V)	Relaxation	0.17 ± 0.26	0.48 ± 0.46	0.06 ± 0.11	0.051 ± 0.041	0.19 ± 0.31
	Contraction	0.99 ± 0.38	1.48 ± 0.66	1.01 ± 0.68	0.71 ± 0.31	1.05 ± 0.59
Contraction time correlation	on	0.95	0.96	0.96	0.97	0.96
	off	0.96	0.98	0.91	0.90	0.94
Envelope correlation		0.91 ± 0.07	0.92 ± 0.038	0.95 ± 0.029	0.93 ± 0.05	0.93 ± 0.052
RMS correlation		0.91 ± 0.06	0.91 ± 0.038	0.95 ± 0.029	0.93 ± 0.05	0.93 ± 0.05
PSD correlation		0.98 ± 0.02	0.95 ± 0.034	0.95 ± 0.046	0.97 ± 0.04	0.96 ± 0.04

Values are expressed as mean ± standard deviation.

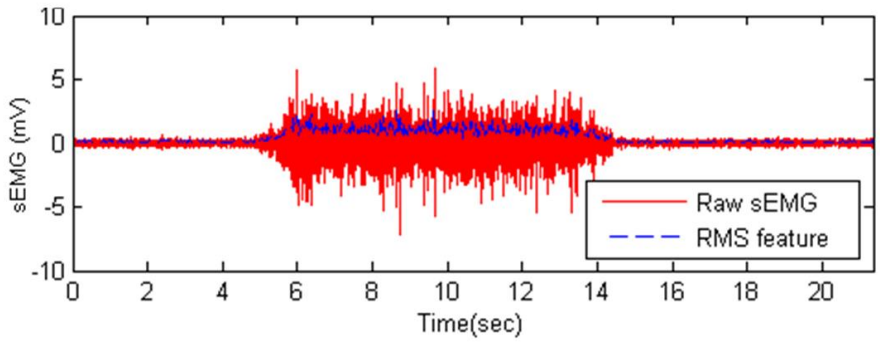

Figure 8.7 – RMS value envelope estimation for a given signal.

the CSA electrodes exhibited a lower noise level than Ag/AgCl during the relaxation phases of the signal while both types of electrodes exhibited similar signal amplitude during the contraction phase.

Table 8.1 contains the results for our interchangeability analysis. No significant differences in amplitude were found between CSA and Ag/AgCl sEMG signals either for relaxation or for contraction stages, for any muscle or in the overall which combines all four types of muscles denoted in Table 8.1. The CSA electrodes exhibited lower amplitude for most of the muscles during muscle relaxation, with the exception of the Tibialis, and higher amplitude during the contraction time for all the muscles. The differences in the relaxation and contraction amplitudes are also present in the overall comparison (gathering results for all muscles together), but they are not found to be statistically significant.

The linear envelope, the RMS value envelope, and the sEMG PSD were highly correlated. The linear envelope and RMS value envelope exhibited a correlation higher than 0.91 for all muscle. Lower correlation was found for the smaller muscles (biceps and triceps), and a stronger correlation was found for the bigger muscles (tibialis and quadriceps). The PSD of the sEMG signals achieved a correlation higher than 0.95 for all the muscles. Figure 8.7 shows the RMS value envelope for a given subject.

On- and off-time contraction time estimations were highly correlated between the two electrodes. Figure 8.8 exemplifies the on- and off-time estimation using the linear envelope and the threshold. We did not use a single value of the sEMG but the mean value of a 25 ms window to determine if a threshold of the occurrence of the muscle contraction or relaxation had occurred. For all the muscles, the correlation of off-time detection was above 0.9. Correlation for on-time estimations was always very high (above 0.95). Notice that the threshold was computed using the same signal during the relaxation stage, i.e. for Ag/AgCl electrodes the threshold was computed using a segment of Ag/AgCl sEMG signal during the relaxation stage. The same time frame of the relaxation stage was used to compute the threshold for CSA and Ag/AgCl signals. Figure 8.9 presents the Bland-Altman plot and a scatter plot of the results for on- and off-time estimation, allowing us to test the interchangeability of the signals for this purpose. Notice the small bias and variance of the error for on- and off-time estimation.

Table 8.2 includes the frequency-domain indices for quality assessment of sEMG signals. The SN ratio was significantly different between the two media for biceps and quadriceps, and in the overall. CSA electrodes showed a higher SN ratio, compared to Ag/AgCl. The SM ratio was different for all the muscles, with CSA electrodes always exhibiting a better response to motion artifacts. The DP ratio was higher for Ag/AgCl electrodes only in the overall, compared to CSA electrodes. Finally, the Ω ratio indicates a significantly higher spectral deformation for the Ag/AgCl electrodes.

Table 8.2 Indices of EMG signal quality estimated using frequency domain measures

		Biceps	Triceps	Tibialis	Quadriceps	Overall
SN ratio (dB)	Ag/AgCl	41.6 ± 14.9	35.2 ± 9.62	24.4 ± 17.3	29.8 ± 15	32.7 ± 15.6
	CSA	50.01 ± 5.89*	34.93 ± 11.9	30.42 ± 5.44	37.83 ± 6.27*	38.3 ± 10.6*
SM ratio (dB)	Ag/AgCl	15.9 ± 7.26	18.4 ± 7.17	19.3 ± 9.49	12.9 ± 9.08	16.6 ± 8.52
	CSA	21.5 ± 12*	22.6 ± 9.56*	30.6 ± 14.5*	21.9 ± 9.95*	24.1 ± 12.1*
DP ratio (dB)	Ag/AgCl	82.8 ± 6.61	62.2 ± 11.7	58.9 ± 13.5	67.7 ± 9.26	67.9 ± 13.9
	CSA	82.9 ± 7.79	60.6 ± 15.3	55.3 ± 9.6	62.8 ± 6.73	65.4 ± 14.6*
Ω ratio (relative units)	Ag/AgCl	1.48 ± 0.14	1.39 ± 0.27	1.42 ± 0.6	1.56 ± 0.38	1.46 ± 0.39
	CSA	1.39 ± 0.12*	1.31 ± 0.12	1.28 ± 0.31	1.3 ± 0.173*	1.32 ± 0.2*

Values are expressed as mean ± standard deviation. *$p<0.05$.

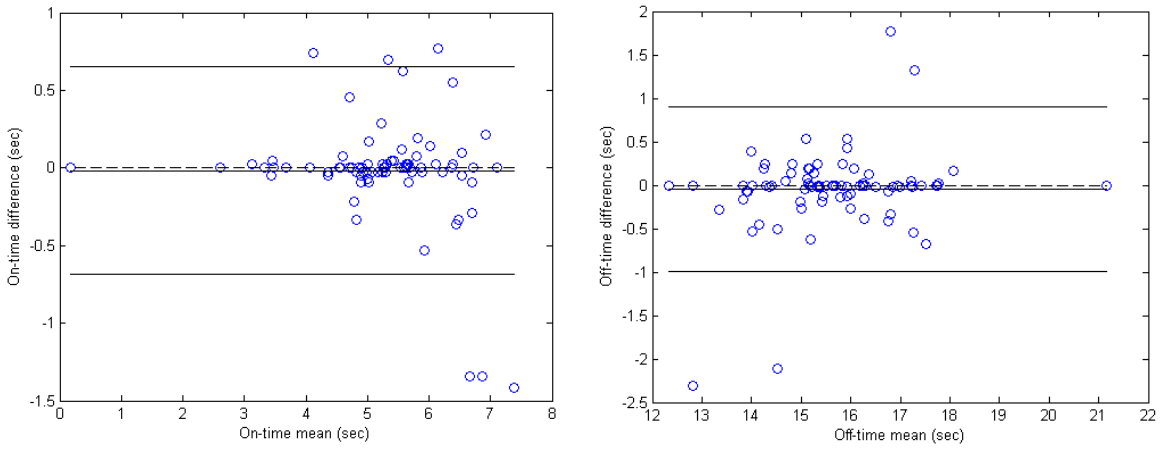

Figure 8.9 – Bland-Altman plot.
(a) On-time estimation (bias = -0.005, variance = 0.1); (b) Off-time estimation (bias = -0.061, variance = 0.23).

8.4 Discussion

First, CSA and Ag/AgCl electrodes were compared by means of impedance measurements. Then, measures of similarity were deployed to evaluate whether CSA sEMG electrodes could replicate dynamics of the Ag/AgCl electrodes. Finally, both time- and frequency-domain indices of sEMG signal quality were introduced to highlight the advantages of using CSA electrodes for the task of sEMG signal collection.

Despite the higher electrode-skin contact impedance exhibited by the CSA electrodes, no significant amplitude differences were found between the signals obtained by the two media. Hence, the impact of the electrode-skin contact impedance on the collected signal amplitude was found to be negligible. Note that impedance results between Ag/AgCl and CSA electrodes are in agreement with what has been reported previously [4], [12]–[14]. Higher impedance was found for CSA electrodes in the current work than in our previous study [4], but this is because the salt concentration was substantially reduced to minimize possible skin irritation. One way to lower the impedance of CSA electrodes is to use higher salt concentrations, but this can lead to possible skin irritation as found in our previous study [4].

The analysis of interchangeability comprises amplitude comparison, linear envelope, on- and off-time estimation, RMS value envelope and PSD correlation. Differences in amplitude estimation during relaxation and contraction stages were not significant, demonstrating that CSA electrodes are at least as sensitive to collect sEMG signals as the Ag/AgCl electrodes. All the correlation values were high and the biases of the measures were low, indicating that CSA electrodes can be used as functional substitutes for Ag/AgCl electrodes for sEMG signal collection.

EMG signal waveforms are more irregular than others (e.g. ECG) and motion artifacts and noise corruption are more difficult to assess by visual inspection of the signal in time or frequency domains. Given this complication, previously-reported and validated indices for automatic evaluation of EMG signal quality were employed. With the only exception of DP ratio (which was higher for Ag/AgCl electrodes only in the overall), the quality indices SN, SM and Ω ratios were in favor of CSA electrodes. These indices suggest that CSA electrodes are more resistant to noise and motion artifact corruption, two highly relevant issues for sEMG signal collection. These are significant benefits of CSA electrodes considering that one of the disadvantages of past dry electrodes, compared to gel electrodes, was the lack of flexible contact provided by the gel. This rigidity produced variations in contact during motion, and tended to introduce motion artifacts to the EMG signal. However, for the CSA electrodes, the Z-direction formation of carbon columns after activation provides a better resistance to shifting against skin, as the electrodes should be less sensitive to X- and Y-direction potentials. Specifically, the main advantage of the CSA electrode is that the conductivity enhancing feature (the bridge) is a low impedance electrically conductive material that produces a lower electrode ohm value by connecting in parallel multiple isolated Z direction (out of plane) conductive pathways in the adhesive. This can be described by

$$\frac{1}{R_{total}} = \frac{1}{R_1} + \frac{1}{R_2} + \frac{1}{R_3} + \cdots + \frac{1}{R_n} \quad \textbf{(4)}$$

where R represents each isolated Z direction pathway. The bridge is specifically designed to balance electrical, mechanical and electrode adhesion properties: its conductive loading level provides

electrical conductivity, its polymeric content and thinness provide mechanical flexibility, and its small area does not significantly reduce the adhesive bonding.

Finally, the lower Ω ratio demonstrates that CSA electrodes are more able to adapt to muscular activity changes derived from muscle fatigue but not from additive disturbances like motion artifact and noise, compared to Ag/AgCl. The higher DP ratio of Ag/AgCl electrodes suggests that the PSD of sEMG signals obtained with such electrodes are more sensitive to detecting the absence of sEMG activity.

8.5 Conclusion

CSA and Ag/AgCl electrodes were quantitatively compared for the task of collecting sEMG signals. It was found that our dry CSA electrodes are comparable to the gold standard Ag/AgCl electrodes in that there were no significant differences in the sEMG amplitude and activation times. Further, CSA electrodes were more resistant to noise and motion artifacts and delivered signals with lower spectral distortion, compared to Ag/AgCl. This is primarily an exciting result because of the two salient disadvantages of Ag/AgCl electrodes that are not a problem for CSA: dehydration with storage or prolonged use, and higher cost. The results of the current work indicate that CSA electrodes represent a suitable and cost-effective alternative to standard Ag/AgCl electrodes for sEMG signal collection. For point-of-care applications, CSA electrodes can be used to monitor the progression of muscular dystrophies or control muscle activities via signal processing of the electromyogram data. Certainly, with the advent of sophisticated machine learning algorithms and robotics, rehabilitation engineering of muscles and limbs will be a good opportunity for more noise-resistant and cost-effective surface EMG electrodes than the current standard hydrogel-based electrodes.

8.6 References

[1] A. Searle and L. Kirkup, “A direct comparison of wet, dry and insulating bioelectric recording electrodes,” *Physiol. Meas.*, vol. 21, no. 2, pp. 271–283, May 2000.

[2] J.-Y. Baek, J.-H. An, J.-M. Choi, K.-S. Park, and S.-H. Lee, “Flexible polymeric dry electrodes for the long-term monitoring of ECG,” *Sens. Actuators Phys.*, vol. 143, no. 2, pp. 423–429, May 2008.

[3] I. Benedek, *Pressure-sensitive adhesives and applications*. CRC Press, 2004.

[4] H. F. Posada-Quintero, B. A. Reyes, K. Burnham, J. Pennace, and K. H. Chon, “Low Impedance Carbon Adhesive Electrodes with Long Shelf Life,” *Ann. Biomed. Eng.*, vol. 43, no. 10, pp. 2374–2382, Oct. 2015.

[5] K. L. Lerner and B. W. Lerner, *The Gale Encyclopedia of Science*. Cengage Gale, 2008.

[6] C. J. De Luca, “The Use of Surface Electromyography in Biomechanics,” *J. Appl. Biomech.*, vol. 13, no. 2, pp. 135–163, May 1997.

[7] R. P. Di Fabio, “Reliability of computerized surface electromyography for determining the onset of muscle activity,” *Phys. Ther.*, vol. 67, no. 1, pp. 43–48, Jan. 1987.

[8] P. W. Hodges and B. H. Bui, “A comparison of computer-based methods for the determination of onset of muscle contraction using electromyography,” *Electroencephalogr. Clin. Neurophysiol.*, vol. 101, no. 6, pp. 511–519, Dec. 1996.

[9] A. Arvidsson, A. Grassino, and L. Lindström, “Automatic selection of uncontaminated electromyogram as applied to respiratory muscle fatigue,” *J. Appl. Physiol.*, vol. 56, no. 3, pp. 568–575, Mar. 1984.

[10] C. Sinderby, L. Lindström, and A. E. Grassino, “Automatic assessment of electromyogram quality,” *J. Appl. Physiol. Bethesda Md 1985*, vol. 79, no. 5, pp. 1803–1815, Nov. 1995.

[11] A. D. Chan and G. C. Green, “Myoelectric control development toolbox,” in *Proceedings of 30th Conference of the Canadian Medical & Biological Engineering Society*, 2007, vol. 1, pp. M0100–1.

[12] A. Gruetzmann, S. Hansen, and J. Müller, “Novel dry electrodes for ECG monitoring,” *Physiol. Meas.*, vol. 28, no. 11, pp. 1375–1390, Nov. 2007.

[13] B. A. Reyes, H. F. Posada-Quintero, J. R. Bales, A. L. Clement, G. D. Pins, A. Swiston, J. Riistama, J. P. Florian, B. Shykoff, M. Qin, and K. H. Chon, “Novel electrodes for underwater ECG monitoring,” *IEEE Trans. Biomed. Eng.*, vol. 61, no. 6, pp. 1863–1876, Jun. 2014.

[14] Y. Noh, J. R. Bales, B. A. Reyes, J. Molignano, A. L. Clement, G. D. Pins, J. P. Florian, and K. H. Chon, “Novel Conductive Carbon Black and Polydimethlysiloxane ECG Electrode: A Comparison with Commercial Electrodes in Fresh, Chlorinated, and Salt Water,” *Ann. Biomed. Eng.*, vol. 44, Jan. 2016.

Chapter 9: Dry Carbon/Salt Adhesive electrodes for recording Electrodermal Activity

(Posada-Quintero, H. F., Rood, R., Noh, Y., Burnham, K., Pennace, J. and Chon, K. H.. Dry Carbon/Salt Adhesive electrodes for recording Electrodermal Activity. Sensors & Actuators: A. Physical. In process of revision for publication)

9.1 Introduction

This paper describes the evaluation of carbon/salt adhesive (CSA) electrodes for measuring electrodermal activity (EDA). CSA electrodes' performance was compared to Silver/Silver Chloride (Ag/AgCl) hydrogel electrodes, the gold standard for electrodermal recording [1]. EDA measures have been traditionally used to assess psychophysiological stress [1], [2], but recently have also been used to assess sympathetic nervous system arousal under stressors of many kinds [3]–[7]. The increasing relevance and popularity of EDA and the ease of data acquisition via wearable devices necessitates the development of better electrodes and instrumentation.

The EDA is a measure of the change in conductance of the skin [1]. When the body is experiencing stressful situations the sympathetic nervous system (SNS) is activated. Sympathetic innervation of sweat glands results in sweat production. As sweat production increases, the conductance of the skin increases, due to high conductivity of the sodium chloride in the sweat. EDA is measured as the modulation produced by such conductivity changes on a power (DC or AC) source [8]. EDA has many potential applications in society. For instance, it could be used for monitoring the stress which the US Navy personnel are experiencing when working in harsh conditions (e.g. battlefield, underwater, prolonged surveillance, etc.). Another possible application could be the use of these electrodes in the automobile industry to alert drivers when they are too tired to be driving because their EDA levels indicate that the driver is falling asleep. In

wearable devices, EDA signals could be used to develop alarms of high or increasing levels of cognitive (related to workload), physical (during workout) or emotional stress, among other things.

EDA data acquisition with Ag/AgCl electrodes requires the application of a paste-like hydrogel over a silver disc. While the hydrogel layer significantly improves the signal quality by effectively lowering the impedance that exists at the electrode-skin interface, impedance increases when the hydrogel layer degrades with time as a result of dehydration. This leads to a loss of signal quality and an increased incidence of motion artifacts and noise [9]. Also, Ag/AgCl electrodes are expensive since silver is an expensive commodity. The Ag/AgCl electrodes we used for this study needed to be taped to the subject's fingers, because they don't have any self-attaching system similar to ECG Ag/AgCl that have an adhesive surrounding the hydrogel.

The most salient advantages of CSA electrodes are their consistently low impedance and no shelf life limitations without the use of a hydrogel layer [10]. These electrodes are cheap to make, and because of their ease of fabrication and flexibility they can be designed, tuned and configured depending on the application. For this study, we have made electrodes in such a way that they wrap around the fingers, with electrode-skin contact surface of around 2 cm2 and a little circular conduction bridge placed directly on a fingertip. We expected these dimensions and characteristics to be suitable for EDA measurements, because of the finger's anatomy and the nature of the EDA signal.

Most EDA devices involve the application of an external constant current or voltage source via electrodes on the skin, either direct current (DC) or alternating current (AC). These are termed exosomatic methods. EDA devices measure the modulated current or voltage (depending on whether the constant source is voltage or current, respectively) to compute the skin conductance. Although AC-source devices have shown advantages over DC-source devices (mainly, avoiding electrode polarization [1]), both types are still widely used.

We aimed to compare CSA to Ag/AgCl electrodes for the task of acquiring EDA signals. First, the electrode-skin impedance was measured for CSA and Ag/AgCl electrodes. The electrodes were tested with

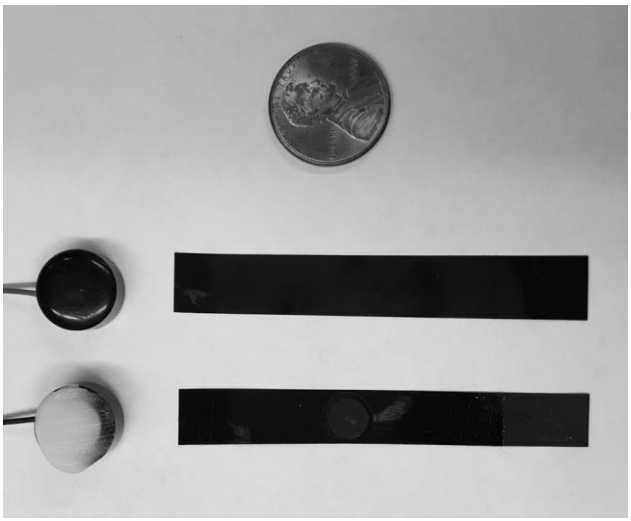

Figure 9.1 – Ag/AgCl hydrogel electrodes (left) and CSA electrodes (right) for EDA

representative types of stressors for which EDA is used, namely physical, emotional, and cognitive stress. The same protocol was followed using DC- and AC-source devices.

9.2 Materials and Methods

Figure 9.1 shows CSA and Ag/AgCl electrodes used to collect EDA signals during this study. FLEXcon developed CSA electrodes to address the issue of dehydration with the current industry gold standard electrodes for collecting bioelectric signals [10]. They were designed by combining a visco-elastic polymeric adhesive [11] with carbon black powder and a quaternary salt. This mixture is potentially much more economical than Ag/AgCl. The process of fabrication of CSA electrodes, and the implemented methods to compare them to Ag/AgCl electrodes are described below.

9.2.1 Fabrication of CSA electrodes for EDA

To create the testable CSA electrodes for EDA measurements, the conductive base layer, the adhesive, and the bridge were prepared beforehand. Details about preparation of the components and a description of the CSA electrode assembly process are included below.

9.2.1.1 Conductive Base layer.

A polyethylene foam carrier is coated with an electrically conductive material consisting of a polymeric binder loaded with conductive fillers. The conductive coating consists of 50% polymeric binder and 50% conductive filler based on the total solids weight of the mixture. The wet coating is prepared by weighing out the desired amounts of each component and smoothly blending them together for about 10 minutes until a uniform appearance is obtained. In the design of CSA electrodes to collect EDA, concentrations of 2% carbon and 15% salt were used. The wet mixture is then coated onto the carrier using a #60 Mayer rod, and then placed into a 71.1 °C oven for 10 minutes to dry. The electrical conductivity of the dried coating is easily checked by measuring its surface resistance to confirm that approximately 150 Ohms per square has been achieved.

9.2.1.2 Adhesive.

A releasable carrier is coated with a doped adhesive such as an acrylic pressure sensitive type loaded with conductive carbon filler & a quaternary ammonium salt. The wet adhesive mixture is prepared by weighing out the desired amounts of each component and smoothly blending together for about 10 minutes until a uniform appearance is obtained. The resulting wet mixture is then coated onto a release liner using a # 18 gap drawdown blade and then placed into a 71.1 °C air flow oven for 10 minutes to dry. The dried adhesive is covered with a second liner to facilitate easy handling.

9.2.1.3 Bridge.

A releasable carrier is coated with an electrically-conductive material such as a polymeric binder loaded with conductive fillers. The conductive coating consists of 50% polymeric binder and 50% conductive filler based on the total solids weight of the mixture. The wet coating mixture is prepared by weighing out the desired amounts of each component and smoothly blending together for about 10 minutes until a uniform appearance is obtained. The wet mixture is then coated onto the carrier using a #60 Mayer rod, and then placed into a 71.1 °C oven for 10 minutes to dry. The electrical conductivity of the dried coating is easily checked by measuring surface resistance to confirm that approximately 150 Ohms per square has been achieved. Discs of the conductive bridge coating/carrier are cut out using a die punch.

9.2.1.4 Electrode Assembly and Activation.

After removing one release carrier from the adhesive, the adhesive layer is laminated to the conductive base layer so that it covers the bottom of the electrodes. The remaining release carrier is removed. The discs of conductive bridge coating/carrier are applied to the adhesive with the bridge against the adhesive. The bridge's release carrier is removed. The lamination is then applied to a release carrier to facilitate easy handling. The lamination is trimmed into 1-1/2" x 3/8" electrodes to complete the process. We cut the material in this shape so the electrode can be wrapped around the finger, with the bridge in contact with the fingertip, providing stability. After the CSA electrodes were fabricated, they were activated by electrophoresis [12]. This produces multiple isolated Z direction (out of plane) conductive pathways in the adhesive. The bridge, or conductivity-enhancing feature, is a low impedance electrically conductive material that produces generally lower electrode impedance by connecting in parallel the Z direction conductive pathways. This can be described by $1/R_{total} = (1/R1)+(1/R2)+(1/R3)+....(1/Rn)$ where R represents each isolated Z direction pathway. The bridge is specifically designed to balance electrical, mechanical and electrode adhesion properties: its conductive loading level provides electrical conductivity, its polymeric content and thinness provide mechanical flexibility, and its small footprint minimizes reduction in adhesive bonding.

9.2.2 Protocol

The study protocol was approved by the Institutional Review Board of The University of Connecticut and all volunteers provided written informed consent to participate in the experiment. Electrode-skin contact impedance was measured for both media. For procuring a fair comparison, skin properties were kept as constant as possible by doing all measurements in a single day, on a single subject. The skin of the test subject was cleaned before each measurement by wiping with a 70% alcohol-impregnated cotton pad, which was allowed to evaporate before applying the electrodes. Two electrodes were mounted, one each on the index and middle fingers. These electrodes were connected to the Hiroki IM3570 impedance analyzer, and each measurement is the result of averaging 10 measurements. The signal

voltage amplitude was set to 1 V and the frequency range from 4 to 200 Hz. N = 7 pairs of CSA electrodes were used for impedance measurements.

To evaluate CSA electrode performance on measuring EDA, three types of stress were monitored throughout this study: physical, emotional, and cognitive. The physical testing consisted of electrical stimulation (shocks), which is a startle-like test; the emotional testing consisted of watching a disturbing video; the cognitive testing consisted of the Stroop test. The latter two are considered tonic-stress tests. With an overall experiment length of just above 40 minutes, subjects experienced each type of stress after a resting period to procure hemodynamic stabilization, and 5 minutes of baseline measurement.

First, the subject went through the electrical stimulation phase. This phase required the use of a commercially available dog collar [13]. The contact points of the receiver were placed on the inside of the subjects forearm. The power level on the transmitter was set to a level just enough to elicit a response on the subjects (amperage of less than 1.5 mA) without any risk, and remained at this level throughout the entire period of electrical stimulation (5-min baseline plus 5-min stimulation). This level of power was chosen because it was just above the threshold of feeling of 1 mA [14]. This also was chosen to adhere to UConn IRB recommendations and reduce any unnecessary discomfort to subjects. After the baseline recordings, there were 5 minutes of test during which the subjects were stimulated twice, at minutes 1 and 4. Subjects were not told when the shocks were going to be given. Each shock lasts about 100 ms. At the end of the five minutes the dog collar was taken off the subject.

The second stage consisted of emotional stimulation by presenting to the subjects a disturbing video (adapted from [15]). After 5 minutes of baseline recordings, subjects were presented a video including images and sounds intended to elicit emotional stress on the subjects (the video was approved by the IRB at The University of Connecticut). Finally, the Stroop test was applied in the same manner as in [16]. Stroop tests induce cognitive stress on subjects. Five minutes of baseline measurements were also recorded for the subject before the Stroop task took place.

9.2.3 Subjects

N= 16 subjects (5 female, 11 male, age 25 ± 7.7 years old) were selected. CSA and Ag-AgCl electrodes were used simultaneously on every subject to collect EDA signals. Subjects were screened to participate in the experiment based on their answers to a preliminary questionnaire. This was a screening process to make sure that candidates who use drugs frequently, sweat often and easily, or have a pre-existing condition that puts them in harm during the experiment were excluded. Subjects were not allowed to drink, smoke or use any other type of drug (excluding daily prescriptions) for a 48 hour period before testing. This eliminated any variables that may affect the response the body has to certain stressful scenarios. Some drugs and daily medications have a direct correlation with skin conductance changes, hence, subjects with these scenarios were excluded. Any candidates that have metal implants, pacemakers, or other implants were not allowed to enter this study to avoid harmful effects of the electrical shock experiment. In addition to this, candidates with severe anxiety problems or cardiac and circulatory conditions such as chronic hypertension or frequent heart palpitations were excluded from this study. Also, candidates who are pregnant or have a past history of seizures did not meet criteria. All other subjects who completed the questionnaire were allowed to participate.

9.2.4 Devices

Data were collected using both DC- and AC-source EDA devices (N=8 for each). AC-source EDA measurement has been documented to be superior to DC-source measurement with respect to electrode polarization and also possible effects of the applied voltage on biological membranes [17]. Despite its known advantages compared to DC, AC has been infrequently used so far [1]. For this reason, we decided to compare CSA and Ag/AgCl electrodes using both types of devices.

Two identical DC-source EDA devices were implemented to perform a fair comparison between the two media. Figure 9.2 shows the schematic diagram of the circuit for the DC-source EDA devices fabricated for this study. It is powered by a source of 3.3 volts. The current source applied a constant current to the subjects' fingers through the electrodes. The signal variations on the resulting voltage were acquired

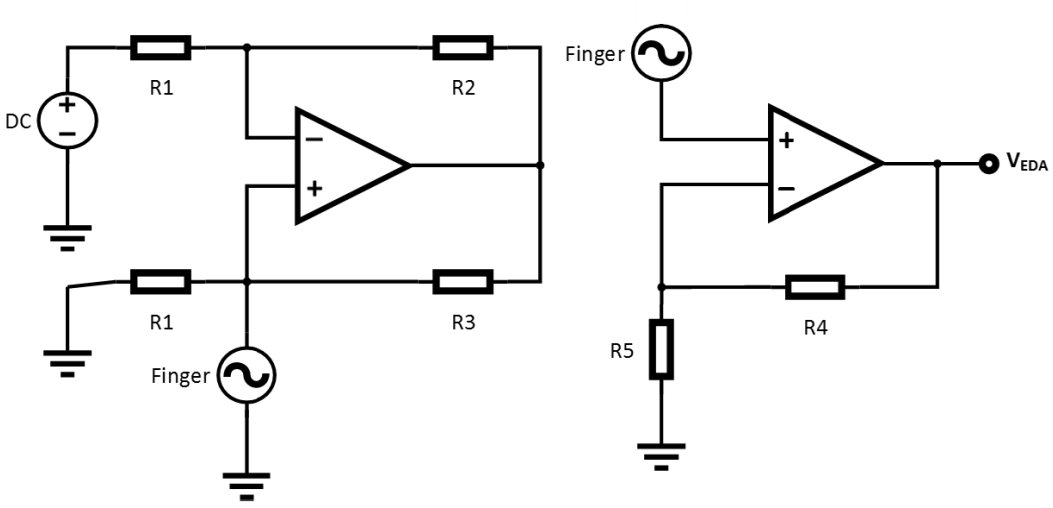

Figure 9.2 – Schematic of circuit used for measuring EDA using DC current source.

through a differential op-amp. Lastly, a filter was used to obtain the EDA signal. Similarly, two identical AC-source fully isolated galvanic skin response amplifiers with low voltage (22 mVrms, 75 Hz AC, FE116, ADInstruments) were employed to collect EDA signals. All EDA signals were digitized through the PowerLab ADC (ADInstruments), sampled at 400 Hz.

In order to collect signals simultaneously from two different media, two pairs of fingers were employed: (1) middle and index, and (2) ring and little. To procure a fair comparison, fingers were interchanged from subject to subject, for both types of devices (for instance, CSA electrodes were placed on middle and index fingers on half of the subjects).

Electrodermal activity is usually measured in conductance units, microsiemens [μS]. In our study, the AC-source devices provided values in μS. However, for the DC-source circuits used in this experiment, the raw voltage signal modulated by changes in subjects' skin conductance was acquired [mV]. Therefore, instead of a conductance increasing when the subject became stressed, we obtained a voltage that decreased at the same rate. This is why for the DC measurements the onset is determined by a drop in magnitude (as shown in the left panel of Figure 9.4).

9.2.5 Signal processing

Once all data were collected, data were separated into the corresponding electrode and task. All EDA signals were down-sampled to a frequency of 2 Hz, which is enough to maintain all the frequency components of the signal (< 0.5 Hz). EDA incorporates both rapid transient events and slow shifts. Rapid transients, called skin conductance responses (SCRs), are elicited through startle tests like the one we implemented in the present study to induce physical stress (electric shocks). The SCR rise time (onset-to-peak time) and amplitude for both signals were measured, for further analysis and comparison.

Amplitude is defined as the absolute value of the difference in level between the onset and the peak of the SCR. Rise time is the difference in time between the same two points. Onset-difference is defined as the time of SCR's onset obtained using Ag/AgCl electrodes minus the time of the onset of the corresponding (ideally simultaneous) SCR obtained through the CSA electrodes, as a reaction to the same stimulus.

Emotional and cognitive stress are elicited to evaluate slow shifts of the EDA signals. Signals for these tests were high-pass filtered to remove any low frequency trend or baseline wander (Butterworth, cutoff frequency = 0.01 Hz). In order to obtain a frequency domain representation of the EDA signals, the power spectra were calculated using Welch's periodogram method with 50% data overlap. A Blackman window (128) was applied to each segment, the Fast Fourier Transform was calculated for each windowed segment, and the power spectra of the segments were averaged. Also, the recently-reported indices of sympathetic control based on frequency-domain and time-frequency domain analysis of EDA (EDASympn and TVSymp) were computed [18], [19]. These indices utilize the spectral power within the band of 0.045 to 0.25 Hz. Frequency and time-frequency domain indices exhibited lower variability compared to time-domain measures of EDA, and acceptable consistency and sensitivity to cognitive stress.

9.2.6 Statistics

Acquired EDA signals using CSA and Ag/AgCl electrodes were compared independently for startle (shocks) and tonic (disturbing video and Stroop task) tests. The resulting SCRs from the electric shocks were compared in terms of their amplitude, onset-to-peak time and onset-differences between simultaneous

recordings obtained using CSA and Ag/AgCl electrodes. T-test analysis was used to determine the significance of the differences in SCRs' amplitude and onset-to-peak time values obtained with the two media, and to evaluate the null hypothesis that the mean of the onset-differences is equal to zero.

EDA signals during emotional and cognitive stress, from CSA and Ag/AgCl electrodes, were compared on each subject by computing the Pearson's Correlation Coefficient in time and frequency domain. Pearson's correlation coefficient mean and standard deviation throughout the subjects for each test were calculated. Difference in values of EDASympn and TVSymp obtained for baseline and test were compared between CSA and Ag/AgCl electrodes by means of t-test. Also, the differences between baseline and test values of EDASympn and TVSymp obtained using each type of electrode were tested to see if they have the same power to distinguish between the two stages. The same analysis was performed for signals obtained with the DC and AC source devices.

9.3 Results

Results for electrode-skin contact measurements are presented in Figure 9.3. Ag/AgCl electrodes exhibited lower impedance compared to CSA electrodes for the range of frequencies of interest (4 Hz to 200 Hz). For an example of what an individual SCR looks like right after electrical stimulation, for the two

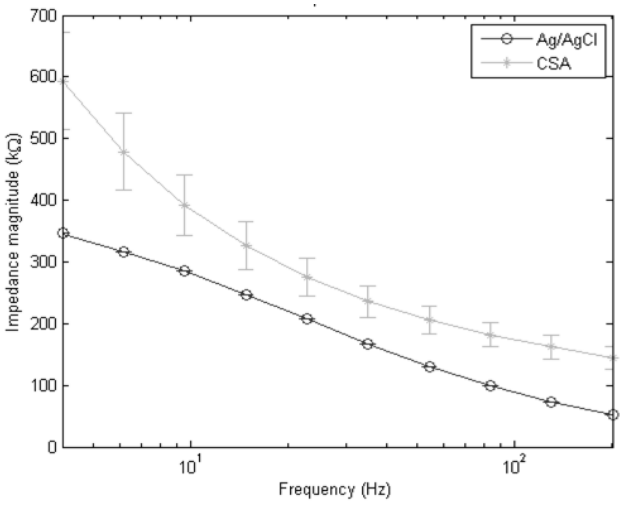

Figure 9.3 – Electrode-skin contact impedance measurements for CSA and Ag/AgCl EDA electrodes.

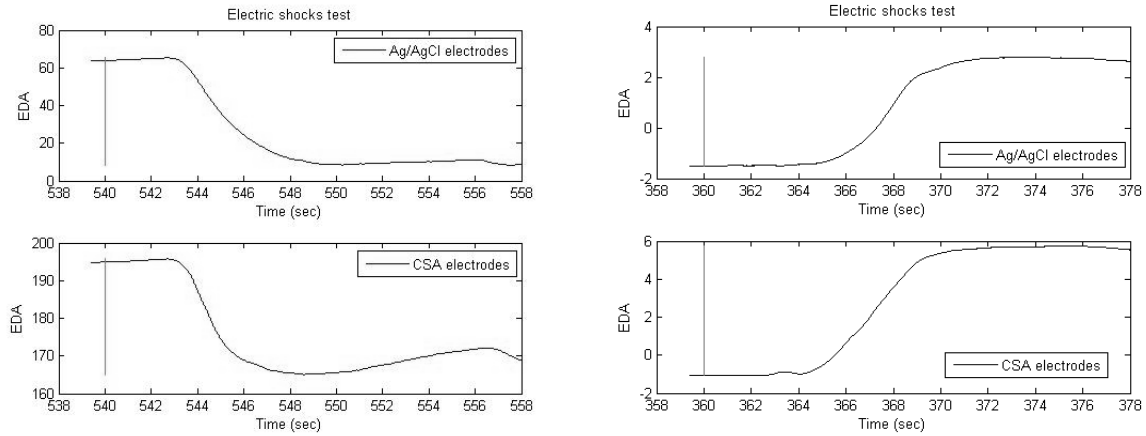

Figure 9.4 – Example of SCR for Ag/AgCl (top) and CSA (bottom) electrodes. Left: DC-source (mV); right: AC-source (μS).

types of electrodes using the two DC- and AC-source devices, see Figure 9.4. The vertical line is the time when the shock was applied. Notice in the Figure 9.4 that there is a delay of about three to five seconds from the actual shock time to the SCR onset. This delay time is in agreement with what has been reported in the literature [1], [8]. For the DC-source devices, given that we acquired the potential produced by a constant current to the skin, an increase in skin impedance is transduced to subsequent reduction in the voltage. Therefore, each time a shock occurs the voltage signal drops significantly. For the AC-source devices, the readings are in μS, so the shock produces an increase in subjects' skin conductivity. Every shock can be recognized fairly easily. The trends are very similar and each shock is well captured by both types of electrodes.

Figure 9.5 displays the results for rise time (left) and amplitude (right) correlation analysis, for DC- (top) and AC-source (bottom) devices. The two most commonly observed waveforms of the SCRs, the uniphasic and biphasic [8], were considered in the analysis. N = 13 and N = 12 SCRs were selected from the DC-source and AC-source data respectively, out of a total of 16 (2 shocks times 8 subjects). Unused shocks either saturated the SCR of one of the electrodes (in all three cases it was the Ag/AgCl) or elicited an SCR that was not distinguishable or was overlapped with other waves (4 times). It is worth mentioning

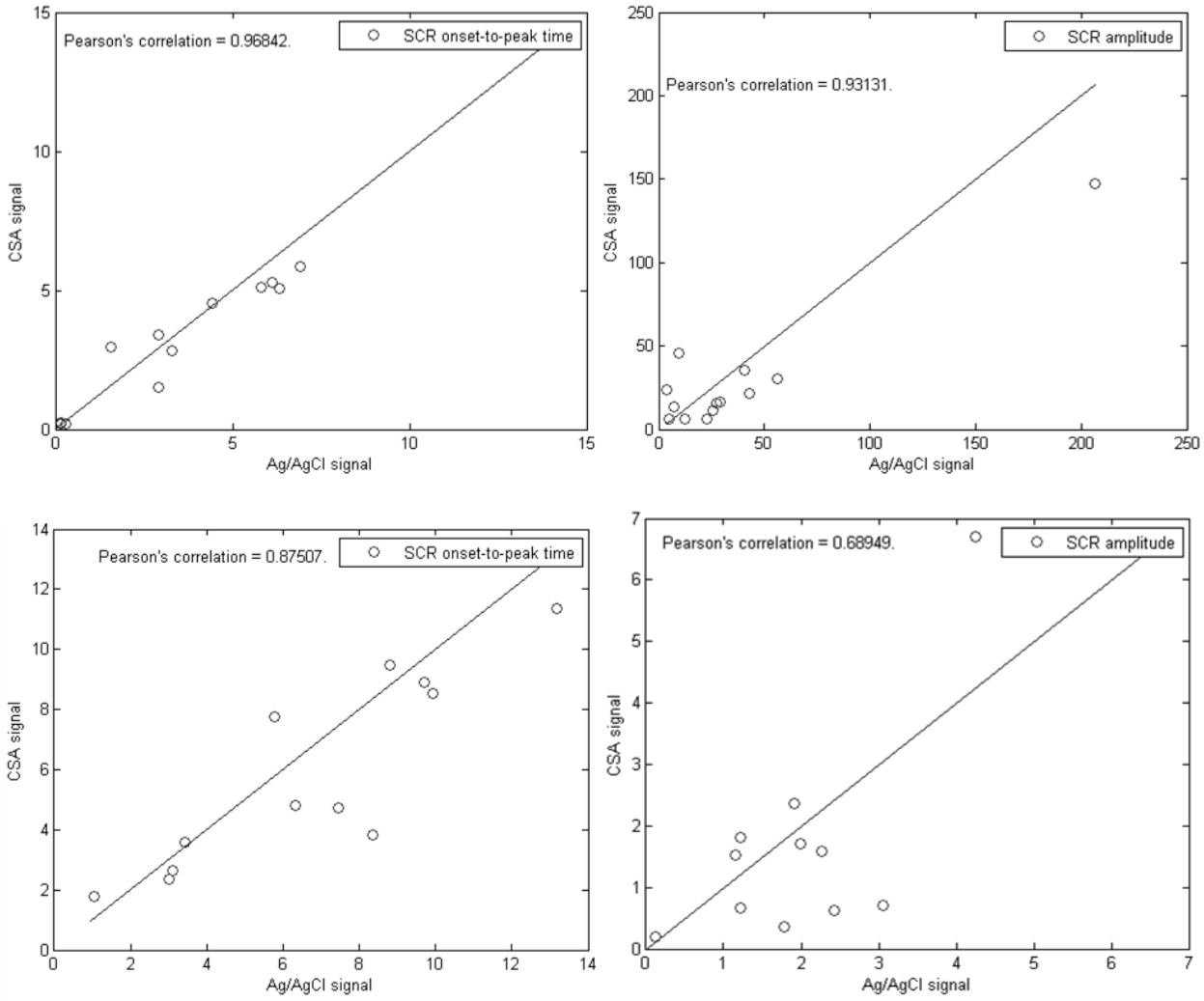

Figure 9.5 – Left: correlation analysis of onset-to-peak time; right: amplitude. Top: DC-source device; bottom: AC-source device. The blue line represents the unitary slope straight line.

that many times Ag/AgCl electrodes tended to polarize with the DC-source device, making it temporarily impossible to measure any EDA values.

Using the DC-source device, an overall correlation of 0.97 for the onset-to-peak time measure was found between the measurements performed using CSA and Ag/AgCl EDA signals. This indicates that both media exhibited a similar time for going from the onset to the peak on the elicited SCRs. Moreover, SCR amplitudes were also highly correlated between CSA and Ag/AgCl electrodes (0.93). With the AC-source

Table 9.1 Results for comparing CSA electrodes to Ag/AgCl electrodes using DC and AC-source devices

		DC-source devices		AC-source devices	
		Electric Shocks (physical stress)			
		Ag/AgCl	**CSA**	**Ag/AgCl**	**CSA**
Onset-to-peak time (sec)		4.12 ± 3.52	3.94 ± 3.66	6.67 ± 3.56	5.82 ± 3.22
Amplitude (mV for DC, μS for AC)		37.62 ± 53.29	29.3 ± 37.4	1.94 ± 1.09	1.66 ± 1.81
Onset-difference (sec)		0.0026 ± 0.13		0.31 ± 0.72	
		Disturbing video			
		Baseline	**Emotional Stress**	**Baseline**	**Emotional Stress**
Time-domain correlation		0.96 ± 0.06	0.84 ± 0.23	0.6 ± 0.35	0.59 ± 0.37
Frequency-domain correlation		0.94 ± 0.08	0.96 ± 0.05	0.64 ± 0.33	0.84 ± 0.25
EDASympn	**Ag/AgCl**	0.12 ± 0.074	0.15 ± 0.085	0.14 ± 0.09	0.15 ± 0.082
	CSA	0.26 ± 0.22	0.19 ± 0.16	0.39 ± 0.33	0.33 ± 0.29
TVSymp	**Ag/AgCl**	0.3 ± 0.18	0.62 ± 0.45#	0.29 ± 0.47	0.47 ± 0.44
	CSA	0.12 ± 0.027*	0.19 ± 0.087*#	0.17 ± 0.05	0.37 ± 0.4
		Stroop test			
		Baseline	**Cognitive Stress**	**Baseline**	**Cognitive Stress**
Time-domain correlation		0.92 ± 0.14	0.87 ± 0.14	0.63 ± 0.37	0.54 ± 0.45
Frequency-domain correlation		0.96 ± 0.04	0.91 ± 0.14	0.73 ± 0.34	0.92 ± 0.07
EDASympn	**Ag/AgCl**	0.1 ± 0.096	0.31 ± 0.21#	0.11 ± 0.068	0.37 ± 0.23#
	CSA	0.16 ± 0.088	0.32 ± 0.14#	0.16 ± 0.14	0.38 ± 0.25#
TVSymp	**Ag/AgCl**	0.37 ± 0.22	0.96 ± 0.44#	0.23 ± 0.17	1.1 ± 0.78#
	CSA	0.13 ± 0.06*	0.23 ± 0.081*#	0.18 ± 0.12	0.48 ± 0.35#

Values are mean ± standard deviation. EDASympn: normalized spectral index of sympathetic control; TVSymp: time-varying index of sympathetic control.

* represents significant differences between Ag/AgCl and CSA

represents significant differences between baseline and test, for the given type of electrodes.

devices, the obtained correlation values were lower, 0.87 for the onset-to-peak time and 0.69 for the amplitude.

Table 9.1 includes the results for DC- and AC-source EDA devices. In general, CSA electrodes seemed to obtain slightly lower SCR amplitudes, due to higher impedance than Ag/AgCl electrodes. Nevertheless, CSA electrodes appeared to capture the transit from onset to peak in a faster manner (somewhat lower onset-to-peak time). However, none of these differences are significant. For both materials the mean of the onset-differences is not statistically different from zero.

The Stroop test elicited noticeable reactions on the subjects' EDA, with both types of electrodes and devices. Figure 9.6 shows representative EDA for a subject undergoing the Stroop task. Responses to disturbing video were more variable, ranging from negligible reaction (common within male subjects), to highly noticeable reaction (noticeable in some female subjects). CSA and Ag/AgCl electrodes demonstrated this same trend, throughout the experiment. The frequency-domain index, EDASympn, was not significantly different between the two types of electrodes, for both emotional and cognitive stress. The index was able to distinguish the differences between baseline and test when subjects underwent cognitive

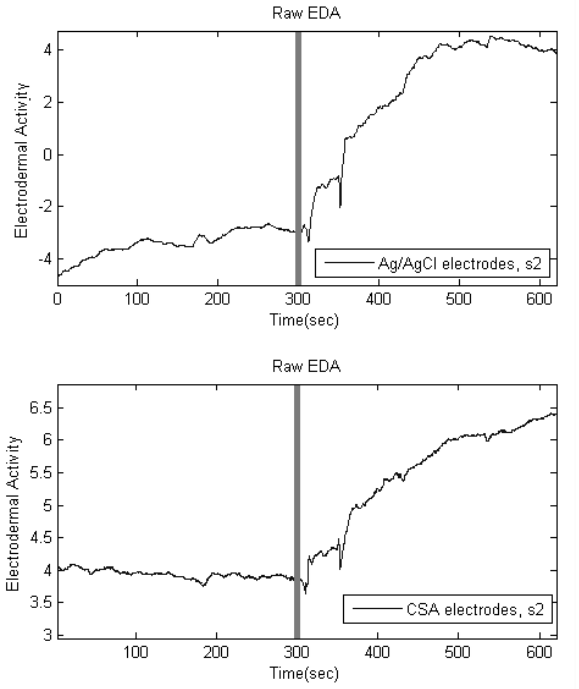

Figure 9.6 – EDA measurements (μS) during baseline (before the line) and cognitive stress test (Stroop task), for Ag/AgCl and CSA electrodes, for a given subject. AC-source device was used for this specific subject.

stress, and as expected, was not sensitive to the elicited emotional stress. Nevertheless, high correlation, with low standard deviation, was found for baseline and test stages of emotional and cognitive stress tests (Table I).

The time-varying spectral index, TVSymp, exhibited significant differences from baseline to cognitive stress, using any type of EDA electrode and device. Beyond that, it was able to detect differences from baseline to emotional stress with both kinds of electrodes, using the DC-source devices. When AC-source devices were used, the index was also insensitive to emotional stress, similar to EDASympn. Interestingly, there are noticeable differences in the TVSymp index computed using signals from Ag/AgCl and CSA electrodes, when the DC-source devices were employed.

9.4 Discussion

The CSA electrode has demonstrated its ability to detect EDA dynamics similarly to Ag/AgCl hydrogel electrodes, using DC- and AC-source devices, in various stressful scenarios. This is in agreement with previous studies that showed how the CSA electrodes are suitable to detect bio potentials [10], [20]. Figure 9.4, Figure 9.5 and Figure 9.6 all illustrate the direct correspondences between the measurements for both media. The results are similar for both media. The effect of the stimulus on the subject, for both the CSA and Ag/AgCl electrodes, can be clearly seen in the figures. Figures show differences in the amplitude of the responses and in the magnitude of the baseline wander of the signals, but the differences are circumstantial, because the measures are simultaneous, with the electrodes placed in different fingers. The comparison showed no significant differences and a high correlation of the results between the two media. It seems that a CSA electrode should be a valid replacement when it comes to recording EDA. This could save a substantial amount of money for hospitals due to the infinite shelf life the CSA electrode has to offer [10]. The CSA electrodes can also be more economical since carbon is cheaper than silver as well as the cheaper fabricating and manufacturing process mentioned earlier.

Electrode-skin impedance was higher for CSA electrodes, compared to Ag/AgCl hydrogels. The difference is more noticeable in the low frequency range, but is consistent throughout the frequency band of interest (4 to 200 Hz). Even though at very low frequencies CSA electrodes exhibited about two times the impedance of Ag/AgCl electrodes (600 compared to 350 Ω), those differences are reduced to less than 100 Ω on average as the frequency increases. We noticed that such difference in electrode-skin impedance did not affect the measures significantly.

Furthermore, as mentioned before, the Ag/AgCl electrodes made it impossible to collect EDA signals on many occasions. The signal was very noisy and in some cases, there was no signal at all. This was due to polarization of the electrodes, impeding the use of the electrodes for a period of time. However, CSA electrodes worked properly when the Ag/AgCl electrodes failed to work. Even though the use of sintered Ag/AgCl electrodes is the standard in order to minimize polarization of the electrode [1], [21],

[22], we have found it to polarize and fail many times during the development of this study. Moderate correlation (>0.5) values found between the two signals (Table 1), can be also explained in the eventual failure of Ag/AgCl electrodes to properly collect EDA signals.

Three different types of stress were induced to verify that the electrodes worked for each type of stress someone may undergo. For the electric-shocks test no significant differences were found for onset-to-peak time, amplitude, or onset-time, for any type of EDA devices. The onset differences were calculated by simply subtracting the values of Ag/AgCl SCR onsets from CSAs' SCR onset times, providing a difference value. If this value was negative then the hydrogel electrode responded first, and vice versa. Once all the values were recorded the mean value was taken, providing a value of 0.0026 ± 0.13 for DC-source devices and 0.31 ± 0.72 for AC-source devices. The mean of these onset differences are not significantly different from zero.

The disturbing video induced negligible changes in participants' stress levels, on average. The main characteristic that subjects reported from the emotional stress test was the subjectivity of the stress induced by the images, which highly varied depending on the novelty of the information, gender, cultural background, and other factors. For our purpose, we found high correlation between Ag/AgCl and CSA recordings. As expected, we found no differences in EDASympn from baseline to test during this test, for any type of electrodes, using either kind of device. Only TVSymp, a highly sensitive index of sympathetic arousal [19], exhibited significant differences from baseline as a result of the exposure to the disturbing video, exclusively when the DC-source devices were used. For its part, Stroop test results were in agreement with previous studies [18], [19]. The computed EDASympn and TVSymp indices were able to distinguish differences between baseline and test using both CSA and Ag/AgCl electrodes, for DC and AC source devices.

Between the two media, there were significant differences only in the computed TVSymp index for the DC-source devices, both for emotional and for cognitive stress. This significant difference resulted from lower standard deviation values and greater sensitivity of the CSA electrodes with stimuli when compared to Ag/AgCl electrodes.

9.5 Conclusion

Overall, CSA electrodes had similar readings to the Ag/AgCl electrodes. The correlation between the signals obtained using the two types of electrodes was moderate to very high and there were only significant differences in the highly sensitive time-varying index of sympathetic control. The electrodes worked using DC- and AC-source EDA devices, for all three different types of stress: emotional, physical, and cognitive. Signals were slightly more correlated in the frequency domain, compared to the time domain. The amplitude and onset-to-peak time testing also verified that the two electrodes were comparable to collect SCRs and there were no significant differences in their characteristics. In conclusion, CSA electrodes for collecting EDA signals are suitable surrogates of Ag/AgCl electrodes.

9.6 References

[1] W. Boucsein *et al.*, "Publication recommendations for electrodermal measurements," *Psychophysiology*, vol. 49, no. 8, pp. 1017–1034, Aug. 2012.

[2] J. T. Cacioppo, L. G. Tassinary, G. Berntson, and & 0 more, *Handbook of Psychophysiology*, 3 edition. Cambridge England ; New York: Cambridge University Press, 2007.

[3] T. P. Zahn and J. L. Rapoport, "Autonomic nervous system effects of acute doses of caffeine in caffeine users and abstainers," *Int. J. Psychophysiol. Off. J. Int. Organ. Psychophysiol.*, vol. 5, no. 1, pp. 33–41, May 1987.

[4] T. P. Zahn, J. L. Rapoport, and C. L. Thompson, "Autonomic effects of dextroamphetamine in normal men: implications for hyperactivity and schizophrenia," *Psychiatry Res.*, vol. 4, no. 1, pp. 39–47, Feb. 1981.

[5] G. Bohlin, "Delayed habituation of the electrodermal orienting response as a function of increased level of arousal," *Psychophysiology*, vol. 13, no. 4, pp. 345–351, Jul. 1976.

[6] E. S. Mezzacappa, R. M. Kelsey, and E. S. Katkin, "Breast feeding, bottle feeding, and maternal autonomic responses to stress," *J. Psychosom. Res.*, vol. 58, no. 4, pp. 351–365, Apr. 2005.

[7] G. H. Prystav, "Electrodermal, Cardiac, and Respiratory Activity to Repeated Cold Pressor Stimulation in Drug Addicts," *J. Gen. Psychol.*, vol. 94, no. 2, pp. 259–270, Apr. 1976.

[8] N. S. Greenfield and R. A. Sternbach, *Handbook of psychophysiology*, vol. xii. Oxford, England: Holt, Rinehart & Winston, 1972.

[9] A. Searle and L. Kirkup, "A direct comparison of wet, dry and insulating bioelectric recording electrodes," *Physiol. Meas.*, vol. 21, no. 2, pp. 271–283, May 2000.

[10] H. F. Posada-Quintero, B. A. Reyes, K. Burnham, J. Pennace, and K. H. Chon, “Low Impedance Carbon Adhesive Electrodes with Long Shelf Life,” *Ann. Biomed. Eng.*, vol. 43, no. 10, pp. 2374–2382, Oct. 2015.

[11] C. Gutsche, “Pressure-sensitive adhesives and applications. István Benedek, second edition, 2004 Marcel Dekker, Inc., New York, ISBN~0-8247-5059-4, 747 pages, price $ 185,” *Colloid Polym. Sci.*, vol. 283, no. 4, pp. 465–465, Jan. 2005.

[12] K. L. Lerner and B. W. Lerner, *The Gale Encyclopedia of Science*. Cengage Gale, 2008.

[13] R. Luijcks, H. J. Hermens, L. Bodar, C. J. Vossen, J. van. Os, and R. Lousberg, “Experimentally Induced Stress Validated by EMG Activity,” *PLoS ONE*, vol. 9, no. 4, p. e95215, Apr. 2014.

[14] C. R. Nave and B. C. Nave, *Physics for the health sciences*. WB Saunders Company, 1985.

[15] B. S. Zheng, M. Murugappan, and S. Yaacob, “Human emotional stress assessment through Heart Rate Detection in a customized protocol experiment,” in *2012 IEEE Symposium on Industrial Electronics and Applications (ISIEA)*, 2012, pp. 293–298.

[16] P. Karthikeyan, M. Murugappan, and S. Yaacob, “Analysis of Stroop Color Word Test-Based Human Stress Detection using Electrocardiography and Heart Rate Variability Signals,” *Arab. J. Sci. Eng.*, vol. 39, no. 3, pp. 1835–1847, Sep. 2013.

[17] R. Edelberg, “Electrical properties of the skin,” *Methods Psychophysiol.*, pp. 1–53, 1967.

[18] H. F. Posada-Quintero, J. P. Florian, A. D. Orjuela-Cañón, T. Aljama-Corrales, S. Charleston-Villalobos, and K. H. Chon, “Power Spectral Density Analysis of Electrodermal Activity for Sympathetic Function Assessment,” *Ann. Biomed. Eng.*, vol. 44, no. 10, pp. 3124–3135, Apr. 2016.

[19] H. F. Posada-Quintero, J. P. Florian, A. D. Orjuela-Canon, and K. H. Chon, “Highly Sensitive Index of Sympathetic Activity based on Time-Frequency Spectral Analysis of Electrodermal Activity,” *Am. J. Physiol. - Regul. Integr. Comp. Physiol.*, p. ajpregu.00180.2016, Jul. 2016.

[20] H. Posada-Quintero, R. Rood, K. Burnham, J. Pennace, and K. Chon, “Assessment of Carbon/Salt/Adhesive Electrodes for Surface Electromyography Measurements,” *IEEE J. Transl. Eng. Health Med.*, vol. PP, no. 99, pp. 1–1, 2016.

[21] D. C. Fowles, “The Eccrine System and Electrodermal Activity,” *Psychophysiol. Syst. Process. Appl.*, pp. 51–96, Jan. 1986.

[22] D. T. Lykken and P. H. Venables, “Direct measurement of skin conductance: a proposal for standardization,” *Psychophysiology*, vol. 8, no. 5, pp. 656–672, Sep. 1971.

Chapter 10: Conclusions and Future Work

10.1 Conclusions

In this thesis we have used signal processing techniques to evaluate how EDA can contribute to better understanding of the dynamics of the sympathetic nervous system. We started with introduction of the power spectral analysis to EDA processing, in order to develop a less variable and more sensitive index of sympathetic control. The EDASymp (chapter 3) index is a suitable discriminator of orthostatic, physical and cognitive stress, and has the potential to be used as a reliable marker of quantitative assessment of the sympathetic function. It was found to be more reliable and sensitive than the LF index of HRV, consistent between the subjects, and exhibited a lower variability compared to the time-domain measures of EDA. Moreover, we established for the first time that frequency bands of the sympathetic nervous activities can be defined to be within 0.045-0.25 Hz based on spectral analysis of EDA.

Subsequently, we used a time-varying approach to analyze the spectrum of EDA. We computed a time-varying index, TVSymp, which proved to be a suitable discriminator of the stress induced by cold pressor test, 70° head-up tilt (HUT) test, stand test, and Stroop task, and has the potential to be used as a reliable marker of quantitative assessment of the sympathetic function. Overall, TVSymp was found to be more reliable and sensitive than indices based on low-frequency components of HRV (commonly used to assess sympathetic tone), was highly consistent between subjects, and exhibited a lower variability compared to the time-domain measures of EDA. Using this time-frequency domain approach, we concluded that the band of frequencies between 0.08 and 0.24 Hz is the most responsive to the sympathetic nervous activities in healthy subjects.

Using the analysis techniques developed in previous stages, along with others available in the literature (i.e. HRV and time-domain EDA), we explored the effects of sleep deprivation on the ANS. We collected EDA and ECG (for HRV) every two hours during a 24-hour period. We found notable differences in the effects of sleep deprivation on lower (SCL) and higher frequencies (NS.SCRs, EDASymp and TVSymp) of EDA. We encountered that information confined to the higher frequency components of EDA

relates to subjects' level of attention or vigilance. For its part, changes on tonic SCL, exhibited a relationship with subjects' reactivity. This information can be utilized for developing tools to prevent the effects of prolonged wakefulness in jobs that require a high number of work hours, along with significant concentration to perform well, to assess and predict impaired cognitive performance.

To better understand what happens to sympathetic and parasympathetic control under exercising conditions, we studied HRV and EDA in subjects undergoing increasing level of exercise. We stablished that the upper band of the sympathetic dynamics shift to 0.35 to 0.4 Hz as a result of moderate to high-intensity exercise. Moreover, we found that the low frequency bounds derived via EDA can be good surrogate measures of the sympathetic dynamics especially during moderate to high-intensity exercises, hence, the upper bound of HRVLF needs to shift to higher frequencies. The varying upper frequency band of the sympathetic dynamics needs to be taken into account to provide a better understanding of the functioning of the branches of autonomic nervous system especially under high-intensity physical activity.

In the field of sensing media, our ultimate goal was to evaluate novel CSA electrodes for the task of recording EDA signals. In the pursuing of such goal, we deployed a comprehensive assessment of CSA electrodes' performance. CSA electrodes were used to collect several biopotential signals and the results were evaluated using suitable measures of signal quality. We started with the most common application, the ECG. First, we demonstrated that dry ECG electrodes can be fabricated from a mixture of carbon powder, salt, and visco-elastic polymeric adhesive. All ECG morphological waveforms and HRV indices were found to be nearly identical to Ag/AgCl electrodes. Moreover, based on CSA electrode's characteristics we determined that they are applicable for defibrillation usage, but the main advantage is their infinite shelf life which lowers both supply chain handling costs and scrap costs when compared to Ag/AgCl electrodes since the latter have a shelf life of only a month.

Subsequently, we carried out a quantitative comparison of CSA and Ag/AgCl electrodes for the task of collecting sEMG signals. It was found that our dry CSA electrodes are comparable to the gold standard Ag/AgCl electrodes in that there were no significant differences in the sEMG amplitude and muscle activation times. CSA electrodes were more resistant to noise and motion artifacts and delivered

signals with lower spectral distortion, compared to Ag/AgCl. The results of the current work indicate that CSA electrodes represent a suitable and cost-effective alternative to standard Ag/AgCl electrodes for sEMG signal collection.

When comparing CSA and Ag/AgCl electrodes for collecting EDA, both media achieved similar results. The correlation between the signals obtained using the two types of electrodes was moderate to very high, and there were only significant differences in the highly sensitive time-varying index of sympathetic control. The electrodes worked using DC- and AC-source EDA devices, for all three tested types of stress: emotional, physical, and cognitive. Signals were slightly more correlated in the frequency domain, compared to the time domain. The amplitude and onset-to-peak time testing also verified that the two electrodes were comparable to collect SCRs and there were no significant differences in their characteristics. In conclusion for this part of the study, CSA electrodes for collecting EDA signals are suitable surrogates of Ag/AgCl electrodes.

The results on evaluation and comparison of CSA electrodes to Ag/AgCl electrodes are exciting because the two salient disadvantages of Ag/AgCl hydrogel electrodes are not a problem for CSA: dehydration with storage or prolonged use, and higher cost. Hence, CSA electrodes have the potential to be a viable and cost-effective alternative to standard Ag/AgCl electrodes for collecting ECG, sEMG and more importantly for us, EDA.

Table 10.1 includes a list of the remarkable results, while providing some details about them. It can be better interpreted when the chapters have been read, and is meant to serve as quick reference if the reader wants to have access to summarized information of the results without the need of searching for them in the specific chapter.

10.2 Future Work

We expect many benefits to arouse from the techniques and sensors reported in this thesis. However, many things need to be studied to potentiate the applicability of EDA. For example, the effects of motion is a common concern for many physiological signals and have been poorly explored in the EDA [1]–[3]. We consider that in the near future, digital processing techniques to identify corrupted data, remove

the adverse effects and reconstruct the signal when possible, and determine the usability of the affected EDA data, are needed.

Table 10.1 Summary of results.

Study	**Remarkable results**	**Comments**
Power spectral density analysis of EDA. Chapter 3.	• Frequency bands of the sympathetic nervous activities on EDA signal. • EDASymp is a suitable discriminator of orthostatic, physical and cognitive stress. • EDASymp exhibited a lower variability compared to the time-domain measures of EDA	0.045 to 0.25 Hz $p < 0.05$ (t-test) CV = 0.55
Time-varying spectral analysis. Chapter 4.	• The components of time-frequency decomposition most sensitive to sympathetic nervous activities in healthy subjects • TVSymp is a suitable discriminator of the stress induced by cold pressor, 70° head-up tilt (HUT) test, stand test, and Stroop task • TVSymp is more reliable and sensitive than HRV indices, was highly consistent between subjects, and exhibited a lower variability compared to the time-domain measures of EDA.	0.08 and 0.24 Hz AUC = [0.8 to 0.92] J = [0.75 to 1.0] Acc = [0.88 to 1.0] ICC = 0.96 (0.9 0.99) CV = 0.67
Exercise. Chapter 5.	• Significant increase in high-frequency bound (Fmax) due to moderate to high-intensity exercise	Dunn's test between stages ($p<0.05$) ~0.35 Hz for moderate ~0.4 for high-intensity exercise
Sleep Deprivation. Chapter 6.	• Indices accounting for higher frequencies of EDA exhibited more significant differences during 24-hour sleep deprivation experiment • Higher frequencies of EDA relate to attention or vigilance • Lower frequencies of EDA relate to reactiveness	Dunn's test between runs ($p<0.05$) Relation found between NSSCRs, EDASymp, TVSymp and Stroop_No_Go, Repeat_No_Go accuracy indices Relation found between SCL and Go_RT index

Table 10.1 Continuation

Study	Remarkable results	Comments
CSA electrodes. Chapters 7 through 9.	• All ECG morphological waveforms and HRV indices can be obtained using CSA electrodes, nearly identical to Ag/AgCl electrodes	$p > 0.05$
	• CSA electrodes are applicable for defibrillation usage, but the main advantage is their long (theoretically infinite) shelf life.	impedance < 2 kΩ Carbon instead of Ag No hydrogel layer
	• For sEMG, amplitude and muscle activation times were not significantly different between CSA electrodes and the gold standard Ag/AgCl electrodes	$p > 0.05$
	• Dry CSA electrodes were more resistant to noise and motion artifacts than Ag/AgCl, for sEMG signals collection.	SM ratio = 24.1 ± 12.1 SN ratio = 38.3 ± 10.6
	• EDA signals collected using CSA and Ag/AgCl, were similar using DC- and AC- source devices.	Moderate to high correlation of EDA signals collected using CSA and Ag/AgCl, for both devices, for all tests.
	• CSA electrodes for collecting EDA signals are suitable surrogates of Ag/AgCl electrodes.	No significant differences on measures of SCRs.

The deployment of indices of EDA on clinical and daily use environments require a systematical exploration of repeatability and robustness of the measures. High inter-subject variability of time-domain measures of EDA has been reported [4], [5]. Indices that account for spectral information of EDA (EDASymp and TVSymp) exhibited less variability and higher consistency. We expect these novel indices to exhibit also lower intra-subject variability and higher consistency than time-domain EDA measures. This has to be evaluated. Repeatability, consistency and variability are important concepts for the applicability of the technique.

Another potential application of EDA is to use it jointly with HRV to develop indices of autonomic function. For instance, as reported in chapter 5, EDA can be used to adjust the bands for spectral analysis of HRV under exercise. Also, adaptive filtering approaches are able to use the information of EDA to filter out sympathetic content of HRV, in order to obtain a pure parasympathetic index, can be also explored. In the past, we have utilized the nonlinear nature of HRV with respect to the ANS dynamics, to separate parasympathetic and sympathetic tones from HRV [6]. The order (i.e., linear or nonlinear) of the

relationship between EDA and the sympathetic tone need to be determined, for being able to successfully carry out studies like the adaptive filtering suggested above.

Furthermore, the possible contributions of EDA for the assessment of sympathetic nervous system in clinical applications need to be explored. The correct diagnosis of many diseases requires more sensitive and reliable measures of sympathetic function. An important example is the diabetic cardiovascular autonomic neuropathy (DCAN), which is present in at least 25% of diabetics. DCAN is a remarkable example of the need for sensitive measures of sympathetic tone [6], [7] because the gold standard procedure for sympathetic assessment in DCAN is the cardiovascular autonomic reflex tests (CARTs) [8], which has low sensitivity (50%) [9]. New quantitative and accessible methods for assessment of sympathetic nervous system are needed. Hence, the analysis techniques for assessing sympathetic control developed in this thesis can contribute to the diagnosis of cardiovascular diseases and conditions (like DCAN) by taking advantage of unique characteristics of EDA signals.

From the sensing point of view, the most efficient way to collect EDA signals have to be established. The proper sensing approach also depends on the specific application and environment to be used. For example, if continuous monitoring needs to be deployed, skin irritation and signal degradation are the key factors. In wearables, the fabrication process and durability of the sensor are more relevant. We found CSA electrodes to be a suitable surrogate of Ag/AgCl electrodes to collect EDA. These electrodes can theoretically be cheaper and last longer. However, they are not reusable. Alternatives like stainless steel electrodes and other carbon-based sensors have to be evaluated for the task of collecting EDA data.

10.3 Envisioned applications

Considering that the ability of the humans' body to respond to a stimulus is linked to the sympathetic nervous system (it is also called the "fight or flight" system), we foresee the deployment of wearable devices as tools to assess stress of many kinds (cognitive, physical, orthostatic, etc.). For instance, in the automobile industry to alert drivers when they are too tired to be driving because their bodies are showing low levels of responsiveness can be of an application for detection of sleep drowsiness. We believe that the most promising tools are those based on EDA, because of the simplicity of the circuitry to collect

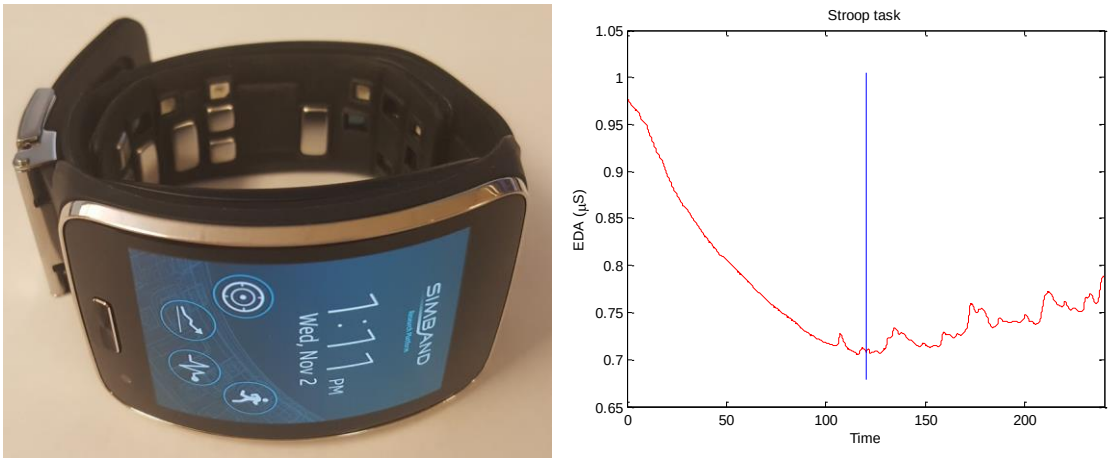

Figure 10.1 – Samsung Simband (left) and EDA data acquired during Stroop task (right). The vertical line represents the time when the Stroop task started.

the signal, and the absence of parasympathetic interference. EDA signals are already collected in some wearable devices (e.g. Samsung Simband, Jawbone's UP3, Empatica's E4, Microsoft band, Moodmetric's mood ring, Sensoree's GER mood sweater, etc.) [10], but its application is limited to functions like detecting if user is wearing the device or basic analysis as computing the mere conductance level.

Based on the positive results obtained from the evaluation of CSA electrodes for ECG, sEMG and EDA, we consider this electrode to be a reliable alternative for many applications in the future. For point-of-care applications, CSA electrodes can be used to collect the electrocardiogram at lower cost and higher quality, compared to Ag/AgCl. All the current clinical information derived from the ECG, plus the research approaches of HRV can be reliable obtained using CSA electrodes. Also, these electrodes can be used to monitor the progression of muscular dystrophies or control muscle activities via signal processing of the electromyogram data. Certainly, with the advent of sophisticated machine learning algorithms and robotics, rehabilitation engineering of muscles and limbs, it will be a good opportunity for more noise-resistant and cost-effective surface EMG electrodes than the current standard hydrogel-based electrodes.

10.4 References

[1] S. Taylor, N. Jaques, W. Chen, S. Fedor, A. Sano, and R. Picard, “Automatic identification of artifacts in electrodermal activity data,” *Conf. Proc. Annu. Int. Conf. IEEE Eng. Med. Biol. Soc. IEEE Eng. Med. Biol. Soc. Annu. Conf.*, vol. 2015, pp. 1934–1937, 2015.

[2] W. Chen, N. Jaques, S. Taylor, A. Sano, S. Fedor, and R. W. Picard, “Wavelet-based motion artifact removal for electrodermal activity,” *Conf. Proc. Annu. Int. Conf. IEEE Eng. Med. Biol. Soc. IEEE Eng. Med. Biol. Soc. Annu. Conf.*, vol. 2015, pp. 6223–6226, 2015.

[3] J. Schumm, M. Bächlin, C. Setz, B. Arnrich, D. Roggen, and G. Tröster, “Effect of movements on the electrodermal response after a startle event,” *Methods Inf. Med.*, vol. 47, no. 3, pp. 186–191, 2008.

[4] A. Crider and R. Lunn, “Electrodermal lability as a personality dimension,” *J. Exp. Res. Personal.*, vol. 5, no. 2, pp. 145–150, 1971.

[5] H. F. Posada-Quintero, J. P. Florian, A. D. Orjuela-Cañón, T. Aljama-Corrales, S. Charleston-Villalobos, and K. H. Chon, “Power Spectral Density Analysis of Electrodermal Activity for Sympathetic Function Assessment,” *Ann. Biomed. Eng.*, vol. 44, no. 10, pp. 3124–3135, Apr. 2016.

[6] K. H. Chon *et al.*, “A novel quantitative method for diabetic cardiac autonomic neuropathy assessment in type 1 diabetic mice,” *J. Diabetes Sci. Technol.*, vol. 8, no. 6, pp. 1157–1167, Nov. 2014.

[7] G. Grassi and M. Esler, “How to assess sympathetic activity in humans,” *J. Hypertens.*, vol. 17, no. 6, pp. 719–734, Jun. 1999.

[8] P. Schwartz, M. La Rovere, and E. Vanoli, “Assessment: Clinical autonomic testing report of the Therapeutics and Technology Assessment Subcommittee of the American Academy of Neurology,” *Neurology*, vol. 46, no. 3, pp. 873–880, Mar. 1996.

[9] V. Spallone, R. Morganti, T. Fedele, C. D’Amato, and M. R. Maiello, “Reappraisal of the diagnostic role of orthostatic hypotension in diabetes,” *Clin. Auton. Res. Off. J. Clin. Auton. Res. Soc.*, vol. 19, no. 1, pp. 58–64, Feb. 2009.

[10] “Design News - Blog - Wearables Get Moody With the GSR Sensor.” [Online]. Available: http://www.designnews.com/author.asp?section_id=1386&doc_id=277976. [Accessed: 17-Mar-2016].

Appendix A. List of Abbreviations

ANS: autonomic nervous system

CSA: Carbon/Salt/Adhesive

ECG: Electrocardiogram

EDA: Electrodermal Activity

EDASymp: electrodermal activity index of sympathetic nervous system

HRV: heart rate variability

HRVLF: low frequency component of heart rate variability

HRVHF: high frequency component of heart rate variability

NSSCRs: non-specific skin conductance responses

PSD: power spectral density

SCL: skin conductance level

sEMG: surface electromyography

SM ratio: Signal-to-motion ratio

SN ratio: Signal-to-noise ratio

RT: reaction time

TFS: time-frequency spectrum

TVSymp: time-varying EDA index of sympathetic control

VFCDM: variable frequency complex demodulation